PHOTOCATALYSIS OF ORGANIC EFFLUENTS

by

H. C. YATMAZ

B.Sc., M.Sc.

Thesis submitted for the degree of Doctor of Philosophy in the Faculty of
Engineering of the University of Newcastle upon Tyne

Department of Chemical and Process Engineering
University of Newcastle upon Tyne
England-UK
July 1993

ABSTRACT

Heterogeneous photocatalytic oxidation is a relatively new technology for the destruction of toxic organic substances in water and so far has concentrated on reaction mechanisms and kinetics, but the engineering side was hardly touched. In this study a detailed investigation for suitable reactor design has been carried out using three different reactor types.

An annular photoreactor was used with two different lamps with different intensities; low pressure and medium pressure mercury lamps. Two types of TiO_2 powder catalysts Degussa P-25 and Tioxide PC1 were used as slurry solutions and Degussa P-25 was found more photocatalytically active than the other. Two main organic reactants salicylic acid and 4-chlorophenol were studied to assess the light intensity effect. Although better reaction rates were achieved with the higher intensity medium pressure lamp, quantum yield results showed that low pressure lamp photons were utilised more effectively.

The falling film reactor (FFR) was used to increase the light intensity utilisation with the stronger medium pressure lamp and using the same reactants in slurries catalysts Degussa P-25 gave superior results to those in annular reactor. Because of the thin film characteristics, FFR provided good oxygen transfer at the film/air interface. A commercial supported catalyst system as a fibre glass gauze was also used inside the reactor and was found as effective as slurry systems.

In order to improve the thin film characteristics and combine these with an immobilised catalyst, a spinning disc reactor (SDR) with catalyst coated borosilicate disc was used to degrade aqueous solutions of 4-chlorophenol and salicylic acid. It was found that the efficiency of the photocatalyst process was dependent upon the type of UV source used. Lamps supplying shorter wavelength UV radiation were found to be more efficient than those whose emissions lay mainly in the near UV region. The method used to coat the disc of the SDR does not appear to meet its operational requirements.

ACKNOWLEDGEMENTS

CONTENTS

I

References

Appendix A

Computer Programs

Appendix B

Experimental and Computational Data

Appendix C

Miscellaneous Calculations

Appendix D

Quantifying Errors in Experimental Measurements

Appendix E

Engineering Design of the Spinning Disc Reactor

Appendix F

Paper to be published

CHAPTER I

1. Introduction

In recent years an increasing amount of attention has been paid to the environmental/health impact of various toxic organic substances present in water. Legislation demands upon industry with regard to the amounts of these substances which are environmentally acceptable and in healthy standards are becoming increasingly rigorous. Hence there is a need for new technology which is capable of efficiently removing such substances from industrial and municipal waste waters. Environmental pressures of the last decade have concentrated on a new technology development trend in water treatment which is not concerning physical methods (activated carbon adsorption, air stripping, ion-exchangers etc.) and tends to destructive technologies which not only degrade contaminants from water but also destroy them in the process.

One solution to this problem has concentrated on utilising chemical oxidation in order to completely mineralise the organic material (i.e. oxidation to carbon dioxide). Most of the available chemical oxidising agents, such as ozone and chlorine, are selective in their oxidising capabilities and it is unlikely that these agents would be capable of producing complete mineralisation. In fact their use can result in the formation of chemicals which have higher levels of toxicity than the original material, for instance trihalomethanes.

The most efficient oxidising agent identified for use in water treatment is the OH· radical, its having a redox potential second only to that of fluorine. It is highly reactive, non-selective and is capable of producing high degrees of mineralisation of a wide range of organic substances. Various techniques have been studied which were aimed at producing these radicals in the aqueous phase. These include H_2O_2/UV, O_3/UV and H_2O_2/O_3 combinations. Another method which is receiving an increased amount of attention is photocatalysis utilising semiconductor materials. Titanium dioxide (TiO_2) has been found the most surface active semiconductor as a photocatalyst among some certain types. An especially revealing research has been carried out to compare the photocatalysed degradation activity of some various solids using the same reactant and reaction conditions, and TiO_2 has been found to have about twice surface activity versus ZnO, CdS, WO_3 and SnO_2 (Barbeni et al. 1985). When a semiconductor such as the white paint pigment, titanium dioxide, exposed to UV light having a higher energy level than its band gap is capable of producing OH· radicals in the aqueous phase. Under continued illumination the resultant surface becomes sufficient oxidising that it can consecutively oxidise the hydroxyl ions on its surface to hydroxyl radicals. These radicals are capable of complete oxidation to carbon dioxide and water. A major advantage of photocatalysis is that unlike competing technologies, such as activated carbon adsorption or air stripping, it does not accumulate, collect or transfer the hazardous contaminant from one medium to another and destroys it at the source.

Most of the earlier work with this photocatalytic oxidation technique has utilised UV-irradiated colloidal suspensions of TiO_2 (Fujihira et al. 1981, Herrmann et al. 1983, Hsiao et al. 1983, Kalyanasundaram 1983, Matthews

1983). A few latter studies have attempted to produce a supported catalyst with some limited success. The advantage of the slurry based system is that it has generally been found to produce a higher catalytic activity than corresponding supported systems. Whether this is due to its higher available catalyst surface area or a more efficient use of the available photons is unclear. Its main disadvantage is that the catalyst has to be separated from the aqueous phase once the treatment is complete. Thus the removal of suspended catalyst particles from the treated water would be costly and laborious.

One area of research in this field that has been neglected in the past is the actual reactor design. Studies have often been performed with reactors which had previously been designed for photochemical processes rather than photocatalytic ones. Hence more attention needs to be paid to the engineering aspects of this process. It is this aspect that this work has concentrated upon using reactors with thin liquid films which can ultimately use immobilised catalysts provided suitable grades of these can be produced.

1.1   Scope of the work

Chapters 2, 3, and 4, which deal with the literature review, have highlighted that most of the earlier research on photocatalysis has been on the reaction mechanism and kinetics. Studies on reactor design concept have not been carried out and this has prevented wide use of photocatalytic reactors. Therefore the scope of this work is to concentrate on reactor configurations and design using thin liquid films. The thin liquid films produced on the surface of the reactors seem ideal for maximising the influence of the catalytic surface effect and increase the mass transfer. Hence the aim of this work is to

show that these factors make an important contribution to the amount of organic degradation, and that the overall degradation performance of the reactors using thin liquid films are superior to that of conventional photochemical reactors operating under similar conditions.

The experimental work described in this thesis falls into three categories:

(i) an examination of the performance of the annular reactor for primary photocatalytic effects

(ii) an examination of the performance of the spinning disc reactor (SDR)

(iii) an examination of the performance of the falling film reactor (FFR)

1.1.1 Photocatalysis in an annular reactor

The first series of experiments were performed in a photochemical type of annular reactor in order to study and indicate the primary photocatalytic effects. The efficiency and comparison of two type of TiO_2 catalysts were used with different loadings as suspended solids in slurry solution. The two different type of UV-lamps, low pressure and medium pressure were also used to indicate the wavelength and light intensity effects. Different initial organic concentrations were also performed for the purpose of kinetic studies.

1.1.2 Photocatalysis on a spinning disc reactor (SDR)

This reactor has been especially designed for mass transfer and hydrodynamic studies, and in particular it has been used for water treatment purposes as an ozone gas-liquid contactor (Barberis 1987, Wallis 1991). In this

4

work, the reactor was modified with the application of UV lamps and used with a borosilicate glass disc with coated catalyst. The main advantage of using a SDR type design is that it reduces the effect of mass transfer limitation. This is unlikely to be significant in a slurry based system where the overall rate is predominantly reaction rate controlled. Also the thin liquid film produced has poor light absorbency properties which mean that a large proportion of the ultraviolet radiation supplied is not efficiently used (i.e. low quantum yield values). The same characteristics of the liquid film which make it unsuitable for a slurry based system are however ideal for a supported catalyst based reactor, where short organic diffusion lengths are a positive advantage.

1.1.3 Photocatalysis in a falling film reactor (FFR)

This has also thin liquid film characteristics and was especially designed for high light efficiency which is one of the most important economic aspects of photocatalytic processes. The FFR used was designed using a borosilicate glass tube 80cm length and 10cm i.d. surrounding a cylindrical medium pressure lamp 54cm length and 48mm diameter to give the most efficient use of the high light intensity. Two type of catalysts were used in a slurry based solution and also a catalyst coated fibre glass gauze was placed inside the reactor surface for use as a supported system. Four type of organics were used with different concentrations.

CHAPTER II

2. Photocatalysis based upon ultraviolet irradiation of TiO_2

.

2.1 The role of the catalyst

It is generally agreed that the oxidation process at the surface of TiO_2 catalysts is initiated by the formation of an electron-positive hole pair caused by the irradiation of the catalyst with UV with an energy level greater than the band gap of TiO_2 (Kalyanasudaram 1983, Teichner and Formenti 1985):

$$h\nu \rightarrow e^- + h^+ \tag{2.1}$$

The electrons are excited to the conduction band of the TiO_2 and positive holes are produced in the valence band. The energy level of the bottom of the conduction band indicates the reducing potential of the electrons produced, whilst that of the top of the valency band is a measure of the oxidising strength of the positive holes (Sakata and Kawai 1983). Initially the generation of an electron-hole pair would result in the electron adding to a Ti^{4+} centre producing Ti^{3+} and the hole being sited on lattice oxygen giving O^- (Anpo 1988). Fujihira et al. (1982) proposed a mechanism similar to aqueous phase Fenton type reactions for the reactions occurring at the surface of TiO_2:

.

$$2h^+ + H_2O \rightarrow \tfrac{1}{2}O_2 + 2H^+ \qquad\qquad (2.2)$$

$$O_2 + 2H^+ + 2e^- \rightarrow H_2O_2 \qquad\qquad (2.3)$$

$$OH^- + h^+ \rightarrow OH\cdot \qquad\qquad (2.4)$$

$$O_2 + e^- \rightarrow O_2\cdot^- \qquad\qquad (2.5)$$

$$H_2O_2 + O_2\cdot^- \rightarrow OH\cdot + OH^- + O_2 \qquad\qquad (2.6)$$

$$H_2O_2 + h\nu \rightarrow 2OH\cdot \qquad\qquad (2.7)$$

$$H_2O_2 + e^- \rightarrow OH\cdot + OH^- \qquad\qquad (2.8)$$

$$H_2O + h^+ \rightarrow OH\cdot + H^+ \qquad\qquad (2.9)$$
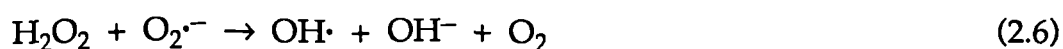
It would therefore appear to be the case that OH· radicals are the major oxidising agent present. The positive holes are "trapped" at the TiO_2 surface by adsorbed water and/or hydroxyl species (reactions 2.2, 2.4, and 2.9) (Bickley and Jayanty 1974); electron trapping is provided by adsorbed oxygen molecules (reactions 2.3 and 2.5). Che and Tench (1983) in a literature review found considerable evidence to support the presence of $O_2\cdot^-$ at the surface of UV irradiated TiO_2. Matthews (1984) demonstrated that reaction 2.7 was not a major source of hydroxyl radicals since addition of aqueous hydrogen peroxide did not effect the rate of photocatalytic degradation of benzoate ions. Even if hydrogen peroxide is involved in the production of oxidising radicals its rate of degradation is very rapid (reactions 2.6, 2.7, 2.8) and very rarely appears in the aqueous phase during photocatalytic studies (Cundall et

7

al. 1976). Tseng et al. (1991) has shown the typical reaction scheme of an n-type semiconductor such as TiO_2 (Figure 2.1).
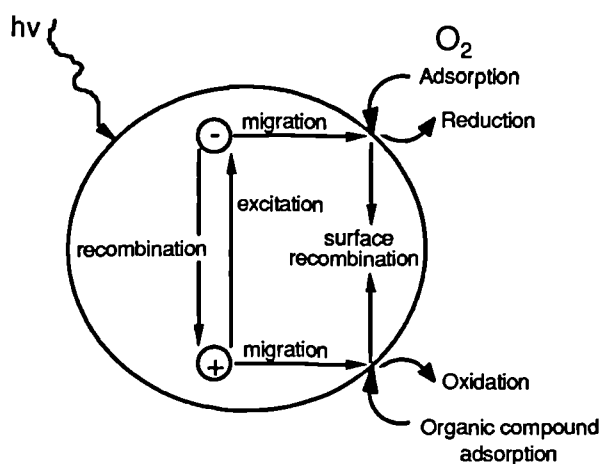
Figure 2.1 The Generation of Holes/Electrons on Semiconductor
and Consequential Interfacial Reactions

Since it is possible for the electron-hole pairs to recombine, if recombination is not to slow the catalytic process, it is necessary that efficient electron and hole traps should be present at the catalyst's surface. For instance, it has been demonstrated that in the absence of oxygen the rate of decomposition of organic subtances slows dramatically (Matthews 1984). Izumi et al. (1980) also showed that the rate of the decomposition of various hydrocarbons could be enhanced by platinization of TiO_2 powder. They suggested that this was due to the fact that the platinum centres tended to draw conduction band electrons to them where they were transferred to molecular oxygen forming $O_2{}^{\cdot-}$. This in turn slowed the rate of electron-hole pair recombination. Due to the rapid rate of electron-hole pair recombination, quantum yields (number of molecules degraded per photon available) for

photocatalytic oxidations are generally fairly low, usually lying in the region of 10^{-2} to 10^{-3} (Pichat 1985, Teichner and Formenti 1985).

Anpo et al. (1989) studied the relationship between catalyst photoluminescence and catalytic activity. They noted that photoluminescence increased with the reactivity of unsaturated hydrocarbons. The extent of the enhancement of the photoluminescence appeared to be related to the ionisation potential of the hydrocarbon being degraded (i.e. the lower the ionisation potential, the higher the observed photoluminescence). The authors related this to the ability of hydrocarbons with high ionisation potentials to form negatively charged adducts via electron capture at the TiO_2 surface, whilst those with low potentials tended to form positive adducts via hole trapping.

Sclafani et al. (1990) conducted a comparative study of the catalytic performance of several TiO_2 catalysts. They found the following order of reactivity (based upon rate of degradation of phenol per unit surface area of catalyst): Carlo Erba RPE > Merck > Tioxide 1601/1 > BDH > Montedison B5 > Degussa P-25 >> Tioxide 1601/2. The two catalysts with the lowest activities had the highest rutile contents (Degussa P-25 20%, Tioxide 1601/2 100%), whereas the others, which had predominantly anatase structures, showed much better activity. This was attributed to the fact that the electron-hole pair recombination reaction is more rapid for rutile. For the anatase catalysts activity appeared to increased with improving crystallinity. However, Tanguay et al. (1989) showed that rutile was more active than anatase for the degradation of dichloromethane. Again the basis for this assessment was the rate of removal of the organic per unit surface area of catalyst.

It has been argued that the catalytic activity of TiO_2 is independent of catalyst surface area since the overall rate of the process is limited by the supply of positive holes to the surface (Sakata and Kawai 1983). If this is the case it is light intensity which controls the rate reaction rather than surface area of the catalyst. The improved catalytic performance of smaller TiO_2 particles when compared to that of larger ones is due to being easier for electrons and holes to migrate to the surface of the catalyst rather than the larger surface area of the former (Teichner and Formenti 1985). This was supported by the findings of Farin et al. (1989) who observed that there was a non-linear relationship between surface area and reaction rate rather than the linear one expected. Anpo (1988) attributed the improvement in catalytic performance of TiO_2 supported on Vicor glass to a particle size effect which enhanced electron-hole separation.

Childs and Ollis (1980) have questioned whether photocatalysis actually occurs in the presence of TiO_2. The authors analysed data obtained from the literature available using a turnover number (molecules reacted divided by the product of reaction time, number of active sites and photons absorbed). They found that approximately half the data studied could not be claimed to be truly catalytic. However the number active sites available on the surface of TiO_2 is not known accurately because they have not been truly identified. If the active sites involved in the reactions were hydroxyl groups then a site number in the region of 5×10^{14} cm^{-2} would be justified, whereas if the active sites were due to surface defects or depletive chemisorption then their concentration would be more likely to be in the region of 10^{12} cm^{-2}.

The mechanistic details of the photooxidative process have generated some controversies. Excitation of aqueous TiO_2 ultimately yields electrons and holes, the latter producing OH· radicals on the particulate surface. In fact some doubt exists as to whether the oxidation reactions in aqueous systems actually occur on the surface of the catalysts at all. It is possible that the oxidising radicals produced by the UV irradiation of TiO_2 can actually free themselves from the catalytic surface and diffuse into the liquid phase. Fox and Chen (1981) claim to have found definite evidence that the oxidation reactions do indeed occur on the surface of TiO_2. They studied the photocatalytic oxidation of olefin to carbonyl derivatives in acetonitrile. They found that it was impossible to account for the oxidation reaction in terms of homogeneous phase chemistry. Hence they concluded that the reaction must have been occurring at the catalyst's surface. However their evidence does not extend to those reactions that occur in aqueous systems, since their experimental conditions precluded the formation of OH· radicals at the surface of the catalyst. Serpone et al. (1991) also argued that photo-oxidation takes place at the surface, and that surface holes and surface OH· radicals are indistinguishable entities. Turchi and Ollis (1990) presented a detailed kinetic analysis of the photocatalytic ozonation process and concluded that hydroxyl radicals could indeed be present as mobile oxidants rather than remaining stationary at the TiO_2 surface.

2.2   Photocatalytic oxidation studies

A large amount of literature is available on the rates of photocatalytic oxidation of aqueous solutions of various organic compounds. These can be divided into two categories:

11

(i) reaction systems where TiO_2 particles are suspended in the aqueous phase forming a catalytic slurry;

(ii) reactors where the TiO_2 is supported on a solid surface inside the reactor and is thus stationary within the reactor.

The former type of system is more common because it is technically easier to obtain. Because of the fairly inert nature of TiO_2 the number of suitable support materials is limited and hence less work has been performed using this type of reactor, since the physical aspects of the reactor are unlikely to effect the basic reaction chemistry.

2.2.1 Mechanistic studies

A large number of reactions have been studied, but the experimental work in this report has concentrated on salicylic acid and 4-chlorophenol degradation, because these organics have been generally used as main model reactants.

Salicylic acid was chosen as the reference contaminant because it is strongly fluorescent and hence can be readily measured in very low concentrations (Matthews 1987a,b,c 1988b, 1990). This possibly makes easy to follow up reaction kinetics. The same author (1983) also indicated additional evidence for OH radicals came from the observed isomer distribution of the hdyroxy-aromatic acids formed.

Matthews (1984) demonstrated that the rate of oxidation of benzoate ions was significantly enhanced at pH values above 8. The major product in this case was salicylate ion, indicating addition of a hydroxyl group to the aromatic ring (Matthews 1983). This was consistent with the assumption that hydroxyl radicals are the main oxidising species present:

$$C_6H_5COO^- + OH\cdot \rightarrow C_6H_5OHCOO\cdot^- \tag{2.10}$$

$$C_6H_5OHCOO\cdot^- + O_2 \rightarrow C_6H_4OHCOO^- + HO_2\cdot \tag{2.11}$$
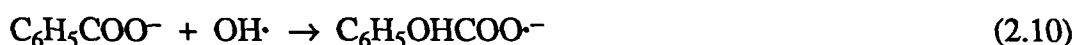
Further attack on the salicylate ions produced according to reaction 2.11 by hydroxyl radicals is then possible (Matthews 1987a):

$$C_6H_4OHCOO^- + OH\cdot \rightarrow \cdot OHC_6H_4OHCOO^- \tag{2.12}$$

Interestingly the rate of degradation of salicylate ion tends to slow with increasing initial concentration. This is because salicylate ion is capable of competing with oxygen for the photogenerated electrons:

$$C_6H_4OHCOO^- + e^- \rightarrow {}^-\cdot C_6H_4OHCOO^- \tag{2.13}$$

$${}^-\cdot C_6H_4OHCOO^- + \cdot OHC_6H_4OHCOO^- \rightarrow 2C_6H_4OHCOO^- + OH^- \tag{2.14}$$
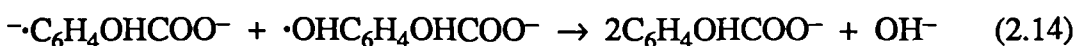
Chlorophenols represent a group of organics frequently found in various industrial effluent and reported in hazardous waste sites (Ellis et al. 1984). Therefore many workers have chosen 4-chlorophenol as a model reactant (Barbeni et al. 1984, Al-Ekabi et al. 1988, 1989, Matthews 1986b,1987b,c 1988b, 1990, Tseng and Huang 1991, Al-Sayyed et al. 1991).

Al-Ekabi et al. (1988, 1989) studied the degradation of chlorophenols in a supported catalyst reactor. Complete mineralisation of 4-chlorophenol was obtained with hydroquinone being present as a major intermediate:

$$OHC_6H_4Cl + OH\cdot \rightarrow OHC_6H_4ClOH\cdot \qquad (2.15)$$
$$OHC_6H_4ClOH\cdot \rightarrow OHC_6H_4OH + Cl\cdot \qquad (2.16)$$
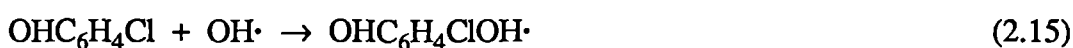
The authors also showed that in a multicomponent system containing 4-CP, 2,4-DCP and 2,4,5-TCP, the organics degraded at similar rates.

Al-Sayyed et al. (1991) studied both photochemical and photocatalytic degradation of 4-chlorophenol and concluded that the latter reached complete mineralisation, furthermore they found that the detected amounts of the identified primary intermediates under photochemical conditions were much larger than in the case of photocatalysis. They also found hydroquinone as the main primary intermediate for both reactions and maximum hydroquinone concentration was much greater under photochemical conditions. They indicated the insignificance of pH to the reaction rate at least in the range of 3.4-6.0.

The above mechanisms indicate the importance of the oxidising radicals (especially OH·) produced at the surface of TiO_2 powders in the organic degradation reactions. Earlier mechanistic studies usually accounted for these types of reaction by assuming that there was a direct reaction between the organic molecules and the positive holes. For instance, Kraeutler and Bard (1978) proposed the following reaction pathway for the photocatalytic oxidation of acetate ion to methane and carbon dioxide:

14

$$CH_3CO_2^- + h^+ \rightarrow CH_3CO_2\cdot \qquad (2.17)$$

$$CH_3CO_2\cdot \rightarrow CH_3\cdot + CO_2 \qquad (2.18)$$

$$CH_3\cdot + e^- \rightarrow CH_3^- \qquad (2.19)$$

$$CH_3^- + H_2O \rightarrow CH_4 + OH^- \qquad (2.20)$$
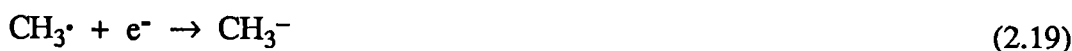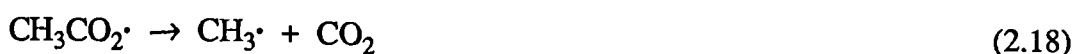
2.2.2 Catalytic slurries

2.2.2.1 Effect of concentration

As shown by Matthews (1987a), TiO_2 concentration is an important experimental parameter as regards to slurry reactors. At low concentrations, catalytic activity tends to increase with increasing slurry loading due to an increased amount of light absorption (Pichat 1985). However, a point is obtained where catalytic activity reaches a maximum and may even start to fall, since at high slurry concentrations the light distribution through the reactor is affected adversely by falling light penetration. The optimum slurry concentration normally lies in the region of 1g/lt (Matthews 1990).

2.2.2.2 Catalyst types

Herrmann et al. (1983) compared the photocatalytic activity of various semiconductor powders in the UV and visible regions by measuring the degradation rate of oxalic acid. The observed rate of activity in the UV region was $TiO_2 > ZrO_2 > CeO_2 \gg Sb_2O_4$, whereas that in the visible region was $TiO_2 > Fe_2O_3 > WO_3$. pH was again shown to exert an influence over the rate of reaction. The authors suggested that this was due to the $HC_2O_4^-$ ion being more reactive than the $C_2O_4^{2-}$.

2.2.2.3 Non-aqueous suspensions

Blatt et al. (1989) studied the selectivity of the photo oxidation of m-phenoxytoluene to m-phenoxybenzaldehyde with a non-aqueous suspension of TiO_2. The most efficient solvent used was xylene. It was found that catalyst deactivation occurred, which was attributed to the presence of unidentified reaction products. The aldehyde was the end product of the reaction due to that compounds inability to form charge transfer complexes with the catalytic surface.

2.2.3 Supported catalysts

Matthews (1987b) has performed a detailed study of a supported catalyst reactor. A thin film of Degussa P-25 catalyst was deposited on the inner surface of a borosilicate glass helix wrapped around a lamp. The author then irradiated the helix whilst passing various organic solutions through it and measured the rates of decomposition. He obtained the following order for the reactivity organics studied: naphthalene > fluorescein > benzoic acid > salicylic acid > phenol > 2-chlorophenol > 2-naphthol > 4-chlorophenol. The same author used the reactor for the oxidation of methylene blue (1989). He found that salicylic acid degraded 1.75 times faster than this compound.

The performance of the thin film TiO_2 helix reactor has been compared to that of an annular reactor containing TiO_2 supported on a woven glass mesh (Matthews 1987c). It was found that the former type of reactor was capable of higher rates of salicylic acid oxidation. When the coil reactor was

placed in a parabolic trough and exposed to solar illumination a thousand-fold decrease in salicylic acid from an initial concentration of 1.38 mM/lt was observed for one liquid pass. However the liquid flow rate used was only 10 cc/min.

Very few direct comparisons have been made between supported catalyst systems and those using suspensions. However Matthews (1990) has assessed the relative efficiencies whilst using the same type of catalyst, light source and reactor geometry. He found that at high organic concentrations (50 mg/lt) the rate of degradation was similar in both cases, whilst at lower concentrations (1 mg/lt) the slurry system achieved a rate of degradation approximately twice as high as that of the supported catalyst. He suggested that in the former case mass transfer limitations did not affect the rate of oxidation, whilst in the latter this had to be considered.

Serpone et al. (1986) used a rather more refined method of depositing TiO_2 on glass. They impregnated the surface of glass beads by high temperature degradation of titanium alkoxides. The coated beads were then loaded into their reactor. The light source used in these experiments produced simulated sun light and the reaction used for assessment of catalytic efficiency was the oxidation of 2,4,5-trichlorophenol. Complete mineralization of the organic was achieved within an irradiation period of 6 minutes.

Tanguay et al. (1989) studied the rates of degradation of dichloromethane with anatase powder and anatase supported on a carbon felt and found that the latter produced the higher rate of organic degradation.

17

Yoneyama et al. (1989) compared the photocatalytic activity of micro crystalline TiO_2 incorporated in the interlayer space of montmorillonite clay with that of TiO_2 powder. It was shown that the TiO_2/clay particles were capable of higher rates of organic degradation than those observed for TiO_2 powder. It was suggested that this was due to the micro crystalline structure of the TiO_2 shifting the conduction band edge to a higher excited electronic state. These authors found that the order of catalytic activity for these clays with carboxylic acids was propionic acid > lactic acid > caprylic acid > acetic acid > valeric acid > capric acid.

2.2.4 Effects of light intensity

Tunesi and Anderson (1987) studied the effects of light intensity and temperature on the photocatalytic degradation of 3,4-dichlorobiphenyl. The observed reaction rate increased in both parameters, with light intensity having the greater effect. The effect of temperature was accounted for in terms of increased conductivity, whilst that of light intensity appeared to be due to increased production of electron-hole pairs at higher intensities. They observed that at low light intensities surface trapping of electrons and holes predominates and hence the rate of reaction is proportional to light intensity. However, at high light intensities the concentrations of electrons and holes are high and the rate of recombination increases accordingly, competing with surface trapping, resulting in a square root relationship between reaction rate and light intensity (Harvey et al. 1983, Pichat 1985). In a recent review of photocatalytic studies Ollis et al. (1991) concluded that increased intensity always results in an increase in volumetric reaction rate, until the mass transfer limit is encountered and they summarised the relationship between

the quantum efficiency Φ (the number of molecules transformed per absorbed photon) and intensity as follows:

Low I: rate varies as $I^{1.0}$ - Φ = constant

Intermediate I: rate varies as $I^{0.5}$ - Φ varies as $I^{-0.5}$

High I (mass transfer limit): rate varies as $I^{0.0}$ (const.) - Φ varies as $I^{-1.0}$

This comparison was also extended to reactor cost efficiency and concluded that as the reactor cost is the most expensive part of the process, increased intensity increases the rate per volume and is worthwhile, whereas if photon collection or generation is a major cost, a lower intensity will provide cheaper treatment.

CHAPTER III

3.   Kinetics of surface catalysed reactions

The main effect of a catalyst on a chemical reaction is to increase its rate, and this must mean to increase its rate coefficient. Measurement of the kinetic parameters of a catalysed reaction is important for two basic reasons.

a) First, knowledge of these, and especially of the orders of reaction with respect to reactants and products, is essential for definition of the mechanism of the reaction, and it is only through some understanding of reaction mechanism that the process of catalyst optimisation may be carried out in a rational and scientific way.

b) Second, the best design of the catalytic reactor, including the size and shape of the catalyst media, depends critically upon information concerning the reaction orders as well as on the thermochemistry of the system.

The fundamental investigator may wish to determine how the rate of a particular reaction varies as catalyst composition is systematically varied, with the aim of relating the results in a fundamental fashion to specific physical or chemical properties of the catalyst. A study of the detailed kinetics of one particular reaction has been a traditional approach to obtaining some understanding, even though indirect, of its mechanism and from this it is desirable to generate a mathematical model to represent the

data. Before the arrival of the sophisticated techniques which are now used routinely to identify surface species, such as Scanning tunnelling spectroscopy (STS), Fourier transform infra-red (FTIR) spectroscopy; Campbell (1988) showed that kinetic studies provided one of the few potential means of gaining some indication of the microscopic action involved in reactions on solid surfaces. Kinetic studies thus feature strongly in many recent accounts of research on heterogeneous catalysis. However in photocatalysis, the study of surface mechanisms and reaction kinetics are relatively new and under intensive investigation. Therefore, most of the photocatalytic studies have concentrated on the most general principles governing the rates of reactions at surfaces (Ollis et al. 1991) rather than detailed mechanistic studies.

3.1   Basic kinetics and order of reaction

3.1.1   Langmuir-Hinshelwood kinetics

The general scheme for a surface catalysed reaction involves five stages, as shown in Figure 3.1 for the conversion of a reactant A into a product P.

Langmuir adsorption isotherm provides a fundamental framework for the observed rate variations and the surface coverage θ is defined by a Langmuir isotherm (Equation 3.1) (Bond-1990).
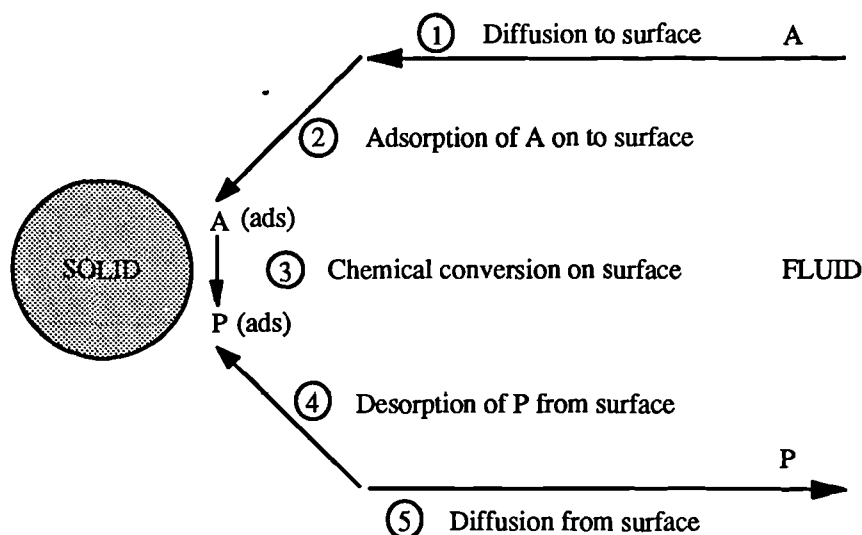
Figure 3.1 Schematic representation of the conversion of a reactant A to a product P
Adsorbed species are indicated by (ads) (Campbell-1988)

$$\theta = \frac{bC}{1 + bC} \qquad (3.1)$$

where C is the solution reactant concentration and b is the apparent binding constant of the organic on the catalyst surface.

The Langmuir-Hinshelwood mechanism for a reaction at a solid surface applies when stage 3 in Figure 3.1 is rate determining. The rate equation for the overall reaction is then predicted by application of the principle of mass action to this surface reaction in conjunction with the Langmuir adsorption isotherm. Considering a unimolecular conversion of a molecule A, adsorbed without dissociation, into a product P that is not adsorbed at all. The rate of removal of A from the liquid phase will depend only on the concentration of adsorbed A, i.e. on its surface coverage; thus (Bond-1990)

$$\frac{-dC_A}{dt} = k\theta_A = \frac{kb_A C_A}{1 + b_A C_A}$$

(3.2)

k being a rate coefficient. There are two important limiting conditions:

(1)   when either b_A or C_A is so small that $b_A C_A$ is much less than unity, θ_A approximates to $b_A C_A$ and the reaction is therefore first order in A, under these conditions θ_A is of course low;

(2)   when either b_A or C_A is so large that $b_A C_A$ is much greater than unity, θ_A becomes almost independent of C_A and the reaction is zero order in A, this occurs when θ_A is in the region of unity.

When neither of these approximations applies, the full form of the rate expression must be used, and the order in A (at least over a limited concentration range) appears to have a positive fractional value between zero and unity. If it were feasible to examine the order of such a reaction over an extended concentration range, it should be first-order behaviour at low concentrations, changing through intermediate values to zero order at high concentrations.

3.1.2   Application of L-H kinetics to photocatalysed reactions

In the analysis of heterogeneous kinetics of photocatalysed reactions, generally it has been agreed that the reactions observed both with catalytic slurries and supported catalysts obey Langmuir-Hinshelwood (L-H) kinetics (Al-Ekabi et al. 1989, Matthews 1986, 1987b, 1989, 1990, Tunesi and Anderson 1987, Ollis et al. 1989, Turchi and Ollis 1990):

$$Rate = r_{LH} = -\frac{dC}{dt} = \frac{k_1 k_2 C}{1 + k_1 C} \qquad (3.3)$$

Integrated form,

$$k_1 k_2 t = \ln\frac{C_0}{C_t} + k_1(C_0 - C_t) \qquad (3.4)$$

and,

$$t = \frac{1}{k_1 k_2}\ln\frac{C_0}{C_t} + \frac{1}{k_2}(C_0 - C_t) \qquad (3.5)$$

where C_0 is the initial concentration of organic in solution and C_t is that remaining after a reaction period of time t. Most authors interpret the values of k_1 and k_2 as follows: k_1 is related to the adsorption affinity of the organic to the catalyst, whilst k_2 is taken to represent the rate of reaction at the catalytic surface. However, Turchi and Ollis (1990) have claimed that these definitions for the constants in the equations are incorrect. Their work indicated that k_2 was independent of the nature of organic being degraded, and that its value could be attributed to the characteristics of the catalyst and the light intensity. They concluded therefore that k_2 was representative of the rate of formation of hydroxyl radicals by the catalyst. It was also found that the values of k_1 showed good agreement with values obtained for the second order rate constants of the aqueous phase reaction of hydroxyl radicals with the same organic material.

They showed that it was possible to delineate surface vs. solution bulk reactions and derived a kinetic model by considered four cases implicating OH radical attack of the organic substrate:

(i)   reaction occurs while both species are adsorbed;

(ii)   reaction occurs between the adsorbed substrate and the free radical;

(iii) reaction occurs between surface-bound OH radical and the substrate in solution; and

(iv)   reaction occurs while both species are in solution.

In all cases, the analytical form of the derived complex rate expression was identical and was similar to that from the Langmuir model.

It can be seen that equation (3.4) comprises both zero and first order kinetics. For low initial concentrations of organic and also small values of k_1, the kinetics tend towards first order $[\ln(C_0/C_t) \gg k_1(C_0 - C_t)]$:

$$\ln \frac{C_0}{C_t} = k_1 k_2 t \qquad\qquad (3.6)$$

In aqueous phases containing more than one dissolved substance, it is possible that there will be competition for the adsorption sites of the TiO_2 amongst the compounds present. This leads to a slowing of the rate of photocatalytic oxidation which is observed for a particular substance. The rate can be described as follows (Al-Ekabi et al. 1989, Hsiao et al. 1983, Ollis et al. 1984, 1985, 1989, Pruden and Ollis 1983):

$$-\frac{dC}{dt} = \frac{kKC}{1 + KC + K_1 C_1 + \cdots + K_n C_n} = \frac{kKC}{1 + KC + \sum K_i C_i} \qquad\qquad (3.7)$$

Hence, as the number of competing compounds increases, the rate of degradation of C tends towards first order behaviour. This was demonstrated by Al-Ekabi et al. (1989) who showed that the rate of degradation of 4-chlorophenol was initially zero order in a single component system, but first order in a multicomponent system. Ollis and Turchi (1990) also demonstrated that rate parameters derived from examination of single compound photocatalysed conversions can be used to provide reasonable estimates of reactor performance while operating with multicomponent feed streams.

Ollis et al. (1991) stated that recent experimental studies have identified active oxygen at the TiO_2 surface and in solution. The reaction therefore may proceed at either or both locations. Moreover, the various light sources used may allow the simultaneous presence of homogeneous and heterogeneous photochemistry. Minero et al. (1992) in their detailed investigation of several aromatic compounds and different forms of TiO_2 supports discussed the use of the L-H model because of its suggestion that the reaction might be occurring at the surface of catalyst and concluded that the degradation rate is not strongly affected by their actual location, whether in solution, on the photocatalyst, or on another *inert* support. They agreed with others who studied aromatic compounds (Terzian et al. 1991) that the disappearance of the organic compound under irradiation in the presence of TiO_2 follows generally a pseudo-first-order kinetics. The change in time of the initial substrate concentration are then fitted with an exponential equation in another form of equation 3.6:

$$C_t/C_0 = \exp(-kt) \qquad (3.8)$$

where C_t and C_0 represent the initial concentration of the substrate and the concentration after time t of irradiation, respectively, and k represents the apparent kinetic rate constant (min^{-1}).

3.2 Effect of mass transfer in catalysed reactions

The above kinetic terms are ideal relationships which assume that there are no mass transfer limitations acting upon the process. Under real conditions the rate of transport of solute to the catalytic surface can exert a significant influence over the observed rate of oxidation. The overall reaction mechanism leading to the final decomposition is in fact rather complex. Once the active oxidising species are generated at the catalyst surface, the subsequent reaction sequence, which leads to the final degradation of the pollutant, can be envisaged to occur several steps.

If the reaction site is at the surface of the photocatalyst, the total process may be broken down into the following five basic steps as in Figure 3.1, any one of which can be rate determining (Pelizzetti and Minero 1993).

1. Transport of reactants to the catalyst

2. Adsorption of the reactants on the catalyst

3. Reaction on the catalyst involving one or more adsorbed reactants

4. Desorption of products from the catalyst

5. Transport of products away from the catalyst

Steps 2,3 and 4 are chemical in nature, and may be regarded as jointly constituting the catalytic reaction, assignment of the slowest step in a

particular case is, as it has been mentioned above, not always self-evident from the observed kinetics. Steps 1 and 5 on the other hand involve no chemical change. Step 1 is the physical process whereby the reactants are brought through the gaseous or liquid phase surrounding the solid catalyst to the active sites on the latter's surface. This is a diffusion process, and the phenomenon is called mass transport or mass transfer. Step 5 is the corresponding process for getting products away from the surface. When either of these is slower than the catalytic rate itself, the rate is determined by the rate of arrival of reactants (or of removal of products), then it can be stated that the rate is diffusion limited or mass-transport limited.

If reaction occurs exclusively (or also) in the bulk solution, the steps are:

1.   Diffusion of photogenerated reactive species from the surface to the bulk solution

2.   Reaction in solution; or, if the reactant to be degraded is adsorbed on the inert surface,

3.   Reaction of the photogenerated reactive species at the surface of the inert support

It is most important in practice to be able to recognise when diffusion limitation is operative, since its occurrence signifies that the catalyst is being used to less than its maximum capacity. There are some occasions when it is preferable that the reaction can be diffusion limited, as when, for example, the isolation of an intermediate product in high yield is desired, but more often it is better to eliminate it to make better use of the catalyst. Diffusion limitation at the external surface of catalyst particles is recognised by the following characteristics.

1. The rate is proportional to the catalyst weight (or to the concentration of the active component) raised to a power less than unity, which in the limit may be zero

2. The rate is increased by improving the movement of the gas or liquid with respect to the catalyst

3. The temperature coefficient is low, and the apparent activation energy may be as low as 10-15 kJ mol^{-1}

Reactions whose rate is governed by a truly chemical step on the other hand show the following features.

1. The rate is accurately proportional to catalyst weight or the concentration of the active component

2. The rate is unaffected by better agitation

3. The apparent activation is usually in excess of 25 kJ mol^{-1}

Reactions where a liquid phase is present are far more likely to become diffusion limited than those where only gaseous reactants participate. This is because diffusion coefficients are much lower in liquids than in gases.

It has been demonstrated that in photocatalytic slurry systems the overall rate is reaction rate limited, whilst in supported catalyst reactors the rate is dependent upon the mass transfer characteristics of the system (Al-Ekabi and Serpone 1988, Matthews 1990, Ollis et al. 1989). Matthews (1988) also stated that no mass-transfer limitation is expected for photocatalysis using slurries of very fine catalyst particles of, e.g., 0.1 wt % Fisher Chemical

or Degussa P25 TiO_2 catalysts since the maximum diffusion distance is very small.

Matthews (1987b) noted that the liquid flow rate, and hence the degree of turbulence, affected the rate of decomposition in his supported catalyst coiled glass-tube reactor. He found that adsorbent coefficient k_1 (equation 3.1)(binding constant) is independent of the flow rate since the author argued that the amount of organic adsorbed on the catalyst was independent of flow rate (Matthews 1989), whereas the k_2 value was found increasing approximately linearly with the flow rate and a high flow rate regime in which the k_2 value is approaching a limiting value, independent of flow rate.

Turchi and Ollis (1988) discussed the mass transfer effects of Matthews (1987b) work and they claimed that the results reported by Matthews were completely or largely dependent on reactant convective diffusion to the tube wall rather than inherent surface reaction kinetics. Matthews (1988) then replied that mass-transport limitations are believed to be responsible for the observed dependence of reaction rate on flow rate in the immobilised system but it seems unlikely that differences in solute reactivity at a constant flow rate can be entirely due to differences in solute diffusion coefficients.

In terms of reactor design, it is clear that enhanced mass transfer processes are important in reactors using immobilised catalysts.

CHAPTER IV

4. Photocatalytic reactor design

If photocatalytic processes for effluent treatment are to be successfully utilised, they must be proven as industrialised processes. Many mechanistic and kinetic studies have been undertaken, but only now photoreactor design has started to receive more attention. Although, the photoreactor design literature to date has been largely concerned with homogeneous systems of quite low optical absorbance, the literature for heterogeneous systems are much more sparse. There has been a great amount of research on homogeneous systems, despite this research efforts poured into their study, the development of commercial photoprocesses remains rather limited. One of the important reasons for such limited development could be because systematic research on photochemical engineering is lagging behind. The amount of research on homogeneous systems has gained more interest when the conversion of solar energy into chemical energy via photochemical routes was found to be more effective. Photocatalytic studies has begun to receive more interest after the success of using photocatalysts in order to achieve the photolysis of water, but there is only little work has been done on the engineering side.

Successful industrial application of photochemical reactions requires detailed investigation of reaction kinetics and reliable design of engineering aspects of the photochemical processes including economics. The modelling

and design of photoreactors are important engineering problems to investigate because the photoreactor is the main part of a photochemical plant.

The studies of homogeneous photoreactor modelling and scale-up were widely done by engineers (Schenck 1987, Yue 1985a,1985b,1988, Rizzuti 1985, Augugliaro 1985, Braun 1988, Rizzuti and Brucato 1988, Braun et al. 1991). These analysis have given detailed knowledge and engineering concept about photochemical reactors, but the modelling of heterogeneous photoreactors however has recently started to receive attention (Yue 1985c,1988, Ollis et al. 1989, Braun et al. 1992). It is therefore that intensive research in especially experimental studies including scale-up and optimisation is needed.

4.1   Factors effecting photoreactor design

The most important factors in photoreactor design compiled by Yue (1985a) are presented below:

- *The phases involved*

> Single phase Gas
>
> > Liquid ·
>
> Multiphase   Gas-liquid
>
> > Gas-solid
> >
> > Liquid-solid (including colloidal suspension)
> >
> > Gas-liquid-solid

Reactions involving only solid and/or liquid phase may be considered either batchwise or continuously in equipment of suitable size.

- Heat exchange

Heat of reaction and the heat produced by the lamp are the important factors to be considered. Efficient means of heat addition or removal must be introduced to keep the reactor temperature within the desired range. For this purpose, the problems of heat transfer within the reactor and means of controlling the reactor temperature should be analysed, hence necessary methods should be developed. Different type of reactors have different way of controlling the heat transfer. Batch and some certain types of reactors have some design features to obtain adequate temperature, such as stirred tank type reactors are suitable to provide large heat exchange surface. Moving beds and fluidised beds have also good design advantages for high rates of heat transfer.

- Mixing and flow characteristics

For homogeneous photoreactions, the reactants' contact with photons and for heterogeneous systems, contact between reactants, photons and catalysts are the important factors that depend on the mixing and flow characteristics within the reactor. The contact efficiency for photoreactors in which solids are present needs to be assessed and can be facilitated in different ways. This is especially important when multiphase photoreactors are used and should be considered with the type of the reactor geometry designed. For liquid-solid photoreactors, agitation of the reaction mixture can be provided by means of a stirrer. The rate-limiting step of the process can

also be overcome by mixing and by changing flow characteristics of the reactor. Rotation of the reactor can easily supply the mixing and desired flow characteristics while causing continues movement of catalyst. Fluidised bed photoreactors are ideally suited for enhancing contact efficiency, but for fixed bed reactor the catalyst is limited to a thin layer and a large reaction surface is required.

- Material of construction

Type of material of photoreactor construction heavily depends on temperature, pressure, corrosion problems due to reactants, products and the catalytic properties of the reactor material. The most important choice to be made is to consider the requirement of light transmission. This is the main restricting factor and means that choice is usually limited to different types of glass. Optical glass, Pyrex glass, Vycor glass and quartz are commercially available glass types. Among them quartz gives the best transmission but at a much higher cost, however at short wavelengths such as under 300 nm region, quartz is the only suitable material.

- The light source

The performance of a photoreactor is always affected by the irradiation source. Two principal factors determine the selection of a light source: its power and its spectral distribution of the emitted light. The choice of lamp can be made according to the reaction energy requirement with the specification of lamps. The spectral distribution should be compatible with the absorption and action spectra of the reactant. The type of lamps usually determine the range of wavelengths of the irradiation in the electromagnetic

spectrum. Therefore light source choice will depend on the reaction type itself. In case of heterogeneous photocatalysis, when TiO_2 is used as a photocatalyst, spectral absorption characteristics of TiO_2 allow its excitation in the UV-C, UV-B and UV-A domain (Braun et al. 1992). Hence, the use of preferentially doped medium pressure mercury arcs of high electrical power is of considerable interest.

- Geometrical configuration

Although the conversion for a given reactor volume is independent of geometry in conventional homogeneous reactors, if the effects of flow characteristics are neglected, for all type of photoreactors the light source and its relation with reactor geometry are the most important design factor to be considered. For the maximum use of irradiation source according to reaction medium, the geometrical configuration of a photoreactor has its importance. The three most commonly used geometries can be classified as cylindrical (tubular), parallel-plate and annular.

4.2   Photoreactor types

4.2.1   Conventional types

Photoreactors, like the usual chemical reactors, may be classified in different types depending on the mode of operation (batch, semibatch or continuous), on the number and type of the phases involved, on the mixing characteristics, etc. But undoubtedly the most important classification for photoreactors is based on the relationship between system geometry and the

light source. Not only determining reaction yields, but also understanding reactor operation factors, the geometry plays the most important role. In making the decision of the possible geometry, the factor to be considered is the power, shape and cooling requirements of available commercial lamps useful for the wavelength required by the reaction.

Batch reactors are suitable for very slow reactions and continuous ones are likely used for rapid reactions. The rate of reaction is a function of kinetics, catalyst, temperature, pressure and condition of the feed. There is therefore some degree of flexibility in the choice of reactor type and careful consideration is needed when design is concern. Under technically feasible conditions, the final decision is usually an economic one.

Immersion well photoreactors

This is one of the first photoreactor types designed to achieve a photochemical reaction on a preparative scale and remains useful for some very specific industrial applications and for laboratory experimentation. It comes from the basic idea of immersing a light source in a reaction mixture which is contained in a conventional reactor, perhaps a mixed one. Although it has the basic advantage of simplicity and high photonic efficiency, it presents serious disadvantages. Radiation only reaches to the absorbing medium through relatively small transparent surfaces; even in a well-mixed reactor, a photochemical reaction will only take place within the volume where light is absorbed. Scale-up is an important problem, even on a preparative size, giving the promising results in smaller, laboratory scale. Another major disadvantage of such a reactor is the formation of deposits on

the lamp external surface (filming) which in turn progressively lowers the amount of radiation reaching the absorbing medium.

Annular photoreactors

In this type of photoreactor, the light source is placed at the axis of a reactor composed of two coaxial cylindrical tubes, Figure 4.1.
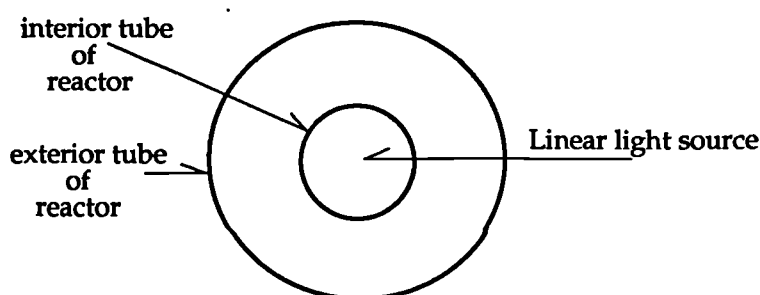
Figure 4.1 Cross-section of an ideal annular photoreactor

This simple geometry allows modelling of the radiation field, and practically all photons emitted by the lamp reach the reacting medium. In the batch type the reaction volume is restricted with the annular volume, whereas in continuous flow the reaction mixture is pumped into the annular volume contained between two cylindrical walls surrounding the lamp and the reagents pass through the irradiated region more than once depending on the reaction completion time. Contrary to an immersion annular reactor which operates in batch mode, a continuous flow type holds only a small part of the total volume of the reaction mixture to be irradiated. Thus, the reactor geometry can be modified in a more flexible way, the size of the reactor and the concentration of the reaction mixture can be reduced. It is also possible to adjust the flow rate of the reaction mixture, an increase in this rate increases the turbulence in the reactor which limits the formation of deposits on the

37

directly irradiated reactor wall. However, a sufficient irradiation time is still needed even with a high throughput.

Several different models derived from continuous flow annular photoreactors are industrially utilised especially in the field of water sterilisation and these models are compiled in detailed manner with different modifications (Schenck 1987, Braun et al. 1991).

Elliptical photoreactor

This kind of photoreactor consists of a cylinder of elliptical cross-section whose internal surface is covered by a reflecting material (Rizzuti and Brucato 1988, Braun et al. 1991). The light source and the tubular reactor are vertically placed at the two foci of an elliptical enclosure, hence it is commonly used method to separate the lamp from reactor. Because of this geometry, most of the photons emitted by the lamp reach the reacting medium radially (Figure 4.2).
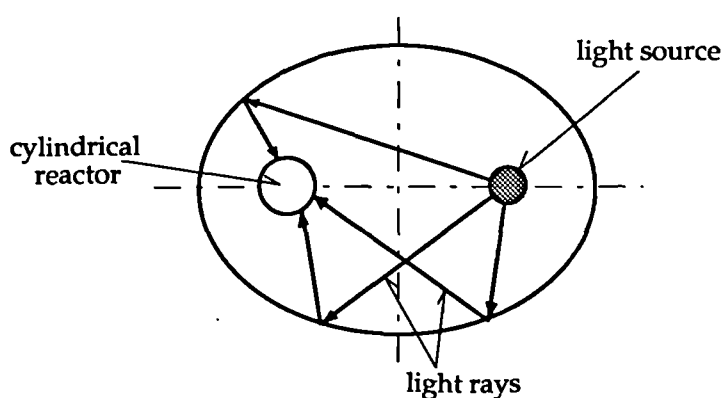
Figure 4.2 Cross-section of an elliptical reflector

Like the annular reactor, the flow path can be arranged in a multipass way. In an apparatus with an elliptical reflector, formation of deposits on the reactor

walls is difficult to avoid, but the physical separation of the lamp and reactor allows an easier cleaning and servicing of the parts.

Parallel plate photoreactor

This reactor type is generally of cylindrical form, and is irradiated by a beam of rays parallel to its axis. The diameter of the beam is of about the same dimension as that of the reactor. External cooling can be used. The combination of the light emitted from the source in the direction of the reactor and the light returned by the reflector in the same direction determines the total radiant power of the beam, which thus depends on the efficiency of the reflector (Figure 4.3) (Braun et al. 1991, Braun 1988).
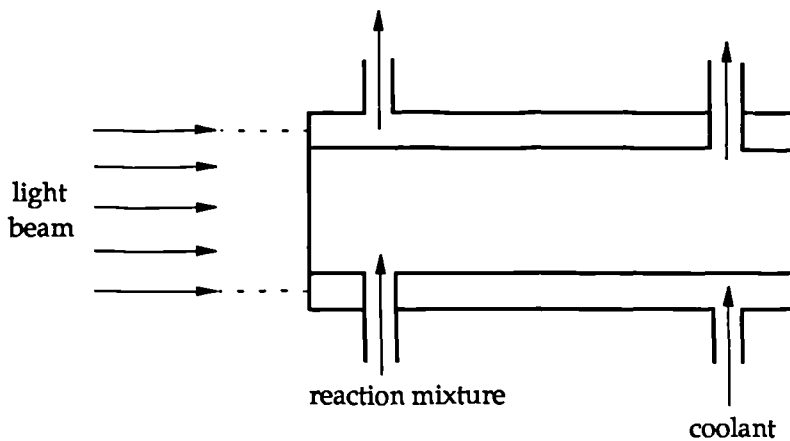
Figure 4.3 Diagram of a parallel plate, cylindrical photochemical reactor

Elliptical mirrors are more efficient than spherical mirrors, but introduce inhomogeneity in the cross-section of the light beam. It is possible to estimate the importance of dispersion of the light in a liquid mixture of reactants by measuring the irradiance along the axis of the reactor.

Multilamp photoreactor

It is possible to create a strongly irradiated region along the axis of a cylindrical photochemical reactor, by surrounding the reactor with many long arc lamps, each of which has a parabolic reflector. This photoreactor design is especially useful when low pressure or fluorescent tube lamps are used, which are usually characterised by small power. This arrangement allows the installation of many of them, thus enabling higher radiant fluxes (Rizzuti and Brucato 1988, Braun et al. 1991).

Experiments have shown that this type of reactor is very efficient for the photolysis of reaction mixtures with low absorbencies, for example sterilisation of drinking water by ultraviolet light. Cylindrical photochemical reactors placed in coaxial radiation fields are often used for carrying out photochlorination reactions, but their most important application remains in the area of water sterilisation (Braun et al. 1991).

4.2.2   Thin liquid film photoreactors

It is clear from the above sections that conventional reactors have problems with light penetrating or being absorbed by the reactant/catalyst mixture or by the wall for this reason thin liquid film/large surface area systems have been considered. Different types of liquid film photoreactors have been constructed. The liquid film covers either the wall of a sloping plane weir, the wall of a vertical, static cylindrical reactor (falling film reactor), or the wall of a horizontal or vertical rotating reactor. The first model proposed was an annular reactor in which a falling film covered the

exterior wall of a transparent tube containing the lamp, but this type of design was found to be inefficient because deposits form very quickly on the wall blocking further irradiation. However, slightly different design of a falling film covering the inside wall of the outer tube of an annular reactor is the basis for the construction of several models of liquid film reactors (Figure 4.4) (Braun et al. 1991). Ashton et al. (1988) also proposed a similar type of photoreactor for their liquid disinfection studies.
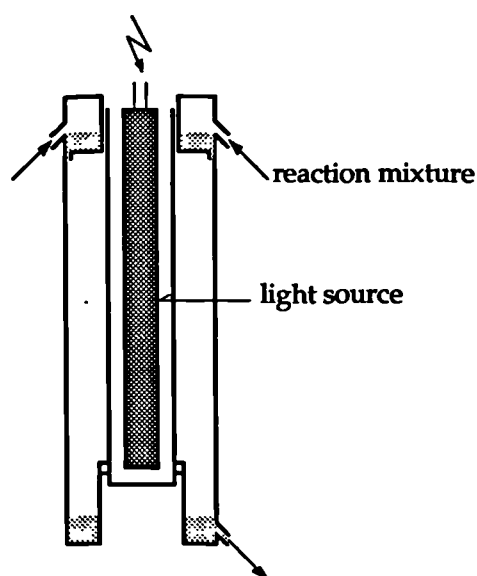
Figure 4.4 Diagram of an annular falling film reactor

Figure 4.5 shows a rotating film reactor in which the liquid film covers the internal wall of the exterior casing of a rotating cylinder. The reactor is a drum rotating horizontally around its axis with the light source placed along this axis (Braun et al. 1991).
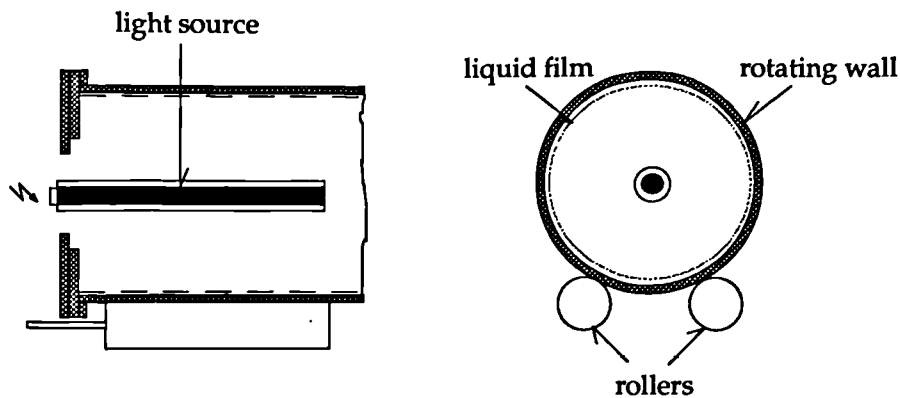
Figure 4.5 Rotating liquid film photoreactor (horizontal)

As a general rule, photoreactors with rotating parts are small, because many mechanical problems appear when reactor size is increased to achieve large-scale production.

Two laboratory model annular falling film photoreactors were also compiled by the same authors and introduced as the best model among the same category. The first model spreads the liquid film on the internal wall of the inner tube of a vertical annular reactor. Here the lamp is suspended from the top of the reactor. The inner reactor tube is open at its upper end: the reaction mixture is pumped up the annular volume between the two tubes constituting the body of the reactor, then overflows the inner tube, forming a falling liquid film on the internal wall which is only at a small distance from the lamp. In this model, the light is absorbed by both the falling film and the rising mixture contained in the annular volume. However, the thickness of the latter in the commercial laboratory reactors is small, and in general, insufficient to provide total absorption. Furthermore, the mixture being introduced near the upper end of the inner tube overflows almost immediately; consequently, much of the mixture contained in the annular volume is only slowly renewed and its radiation time is poorly controlled.

These disadvantages are removed if the reaction mixture is introduced at the bottom of a reactor with a large exterior diameter (Braun 1988). This diameter must be sufficiently large to allow efficient absorption of the light (total absorption), as well as the installation of gas inlet thermostat. This reactor model is equally well suited for either pilot scale experiments or for production scale.

4.3   Heterogeneous photocatalytic reactors

The kinetic modelling in heterogeneous catalysis, in order to get at the true mechanism of the reaction on a surface, is a much difficult problem. The kinetic model is indeed more useful for less ambitious reasons such as to be consistent with experimental rate data, to allow reactor design, to suggest new experiments based on predictions of the model, to contribute qualitative insight into a possible reaction path. As practical suggestion in kinetic model building, if the objective is to find a rate equation consistent with kinetic measurements and also useful for designing a reactor, then the best model is the simplest one that works.

For heterogeneous systems at least two phases are involved, such as photocatalytic water or effluent treatment there are at least two phases, i.e. liquid and solid, present in water. With certain reactor designs, it may be desirable to introduce a gaseous phase into the reactor. For example, oxygen or air may be fed into a reactor for the photocatalytic oxidation of organic pollutants in an aqueous effluent. In this case photocatalytic reactor design, modelling and scale-up are to be concerned as liquid-solid or gas-liquid-solid systems, and the position of solid phase can be considered as the solid phase

43

is stationary within the reactor and the solid phase is dispersed (slurry) within the reactor. Each one of these cases has advantages and disadvantages and are suited for different modes of operation and application.

The design of multiphasic heterogeneous photoreactors involves the selection of the photon source, reactor geometry, reactor configuration, special arrangement of lamp-reactor combination, type of photocatalyst, the size, distribution and concentration of catalyst between fluid and catalyst particles and the mode of operation. The problem of scale-up of these multiphasic photoreactors is considerably more complex than that of conventional chemical reactors or homogeneous photoreactors.

Because the early studies in heterogeneous photocatalysis were mainly based on understanding the reaction mechanisms between catalyst particle, light photons and solution and therefore reaction kinetics, the photoreactors used in this field were mostly small size annular type batch reactors (Pruden and Ollis 1983, Turchi and Ollis 1989, Sclafani et al. 1990,1991, D'Oliveira et al. 1990) and even sometimes small size batch vessel types (Tunesi and Anderson 1987, Tseng and Huang 1991), or such as quartz tubes (Blatt et al. 1989, Pelizzetti et al. 1989, Minero et al. 1992). It is quite common to find that many of the slurry reactors are poorly designed since only a small proportion of the slurry volume is active at any one time. For instance, Harvey et al. (1983) showed that only 2% of TiO_2 catalyst was exposed to UV irradiation in the reactor configuration used in their experimental study. This was due to the inability of the light to penetrate into the slurry by more than 4% of the total available path-length.

The immobilised catalyst type reactors were also in small size glass tubes which catalyst was coated inside and coiled around the lamp source (Matthews 1987b, 1987c, 1988b, 1989, Al-Ekabi and Serpone 1988, Al-Ekabi et al. 1989). Catalyst coated glass beads were also used in small vessels (Serpone et al. 1986, Minero et al. 1992) and similarly catalyst coated sand was used in borosilicate glass dishes (14.5cm i.d. 7cm wall height) (Matthews 1991).

Ollis and Turchi (1990) studied reaction kinetics and reactor design for heterogeneous photocatalysis and proposed elementary mathematical models for different reactor geometries with different liquid velocity profiles.

Ahmed and Ollis (1984) showed that it was possible to achieve complete mineralisation of trichloroethylene and trichloromethane (initial concentration was 50ppm in both cases) in a parabolic trough reactor using solar illumination within a period of 3 to 4 hours. However only a small volume of liquid was treated (1.6 litres).

Pacheco and Tyner (1990) also designed line focusing parabolic troughs having aluminised reflective surfaces that reflect 69% of the incident solar ultraviolet energy (300-400nm). The troughs have an aperture width of 2.1m and concentrate the solar energy about 50 times. The length of the troughs is 218m for an aperture area of 465m². The reactor is a 3.8cm inside diameter by 218m borosilicate glass pipe mounted at the focus of the trough.

The same authors proposed a second system which uses large tracking heliostats, 37m² each, to reflect and concentrate solar radiation onto a falling film reactor mounted in a tower 37m above ground. The falling film reactor is a vertical aluminium panel 3.5m high by 1.0m wide, on which the

contaminated water flows as a thin film (~3mm thick) down the face of the panel and 380 liters of tap water with salicylic acid was circulated through the reactor. The residence time was approximately 2.9 seconds per pass. A cooler was also used in this system. The heliostats have silvered mirrors, which reflect about 66% of the solar ultraviolet.

A novel thin-film-fixed-bed reactor was proposed by Bockelmann et al. (1992) for solar radiation. The most important part of the thin-film-fixed-bed reactor is a sloping plate (width 0.6m, height 1.2m) covered with photocatalyst (TiO_2-Degussa P25) and rinsed with the polluted water in a very thin film (~100μm).

CHAPTER V

5. Estimation of the average intensity in a UV reactor

The intensity is the rate, or flux, of delivery of photons to the target and it is one of the important elements of photocatalysis. It has already been pointed out that the degree of intensity effects the photocatalytic degradation (Ollis et al. 1991 and section 2.2.4). Therefore, it becomes important to be able to quantify the intensity in a given system. The intensity in a reactor is a function of the UV source output, the physical arrangement of the source relative to the effluent treatment (the arrangement of the lamp or lamps and their placement in or out of the liquid), and absorbing media which will attenuate the source output before it can be utilised for photocatalytic purposes.

Determining the intensity at any point in complex lamp reactors is not straightforward. At present, there is no commercially available detector which can measure the true intensity in such a system. The problem lies in the fact that the detectors are planar receptors; only energy striking a flat will be measured. Such detectors will intercept fractions of light striking the surface at an angle. Only light which is normal to the surface, i.e., collimated light, however, will be wholly measured. "Cosine-corrected" detectors attempt to compensate for this by adjusting for the angular light. These still measure, however, only the planar intensity. Where light is not collimated, as is the case with a multi-lamp UV reactor, the flux of energy is three-

dimensional. When the target of the radiation is considered, in slurry systems the hydrodynamic of the mixture is important, thus in rapid turbulent motion, all particles can be expected to receive equal exposure.

Several approaches have been proposed to estimate light intensity; broadly the split into *indirect* techniques such as photocell, chemical actinometry, biological assay measurement and *direct* calculation. Direct calculation of intensity can be accomplished by the point source summation method as detailed below.

5.1   Calculation of the average intensity by the point source summation method

The calculation approach is suggested as the method of choice because of versatility and flexible application to varying configurations. The technique used to calculate intensity is the point source summation method. This technique was evaluated by Jacob and Dranoff (1970) for light intensity profiles in a perfectly mixed photoreactor. It presumes that the lamp is a finite series of point sources that emit energy radially in all directions. The intensity at a given point in a reactor would be the sum of intensities from each of these point sources.

Intensity Attenuation.   UV intensity will attenuate as the distance from the source increases. This occurs by two basic mechanisms: dissipation and absorption. Dissipation is simply the dilution of the energy as it moves away from the source. The area upon which the energy is being projected is

increasing. This dissipation can be calculated by surrounding the point source by a sphere of radius R:

$$I = \frac{S}{4\pi R^2}$$ (5.1)

where I is the intensity at a distance R in μWatts/cm^2, R is the distance in centimetres, S is power available from the UV source in μWatts. Thus, dissipation is seen to attenuate the intensity as the inverse of the radius squared.

The second attenuation mechanism relates to the absorptive properties of the medium through which the energy is transmitted. This is best described by Beer's Law:

$$I = I_o \exp[-\alpha R]$$ (5.2)

where I_0 is the intensity at a given surface on the source (μWatts/cm^2), α is the absorbance coefficient of the medium through which the energy is passing (cm^{-1}), and R is the distance at which I is measured relative to the point represented by I_0. The absorbance coefficient reflects the absorbance at the specific wavelength being emitted; in case of the low pressure mercury arc lamps, the wavelength is 253.7nm.

Combining Equations (5.1) and (5.2) yields an expression which describes the intensity at a given distance from a single point source of energy:

$$I = \left[\frac{S}{\left(4\pi R^2\right)} \right] \exp(-\alpha R) \qquad (5.3)$$

This equation serves as the basis for the point source summation calculation technique. A basic assumption is that a receiver (i.e. a catalyst particle) passing through the reactor or supported on a surface is infinitely small and is spherical; by this it can then be presumed that the energy emitted from any point source element of the lamp will strike the receiver normal to its surface.

The model analysis also neglects the phenomena of reflection, refraction, diffusion, and diffraction of light and assumes that the absorptive properties of the liquid are independent of the light intensity. The intensity at a receiver is then the summation of the intensities from each of the point source elements of a lamp, (or lamps in a multi-lamp system). Figure 5.1 is a schematic representation of this calculation.
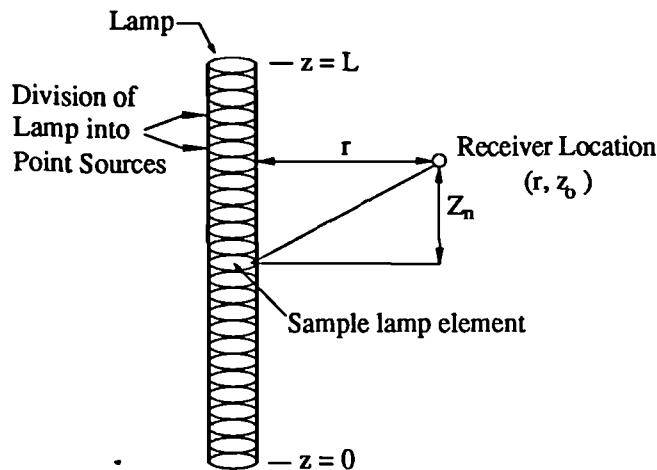
Figure 5.1   Lamp geometry for point source summation approximation of intensity

As shown, the intensity at the receiver location (r,z₀) is the summation of the intensities from each of the lamp elements:

$$I(r,z_0) = \sum_{n=1}^{n=N} \frac{S/N}{4\pi(r^2 + z_n^2)} \exp\left[-\alpha(r^2 + z_n^2)^{1/2}\right] \qquad (5.4)$$

where N is the number of point source elements in the lamp. The value of z_n is:

$$z_n = z_0 - L(n/N) \qquad (5.5)$$

The model takes into account the geometry of a system, the characteristics of the lamps and enclosures (i.e. quartz or Teflon), and the given UV absorption properties of the liquid. Since the low pressure mercury arc lamps are excellent absorbers of light at the 253.7nm wavelength, the model calculations presume that any energy at this wavelength entering a lamp element from a neighbouring element will be completely absorbed.

Computationally, the point source summation method is not convenient and gets complicated when different lamp configurations are used, therefore it is best handled by computer with the appropriate software. However, developing reactor design and the lamp configurations in combination make the model more complicated and often indirect measurement techniques are employed as detailed in the following sections.

5.2 Indirect measurement methods

5.2.1 Bioassay measurement procedure

The bioassay procedure has been applied in a limited fashion for a number of design specifications, primarily as a technique for quantifying the dose delivered by a specific piece of UV equipment (Qualls and Johnson 1983) and more relevant for disinfection purposes. It can also be used to implicitly derive the intensity within a system.

The steady-state bioassay method, generally using *Basillus subtilis* spores, has been used as a specification in demonstrating the dose capacity of a given system. The dose is estimated as a function of flow rate through a scaleable pilot module. A minimum dose is then cited for the equipment specification.

The bioassay procedure, although a valid and unique experimental design, has several disadvantages which is the difficulty and workmanship of its use as routine testing and evaluation procedure. It is not standardised, and results can vary from lab to lab, both in the calibration and system assays. It can be costly and also wholly empirical and limited in its use for extrapolation to alternative system configurations. On the positive side, however, the bioassay can offer several advantages. It is an independent verification of system design, and implicitly of design procedures.

5.2.2 Photometric measurement method

Masschelein et al. (1991) have proposed a photometric measurement method for the evaluation of UV-intensity at 254nm. The model is developed which takes into account the absorption of light according to Beer's law as well as the relative dimensions of both lamp and reactors.

The procedure used for photometric measurement is represented schematically in Figure 5.2, and requires a calibrated detector. In this work a broad-angle detector, the so called "cosinusoïdal detector" was reported to be found better than a "cylindrical detector".
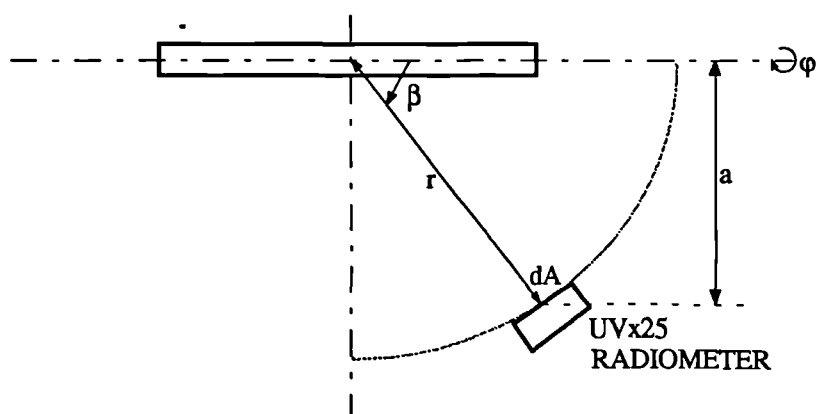
Figure 5.2 Schematic diagram for direct measurement of UV-intensity

The cell used in this work is the Radiometer UV-X25, calibrated for the 254nm wavelength.

In Figure 5.2 the detector is rotated along an arc of 0.8m radius from a reference point, usually at the centre of the lamp, and measurements are

recorded at different values of β. The mathematical treatment produces a simple expression of the power, as a function of the geometry of the system.

$$P = 2 \int_{90^\circ}^{0} \int_{0}^{2\pi} I(\beta)\, d\varphi\, dA(\beta) \qquad (5.6)$$

or $\qquad \int_{0}^{2\pi} I_A(\beta)\, d\varphi = 2\pi\, a(\beta)\, I(\beta) \qquad (5.7)$

and $d_A\beta = rd\beta$

where:

P = total UV power (Watt)

I = intensity (in Watt/cm^2) at a point on the rotational space with a radius, r, around the centre of the lamp [and is a function of β]

A = position on the arc of rotation with radius r

β = apex angle between the position of the detector versus the axis of the emitting lamp

φ = rotational angle of the light source versus the axis of the emitting lamp

r = distance between the photocell and the lamp centre

a = orthogonal distance between the photocell and the lamp

Therefore:

$$P = 2 \int_{90}^{0} 2\pi A\, a(\beta)\, I(\beta)\, rd(\beta) \qquad (5.8)$$

wherein: $a(\beta) = r\, \sin\beta$

$$\frac{P}{2} = \frac{1}{2}\frac{dP}{d\beta} = 4.022\, {}_x I\, {}_x \sin\beta \qquad (5.9)$$

In the standard arrangement, the cell is placed either facing the very centre of the tubular lamp or facing the very centre of one side of the U-shaped lamp, while the other side is masked. The cell is rotated either to the right or to the left. The experiments are eventually repeated by rotating the tubular lamp. A schematic representation of this measurement is shown in Figure 5.3.
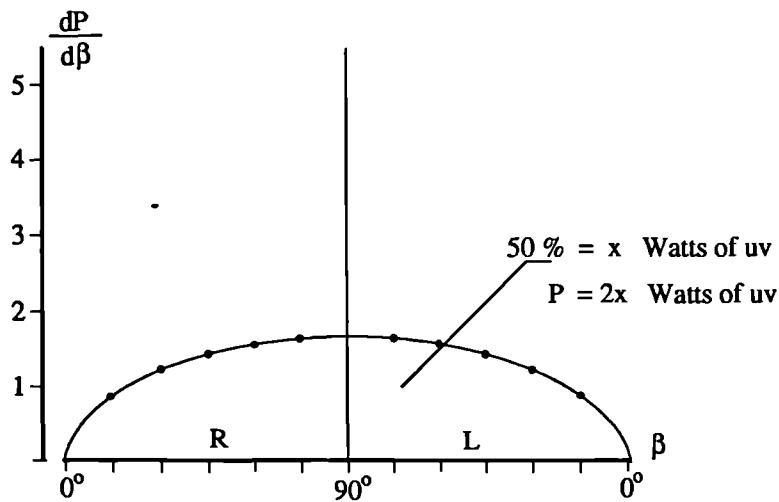
Figure 5.3 Standard measurements of U-shaped tube

The UV power of the lamp (P) is obtained by numerical integration of the surface determined by a curve of $dP/d\beta$ as a function of β (Figure 5.3).

Masschelein et al. (1991) concluded that knowledge of the UV-intensity emitted by lamps applied in experimental work or operational use of UV, in disinfection or advanced oxidation of water, often remains unprecise. Therefore, the data obtained, even when precise description of reactor dimensions and nominal lamp characteristics are given, remain essentially empirical and are based on a trial and error procedure.

5.2.3   Determination of UV light intensities by chemical actinometers

The principle of this is that chemicals are activated by UV into a form which can be analysed. The chemicals must not be influenced by the length of exposure hence uranyl oxalate and potassium ferrioxalate are used. The determination of absorbed light intensities and quantum yields in photochemical systems through photometric measurements generally requires that corrections be made for reflection and scattering of light at surfaces. Photochemists have determined quantum yields of products of many photochemical systems by using photometric methods. Several systems show a product quantum yield which is rather insensitive to changes in temperature, concentration of reactant, light intensity, and wavelength of the absorbed light over quite a wide range of the variables, and the analysis for the product is simple and precise. These systems provide ideal secondary standards which are most useful for rapid and highly accurate light-intensity determinations. A small but important advantage is gained by choosing a liquid-phase actinometer for photochemical studies involving liquids and a gas-phase actinometer for studies involving gases. Not only is the introduction of the actinometer to the photolysis cell usually easier for this choice, but also corrections are eliminated for differences between the fraction of incident light reflected from the front window of the photolysis cell for experiments using the actinometer and the fraction reflected in the actual photochemical study.

Photochemists -who have used both the photometric methods and the chemical actinometer systems to determine UV light intensities generally agree today that results obtained with a well chosen, sensitive chemical actinometer are not only much simpler to determine but also are often more

reproducible and more reliable than those obtained with the photometric systems.

The use of the actinometer for the measurement of the light intensity just inside the front cell window (I_o^i) (Eq. 5.10) can be determined in relative simplicity (Calvert and Pitts 1966). For instance, to find the intensity of a monochromatic beam within a simple reaction cell, a suitable reactant A is chosen which absorbs light of the wavelength of interest and for which the quantum yield Φ_B of some product B is known accurately for specific experimental conditions. Reactant A can be placed within the photolysis cell and with the exact optical train, which is to be used in the photochemical study. The temperature and pressure or concentration of reactant A is adjusted to the required range, and an exposure of A to the light beam is made for t second.

The fraction of the incident light absorbed by A, $1-(I/I_0)=1-10^{-\epsilon[A]l}$ is either measured experimentally or calculated from known values of ϵ, concentration of A, and path length l. The number of molecules of product B formed, n_B, in the time t is determined by analysis. From these data, the intensity of the light beam incident just within the photolysis cell front window, I_o^i, can be calculated from Eq. 5.10 (When the fraction of incident light which is absorbed small, complications due to reflected light arise).

$$I_o^i = \frac{n_B}{\Phi_B \, t \left(1 - 10^{-\epsilon[A]l}\right)} \quad \text{quanta / s} \qquad (5.10)$$

For more complicated geometries Potassium-Ferrioxalate liquid phase chemical actinometry system is often used and this is detailed below.

5.2.3.1 Liquid-phase chemical actinometry

As indicated in section 5.2.3, there are two main chemical reactants which can be used, Potassium-ferrioxalate or Uranyl-oxalate. The most detailed and described solution-phase chemical actinometer for photochemical research today is the potassium ferrioxalate system developed by Hatchard and Parker (1956). It is very sensitive over a wide range of wavelengths, and it is simple to use. The very high absorption coefficient of the complex makes possible useful exposures about one hundredth of the duration required for the uranyl oxalate actinometer procedures. When sulphuric acid solutions of $K_3Fe(C_2O_4)_3$ are irradiated in the range from 250 to 577nm, simultaneous reduction of iron to the ferrous state and oxidation of oxalate ion occur. The quantum yields of Fe^{2+} formation have been accurately determined, and light absorption by the reactant is good for the range 480-253nm. The product ferrous ion and its oxalate complex in these solutions do not absorb the incident radiation measurably during the photolysis, but after the exposure the ferrous ion can be made to be highly absorbing and thus easily analysable by formation of the red-coloured 1,10-phenanthroline-Fe^{2+} complex.

The quantum yields increase only slowly and in a regular fashion with decrease in wavelength. The very small dependence of these yields on reactant and product concentrations, intensity of the incident light, and temperature over a considerable range adds to the utility of this actinometer. This technique was the one adopted in this work.

5.3 The determination of quantum yields

.

To determine the quantum yield (Φ_B) of a given product of a photo-chemical reaction, the number of product molecules n_B of the given type B must be calculated for a given length of exposure t. The calculation requires the determination of the light intensity incident on the reactant I_0^i and the fraction of this light which is absorbed by the reactant (I_a/I_0^i). From these data the respective quantum yields of product B (Φ_B) can be calculated using Eq. 5.11 (Calvert and Pitts 1966, Braun et al. 1991):

$$\Phi_B = \frac{n_B}{I_o^i\left(I_a/I_o^i\right)t} = \frac{n_B}{I_a t} \tag{5.11}$$

.

In photochemical studies, the same experimental measurements are also applied to calculate the fluorescence quantum yield (φ_f). For this, the number of quanta absorbed from a directed beam of monochromatic light is compared with the number of quanta of polychromatic fluorescent light, whose distribution in space may be geometrically complicated. The model is also similar and the number of quanta n_f emitted by the reactant must be determined for the length of exposure t. Hence, fluorescence quantum yields (φ_f) can be calculated from Eq. 5.12:

$$\varphi_f = \frac{n_f}{I_o^i\left(I_a/I_o^i\right)t} = \frac{n_f}{I_a t} \tag{5.12}$$

.

Since the UV lamps mainly emit monochromatic light beams and the number of product molecules n_B of the given type B is to be determined, the term of the quantum yield (Φ_B) is used for model calculations.

Although the quantum yield determination is always basically that outlined, there are different modifications of the main model used for product quantum yield determinations based on the measurement system; such as chemical actinometer or photometric measurement technique and the design of reactor and the lamp type used.

CHAPTER VI

6. Flow of liquids in thin layers

The use of thin films to enhance mass transfer is a well known chemical engineering unit operation and reactors using this phenomena are used in this work. It is therefore important to fully understand the hydrodynamics.

6.1 The hydrodynamics of falling liquid films

The falling film reactor (FFR) is particularly designed to increase the effective photon utilisation for large scale use. Slurry reactors have problems especially in the trade-off between increased catalyst surface and decreased photon distribution when increasing catalyst particle concentrations. Another important design aspect of creating a thin film is to provide high mass transfer in order to promote:

    a) Improved reactant/catalyst interaction or absorption

    b) Improved oxygen take up at the gas/liquid interface

6.1.1 Shell momentum balance for a falling film

Liquid films, falling over an inclined or vertical surface under the influence of gravity have been used to study various phenomena in mass transfer (Bird et al. 1960, Sherwood et al. 1975); coatings on surfaces, wetted

wall towers, evaporation and gas absorption experiments and so on. Liquid flow down a vertical plate is essentially the same as for liquid flow down either the inside or outside surface of a vertical tube, providing the tube radius is large compared with the thickness of the flowing liquid film. Here, an approach similar to that used for laminar flow inside a pipe for the case of flow of a liquid as a thin film in laminar flow down a vertical surface is used. The viscosity and density of the liquid are considered to be constant.

The control volume for the falling film is shown in Figure 6.1a, where the shell of liquid considered is Δx thick and has a length of L in the vertical z direction. This region is sufficiently far from the entrance and exit regions so that the flow is not affected by these regions. This means the velocity $V_z(x)$ does not depend on position z.
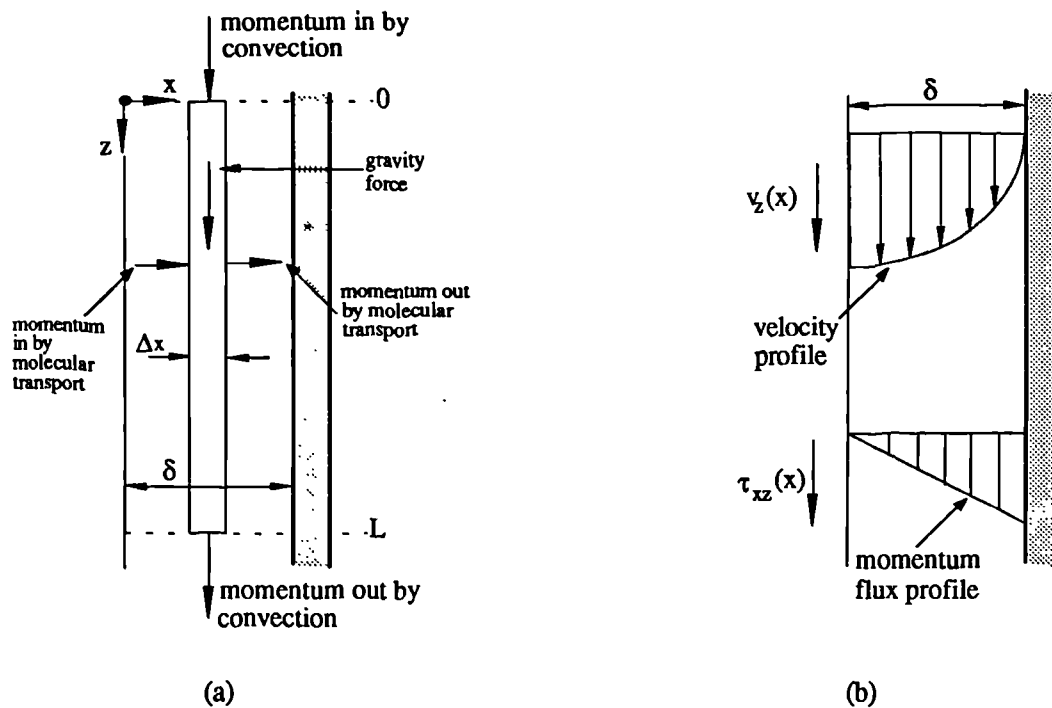
Figure 6.1 Vertical laminar flow of a liquid film : (a) shell momentum balance for a control volume Δx thick, (b) velocity and momentum flux profiles

To start, a momentum balance is set up in the z-direction over a system Δx thick, bounded in the z-direction by the planes $z=0$ and $z=L$, and extending a distance W in the y-direction. The various components of the momentum balance are then,

rate of z-momentum
in across surface at x

$$(LW)(\tau_{xz})\big|_x \qquad (6.1)$$

rate of z-momentum
out across surface at x+Δx

$$(LW)(\tau_{xz})\big|_{x+\Delta x} \qquad (6.2)$$

rate of z-momentum
in across surface at z=0

$$(W\Delta x v_z)(\rho v_z)\big|_{z=0} \qquad (6.3)$$

rate of z-momentum
out across surface at z=L

$$(W\Delta x v_z)(\rho v_z)\big|_{z=L} \qquad (6.4)$$

gravity force
acting on liquid

$$(LW\Delta x)(\rho g) \qquad (6.5)$$

First, it is considered the momentum flux due to molecular transport. The rate of momentum out-rate of momentum in is the momentum flux at point x+Δx minus that at x times the area LW.

$$\text{net efflux} = LW(\tau_{xz})\big|_{x+\Delta x} - LW(\tau_{xz})\big|_x \qquad (6.6)$$

The net convective momentum flux is the rate of momentum entering the area $\Delta x W$ at $z = L$ minus that leaving at $z = 0$. This net efflux is equal to v_x at $z = L$ for each value of x.

$$\text{net efflux} \;=\; \Delta x W v_z (\rho v_z)\big|_{z=L} - \Delta x W v_z (\rho v_z)\big|_{z=0} = 0 \qquad (6.7)$$

The gravity force acting on the fluid is

$$\text{gravity force} \;=\; \Delta x W L \,(\rho g) \qquad (6.8)$$

Then using overall momentum balance:

$$\begin{bmatrix} \text{sum of forces acting} \\ \text{on control volume} \end{bmatrix} = \begin{bmatrix} \text{rate of momentum} \\ \text{out of control volume} \end{bmatrix} - \begin{bmatrix} \text{rate of momentum} \\ \text{into control volume} \end{bmatrix}$$
$$+ \begin{bmatrix} \text{rate of accumulation of momentum} \\ \text{in control volume} \end{bmatrix}$$

for the conservation of momentum at steady state,

$$\Delta x W L \,(\rho g) = L W (\tau_{xz})\big|_{x+\Delta x} - L W (\tau_{xz})\big|_{x} + 0 \qquad (6.9)$$

Rearranging Eq.(6.9) and letting $\Delta x \rightarrow 0$,

$$\frac{\tau_{xz}\big|_{x+\Delta x} - \tau_{xz}\big|_{x}}{\Delta x} = \rho g \qquad (6.10)$$

$$\frac{d}{dx}\tau_{xz} = \rho g \qquad (6.11)$$

Integrating using the boundary conditions at $x=0$, $\tau_{xz}=0$ at the free liquid surface and at $x=x$, $\tau_{xz}=\tau_{xz}$,

$$\tau_{xz} = \rho g x \qquad (6.12)$$

This means the momentum-flux profile is linear as shown in Figure 6.1b and the maximum value is at the wall. For a Newtonian fluid using Newton's law of viscosity,

$$\tau_{xz} = -\mu \frac{dv_z}{dx} \qquad (6.13)$$

Combining Eqs.(6.12) and (6.13) we obtain the following differential equation for the velocity:

$$\frac{dv_z}{dx} = -\left(\frac{\rho g}{\mu}\right) x \qquad (6.14)$$

Separating variables and integrating,

$$v_z = -\left(\frac{\rho g}{2\mu}\right) x^2 + C_1 \qquad (6.15)$$

Using the boundary condition that $v_z=0$ at $x=\delta$, $C_1 = (\rho g/2\mu)\delta^2$. Hence, the velocity distribution equation becomes

$$v_z = \frac{\rho g \delta^2}{2\mu}\left[1 - \left(\frac{x}{\delta}\right)^2\right] \qquad (6.16)$$

This means the velocity profile is parabolic as shown in Figure 6.1b. The maximum velocity occurs at $x = 0$ in Eq.(6.16) and is

$$v_{z_{max}} = \frac{\rho g \delta^2}{2\mu} \tag{6.17}$$

The average velocity over a cross section of the film can be found by the following calculation:

$$v_{z_{av}} = \frac{1}{A}\iint\limits_A v_z dA = \frac{\int\limits_0^W\int\limits_0^\delta v_z dx dy}{\int\limits_0^W\int\limits_0^\delta dx dy} = \frac{1}{W\delta}\int\limits_0^W\int\limits_0^\delta v_z dx dy = \frac{W}{W\delta}\int\limits_0^\delta v_z dx \tag{6.18}$$

Substituting Eq.(6.16) into (6.18),

$$v_{z_{av}} = \frac{\rho g \delta^2}{2\mu}\int\limits_0^1\left[1-\left(\frac{x}{\delta}\right)^2\right]d\left(\frac{x}{\delta}\right) \tag{6.19}$$

and integrating,

$$v_{z_{av}} = \frac{\rho g \delta^2}{3\mu} \tag{6.20}$$

Combining Eqs.(6.17) and (6.20), we obtain $v_{zav} = (2/3)v_{z max}$. The volumetric flow rate Q is obtained by multiplying the average velocity v_{zav} times the cross-sectional area δW.

$$Q = W\delta v_{z_{av}} = \frac{\rho g W \delta^3}{3\mu} \qquad (6.21)$$

The film thickness δ can be given in terms of the average velocity and the volume rate of flow.

$$\delta = \sqrt{\frac{3\mu v_{z_{av}}}{\rho g}} = \sqrt[3]{\frac{3\mu Q}{\rho g W}} \qquad (6.22)$$

The foregoing analytical results are acceptable with laminar flow of falling films in straight streamlines. From experimental results, Bird et al. (1960) reported that the film velocity $v_{z_{av}}$ increases, as the thickness of the film δ increases, and as the kinematic viscosity $v = \mu/\rho$ decreases, the nature of the flow gradually changes and therefore, in this gradual change they classified three different types of flow: (a) laminar flow with straight streamlines, (b) laminar flow with rippling, and (c) turbulent flow. For this, a dimensionless group is defined as *Reynolds number* (Re) for this system.

$$Re = \frac{4\delta \rho v_{z_{av}}}{\mu} \qquad (6.23)$$

The following classification for vertical walls is given by Bird et al. (1960):

laminar flow without rippling	Re < 4 to 25
laminar flow with rippling	4 to 25 < Re < 1000 to 2000
turbulent flow ·	Re > 1000 to 2000

6.1.2 Diffusion in a laminar falling film

After derivation of the equation for the velocity profile in a falling film, mass transfer of solute A into a laminar falling film that the velocity field can be considered virtually unaffected by the diffusion is taken into consideration. This is especially important in wetted-wall columns, in developing theories to explain mass transfer in stagnant pockets of fluids, and in turbulent mass transfer (Bird et al. 1960). The solute A in the gas is absorbed at the interface and then diffuses a distance into the liquid so that it has not penetrated the whole distance $x = \delta$ at the wall. At steady state the inlet concentration $C_A = 0$. At a point z distance from the inlet the concentration profile of C_A is shown in Figure 6.2a.

(a)   (b)
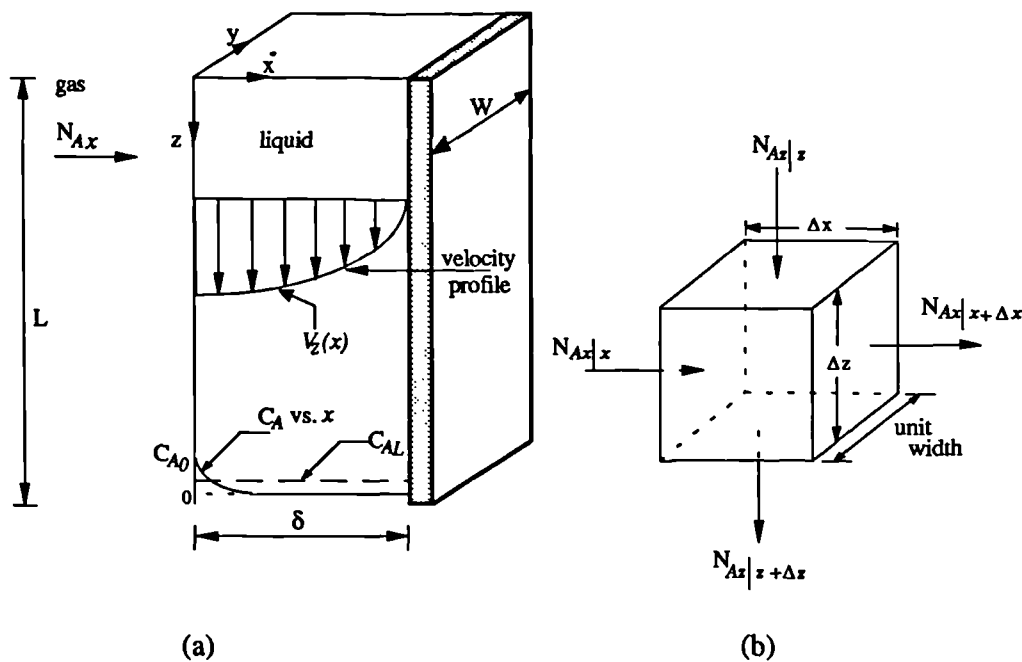
Figure 6.2 Diffusion of solute A in a laminar falling film: (a) velocity profile and concentration profile, (b) small element for mass balance

68

A mass balance will be made on the element shown in Figure 6.2b. For steady state, *rate of input = rate of output*.

$$N_{Ax|x}(W\Delta z) + N_{Az|z}(W\Delta x) = N_{Ax|x+\Delta x}(W\Delta z) + N_{Az|z+\Delta z}(W\Delta x) \qquad (6.24)$$

Inserting the expressions for N_{Ax} and N_{Az} by making appropriate simplifications of the molar flux to the concentration gradient (Bird et al. 1960)

$$N_{Az} = -cD_{AB}\frac{\partial x_A}{\partial z} + x_A(N_{Az} + N_{Bz}) \qquad (6.25)$$

where $x_A = c_A/c = $ mole fraction of A

For a dilute solution the diffusion equation for A in the x direction is

$$N_{Ax} = -D_{AB}\frac{\partial c_A}{\partial x} + x_A(N_{Ax} + N_{Bx}) \qquad (6.26)$$

$$N_{Ax} = -D_{AB}\frac{\partial c_A}{\partial x} + \text{ zero convection} \approx -D_{AB}\frac{\partial c_A}{\partial x} \qquad (6.27)$$

For the z direction the diffusion is negligible.

$$N_{Az} = -D_{AB}\frac{\partial c_A}{\partial z} + c_A v_z(x) \approx c_A v_z(x) \qquad (6.28)$$

Dividing Eq. (6.24) by $W\Delta x\,\Delta z$, letting Δx and Δz approach zero, and substituting Eqs. (6.27) and (6.28) into the result, we obtain

$$v_z \frac{\partial c_A}{\partial z} = D_{AB} \frac{\partial^2 c_A}{\partial x^2} \qquad\qquad (6.29)$$

From Eqs. (6.16) and (6.17), the velocity profile is parabolic and is $v_z = v_{z\,max}[1 - (x/\delta^2)]$. Also, $v_{z\,max} = (3/2)v_{z\,av}$.

$$v_{z\,max}\left[1 - \left(\frac{x}{\delta}\right)^2\right]\frac{\partial c_A}{\partial z} = D_{AB} \frac{\partial^2 c_A}{\partial x^2} \qquad\qquad (6.30)$$

If the solute has penetrated only a short distance into the fluid $(x = \delta)$, i.e., short contact times of t seconds equals z/v_{max}, then the A that has diffused has been carried along at the velocity $v_{z\,max}$ or v_{max} if the subscript z is dropped. Then Eq. (6.30) becomes

$$\frac{\partial c_A}{\partial (z/v_{max})} = D_{AB} \frac{\partial^2 c_A}{\partial x^2} \qquad\qquad (6.31)$$

Using the boundary conditions of $c_A = 0$ at $z = 0$, $c_A = c_{Ao}$ at $x = 0$, and $c_A = 0$ at $x = \infty$, we can integrate Eq.(6.31) to obtain (Bird et al. 1960)

$$\frac{c_A}{c_{Ao}} = 1 - \mathrm{erf}\left(\frac{x}{\sqrt{4D_{AB}\,z/v_{max}}}\right)$$

$$= \mathrm{erfc}\left(\frac{x}{\sqrt{4D_{AB}\,z/v_{max}}}\right) \qquad\qquad (6.32)$$

where $\mathrm{erf}\,y$ is the error function and $\mathrm{erfc}\,y = 1 - \mathrm{erf}\,y$. Values of $\mathrm{erf}\,y$ are standard tabulated functions.

To determine the local molar flux at the surface $x = 0$ at position z from the top entrance, this can be written (Bird et al. 1960)

$$N_{Ax}(z)\big|_{x=0} = -D_{AB}\frac{\partial c_A}{\partial x}\bigg|_{x=0} = c_{Ao}\sqrt{\frac{D_{AB}v_{max}}{\pi z}} \qquad (6.33)$$

The total moles of A transferred per second from the gas to the liquid film over the entire length $z = 0$ to $z = L$, where the vertical surface is W width

$$N_A(LW) = (W)\int_0^L (N_{Ax|x=0})dz = (W)c_{Ao}\left(\frac{D_{AB}v_{max}}{\pi}\right)^{1/2}\int_0^L \frac{1}{z^{1/2}}\ dz$$

$$= (LW)c_{Ao}\sqrt{\frac{4D_{AB}v_{max}}{\pi L}} \qquad (6.34)$$

The term L/v_{max} is t_L, time of exposure of the liquid to the solute A in the gas. This means the rate of mass transfer is proportional to $D_{AB}^{0.5}$ and $1/t_L^{0.5}$.

6.2   Films produced by centrifuged fluids on rotating surfaces

Thin liquid films used for gas absorption processes have indicated that they have certain advantages over contactors which disperse the gas phase through a continuous liquid phase. Falling liquid films in wetted-wall columns have shown that ripples are present at the surface of the liquid. Comparison of these films with films which have flat interfaces indicates that the presence of these ripples results in an increase in the rate of absorption of a gas. It has been demonstrated that an increase of 250% in the rates of absorption of oxygen and carbondioxide occurs when the ripples were

71

present (Emmert and Pigford 1954). They proposed that this effect was due to a combination of increased interfacial area and enhanced mixing in the bulk liquid. Liquid flowing across the surface of a rotating disc also demonstrate this type of wave formation. However, the film formed under these circumstances is much thinner, due to the centrifugal forces which are applied to it, than that which would be obtained in a falling liquid film. This fact implies that a system which produced such films would be able to produce higher rates of mass transfer than other systems. It was this idea that implied the developing of the spinning disc contactor.

Spinning disc reactors (SDR) have been studied in the past in connection with gas-liquid reactions in different modifications (Barberis 1987, Wallis 1991). They produce a thinner and more controllable liquid film than the falling film reactor and the thin liquid films produced in these reactors possess a high degree of turbulence and hence correspondingly high values for their gas-liquid mass transfer coefficients. Therefore, the fundamental advantage of using a SDR type design is that it reduces the effect of mass transfer limitation.

However, mass transfer effect is unlikely to be significant in a slurry based system where the overall rate is predominantly reaction rate controlled (Matthews 1988, Turchi and Ollis 1988, Ollis et al. 1991), hence the same characteristics of the liquid film on a spinning disc which make it unsuitable for a slurry based system might be ideal for a supported catalyst based reactor, where short organic diffusion lengths are a positive advantage.

Therefore the use of the SDR as a supported catalyst reactor is recommended and the experimental work is performed using the SDR which

utilised titanium dioxide catalyst supported on a borosilicate glass disc to degrade aqueous solutions of various organic substances.

The following work is based on the hydrodynamics of thin films formed on smooth rotating surfaces.

6.2.1 The hydrodynamics of thin films formed on smooth rotating discs

Liquid films formed on a smooth rotating surface can, for modelling purposes, be assumed to be laminar in character. The two mathematical models which are most commonly used to describe the characteristics of the liquid film are the centrifugal and coriolis models.

The centrifugal model is the easiest to derive of the two. It is based upon the following assumptions (Lim 1980, Venkataraman 1966):

a)   the viscous and centrifugal forces are in equilibrium and act in opposite directions,

b)   the thickness of the film is small compared to the radius,

c)   the effects of surface tension, gravity and friction at the free liquid surface are insignificant,

d)   the effects of coriolis and inertial forces upon the liquid are negligible.

Hence:

$$v\frac{d^2u_r}{dy^2} = -w^2r \qquad (6.35)$$

where:

v = kinematic viscosity

u_r = radial velocity of the liquid

y = distance perpendicular to the plane of the disc

w = angular velocity of the disc

r = radius

Integration of equation (6.35) leads to the following expression for the radial velocity:

$$u_r = \frac{w^2 r}{v}(\delta y - y^2/2) \tag{6.36}$$

The average velocity is thus,

$$\bar{u}_r = \frac{w^2 r \delta^2}{3v} \tag{6.37}$$

The continuity of flow is given by,

$$Q = 2\pi r \, \delta \, \bar{u}_r \tag{6.38}$$

where Q = liquid volumetric flow rate

Combining equations (6.37) and (6.38) results in the following expression for the liquid film thickness,

$$\delta = (3Qv)^{1/3}\left(2\pi w^2 r^2\right)^{-1/3} \tag{6.39}$$

This can be rewritten in terms of dimensionless groups (Venkataraman 1966),

$$\frac{\delta}{r} = 1.145 \ Re^{0.33} \ Ta^{-0.67} \tag{6.40}$$

where; Reynolds Number, $Re = \dfrac{Q}{rv}$ and Taylors Number, $Ta = \dfrac{wr^2}{v}$

An expression for the mean residence time of the liquid film upon the disc surface can be found by combining Eqs. (6.37) and (6.39) and then integrating to give,

$$t_r = 3.683 \left(v(r_e^4 - r_i^4) \right)^{0.33} (wQ)^{-2.33} \tag{6.41}$$

where; r_e = the outer radius of the disc

r_i = the distributor radius

When a liquid film flows over a rotating surface, it has been observed that the film never reaches the angular velocity of the surface. This effect has been suggested that it is due to a force, known as the coriolis force, which acts in the circumferential direction opposite to that for rotation. The effect of the coriolis force upon the liquid film increases with increasing film thickness and decreasing liquid viscosity. Hence, it tends to have the greatest significance at low radii and high liquid flow rates. At larger radii, its effect is reduced and the liquid film's flow pattern can be described adequately by the centrifugal model. Incorporation of this force into the derivation of the centrifugal model results in the coriolis model (Venkataraman 1966),

$$v\frac{d^2u_r}{dy^2} = -wr^2 \qquad (6.42)$$

$$v\frac{d^2u_\theta}{dy^2} = 2wu_r \qquad (6.43)$$

where; u_θ = angular velocity of the liquid

It has been hypothesised that flow across a smooth rotating disc is turbulent in nature, with a laminar sublayer occurring at the free surface of the liquid film (Venkataraman 1966). The sublayer is produced by suppression of the eddy currents inside the film by the surface tension of the liquid. The thickness of this sublayers appears to be fairly constant and hence the proportion of the liquid film showing laminar behaviour increases at larger disc radii, due to the decrease in the overall thickness of the film.

CHAPTER VII

7. Experimental equipment design and construction

7.1 Design of the quartz annular photoreactor

Picture 7.1 shows the annular photoreactor and the ultraviolet source. The annular photoreactor was constructed entirely of quartz to minimise light absorbance at 254nm, design features are shown in Figure 7.1.

The annular photoreactor has been designed to give a maximum liquid irradiation since the ultraviolet lamp is effectively surrounded by the solution. It comprises of a double-walled well (model 3230, Applied Photophysics Ltd.) which houses the irradiation lamp.

A small diameter inlet PTFE tube (i.d. = 5 mm) extends to the bottom of the annular space to allow liquid flow from the bottom of the well upwards and the actual volume of annular reactor is 360ml.

The ultraviolet source consists of two different type of lamps supplied from Applied Photophysics Ltd. The first one is a mercury low pressure lamp (model 3016) which emits over 90% of its radiation at 254nm. The second one is a mercury medium pressure lamp (model 3040) which has a much more intense arc and radiates predominantly 365-366nm radiation with smaller

amounts in the UV region at 265, 297, 303, 313, and 334nm as well as significant amounts in the visible region at 404-408, 436, 546 and 577-579nm. Other lamp characteristics were as follows:

Nominal wattage (watts)	Overall length (mm)	Discharge length (mm)	Diameter (mm)	Light Output[a]
16	380	275	20	3.10^{18}
400	375	90	30	$>5.10^{19}$

[a] Photon/s measured by ferrioxalate actinometry in quartz well
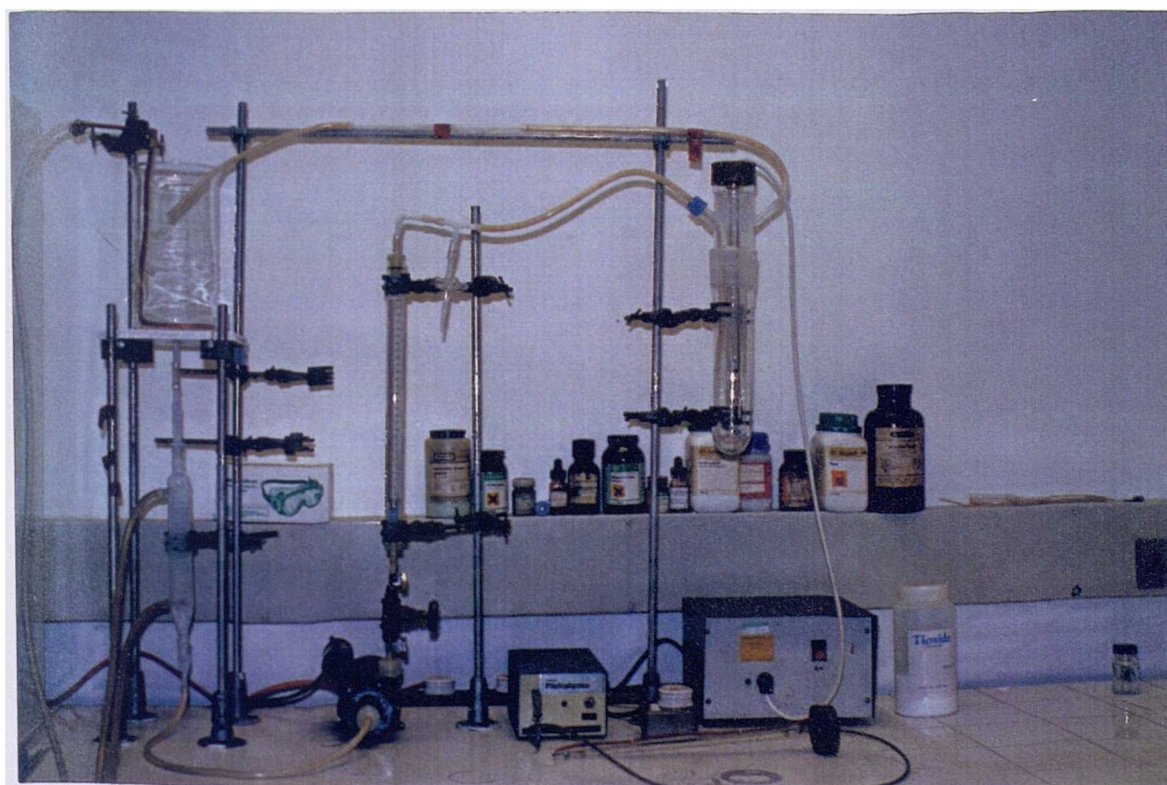
Picture 7.1 The quartz annular photoreactor and the UV lamps

the lamp

annular reactor

power
unit

sampling point

rotameter
to 1.3 lt/min

30W pump

pH and temperature
measurement

vessel
2lt

cooling
water
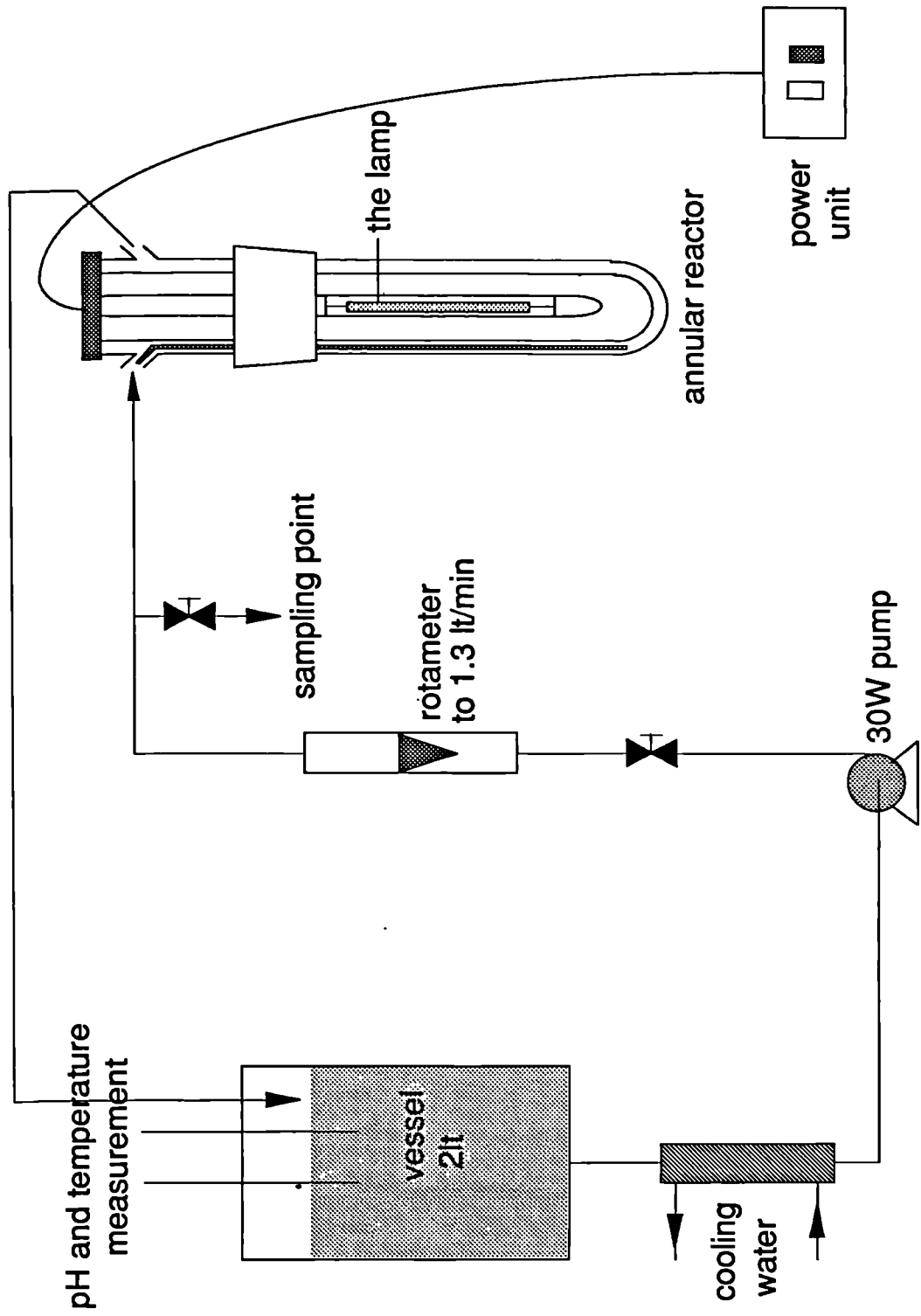
Figure 7.2 Schematic diagram of the annular photoreactor process

7.2   Design of the spinning disc reactor (SDR)

The spinning disc reactor used during this study was basically that used by Barberis (1987) and Wallis (1991) for their ozonation studies. However a few modifications were made to the SDR. A borosilicate glass disc (38cm diameter) was fitted (Picture 7.2 and 7.3) and two different UV lamp configurations were applied (Figure 7.3). These two lamp types were used in configuration:

- Two 15 watt low pressure mercury lamps (Hanovia Ltd.), producing 4×10^{17} photon/s at a UV peak wavelength of 254nm (Picture 7.4).

- A 400 watt medium pressure mercury lamp (Applied Photophysics Ltd.), producing 5×10^{19} photon/s at a UV peak wavelength of 365-366nm (the same type used in the annular reactor).

A -   B

liquid out

liquid in

(Engineering design of the SDR
is shown in Appendix-E)

liquid out
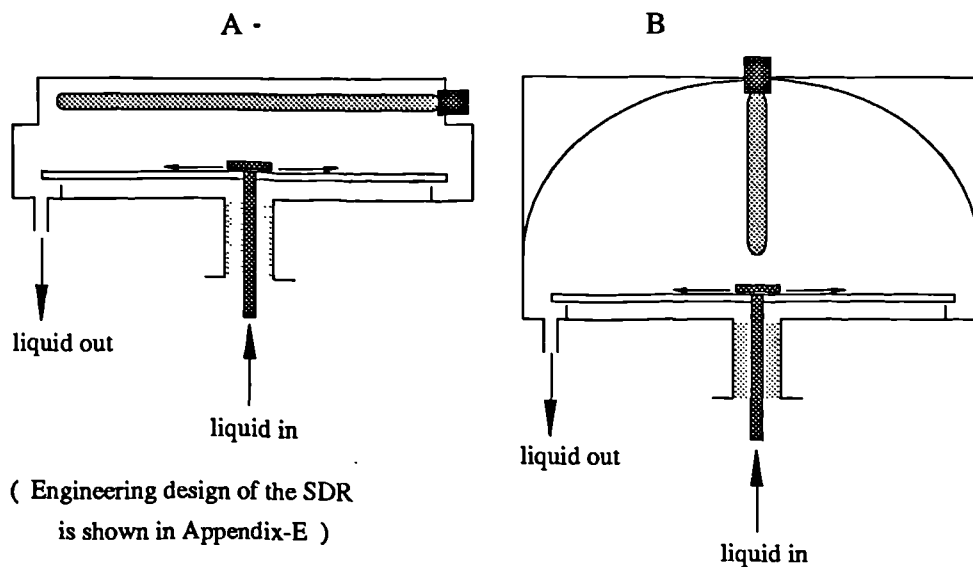
liquid in

Figure 7.3 Lamp configurations used for the SDR (arrows indicate direction of liquid flow); (A) 2 x 15 watt low pressure mercury lamps, (B) 400 watt medium pressure mercury lamp
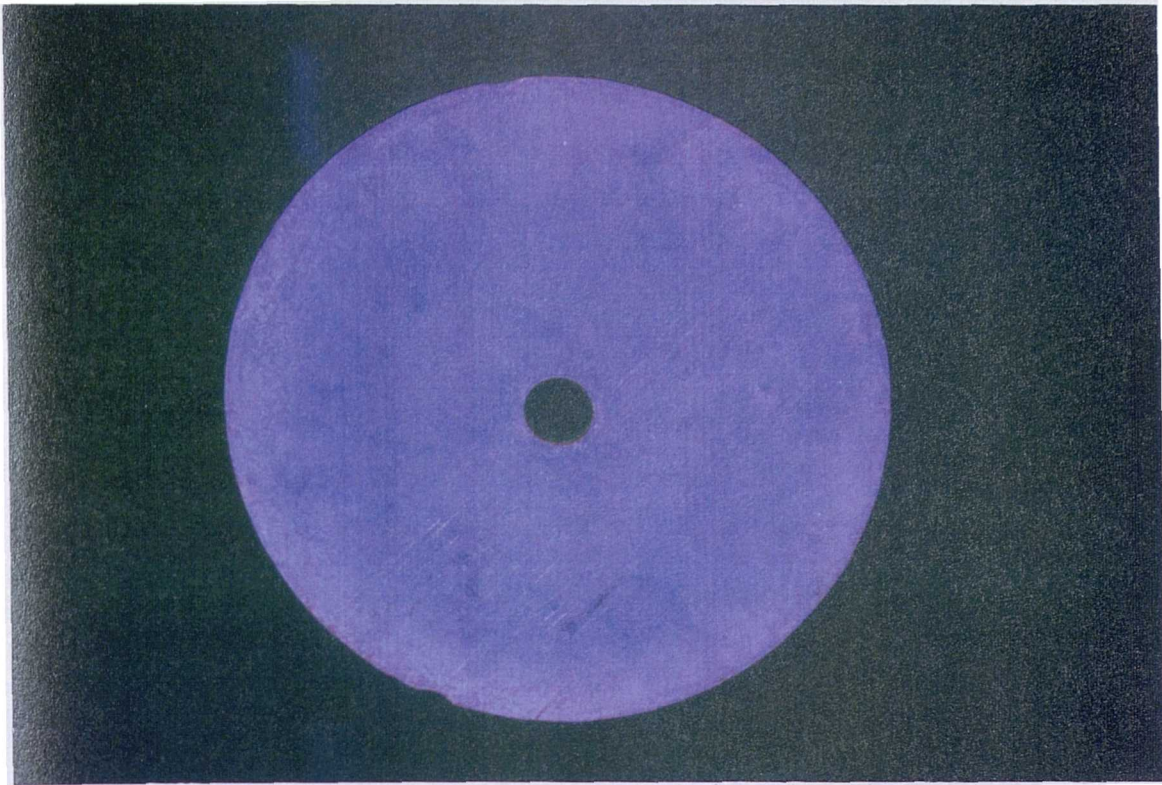
Picture 7.2 The borosilicate glass spinning disc (38cm diameter)
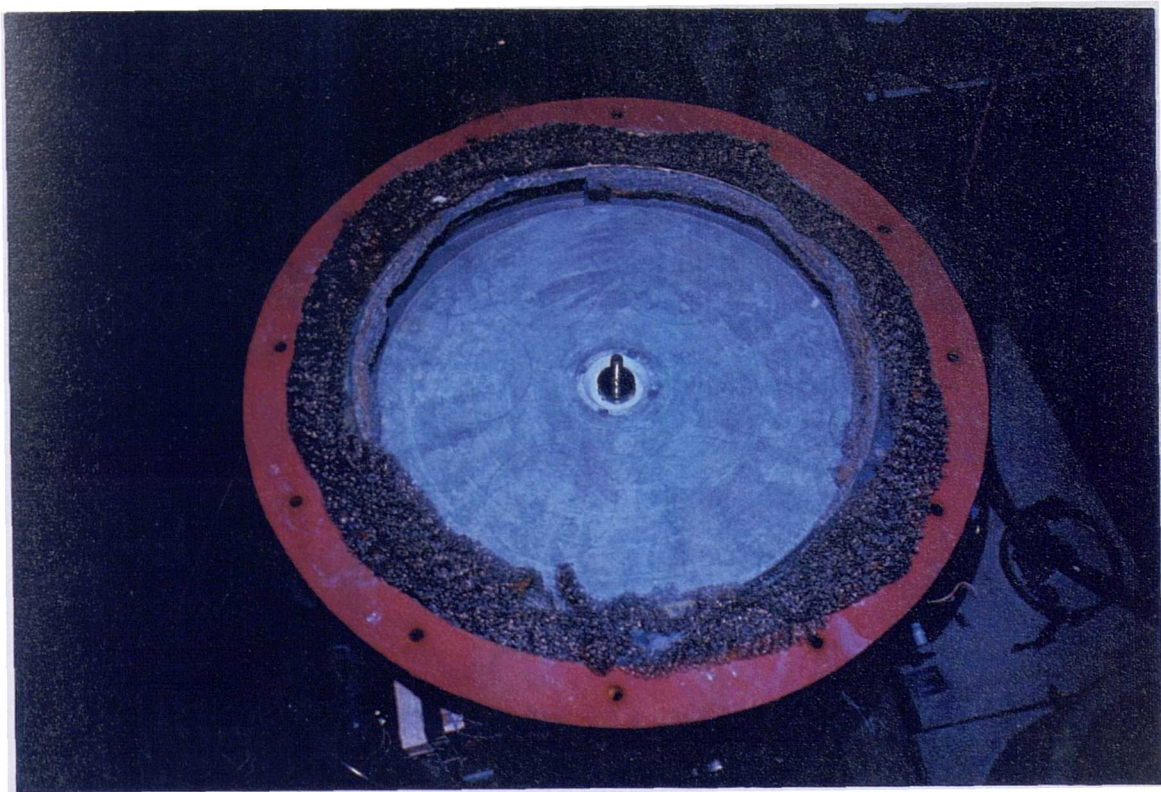
Picture 7.3 The disc fitted to the SDR
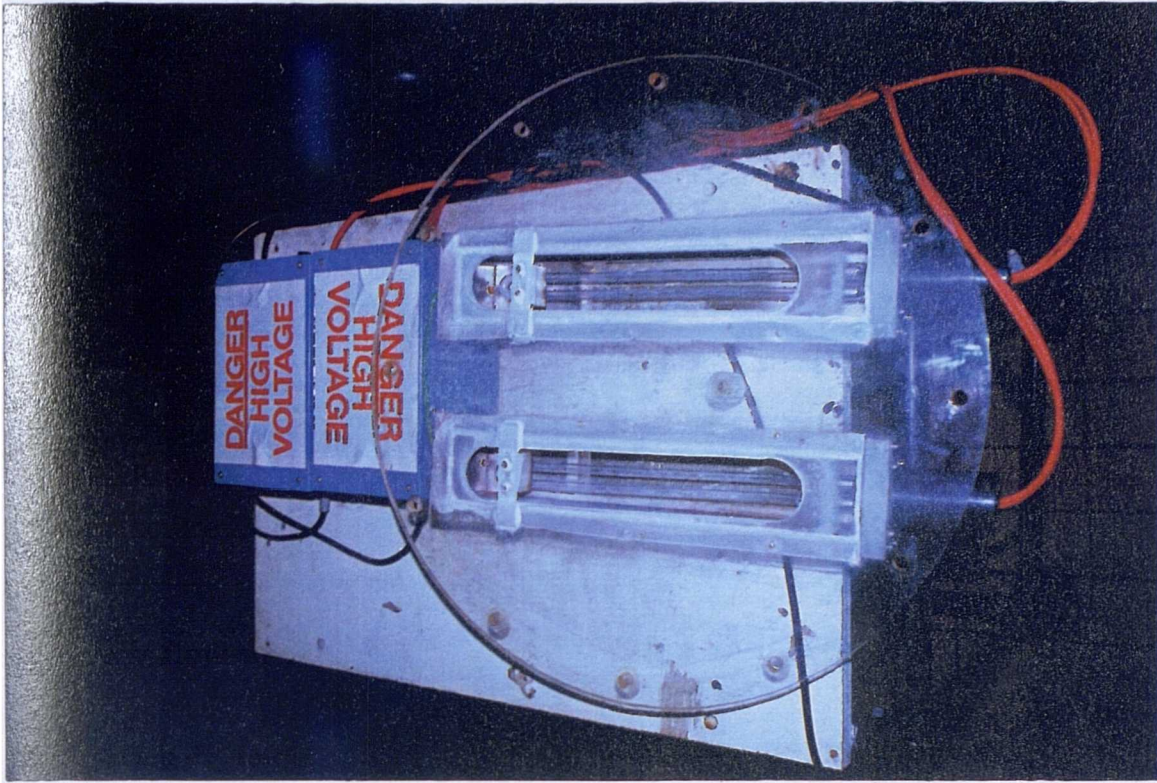
Picture 7.4 The 2 x 15 watt low pressure mercury lamps

The process flow sheet of SDR was shown in Figure 7.4.
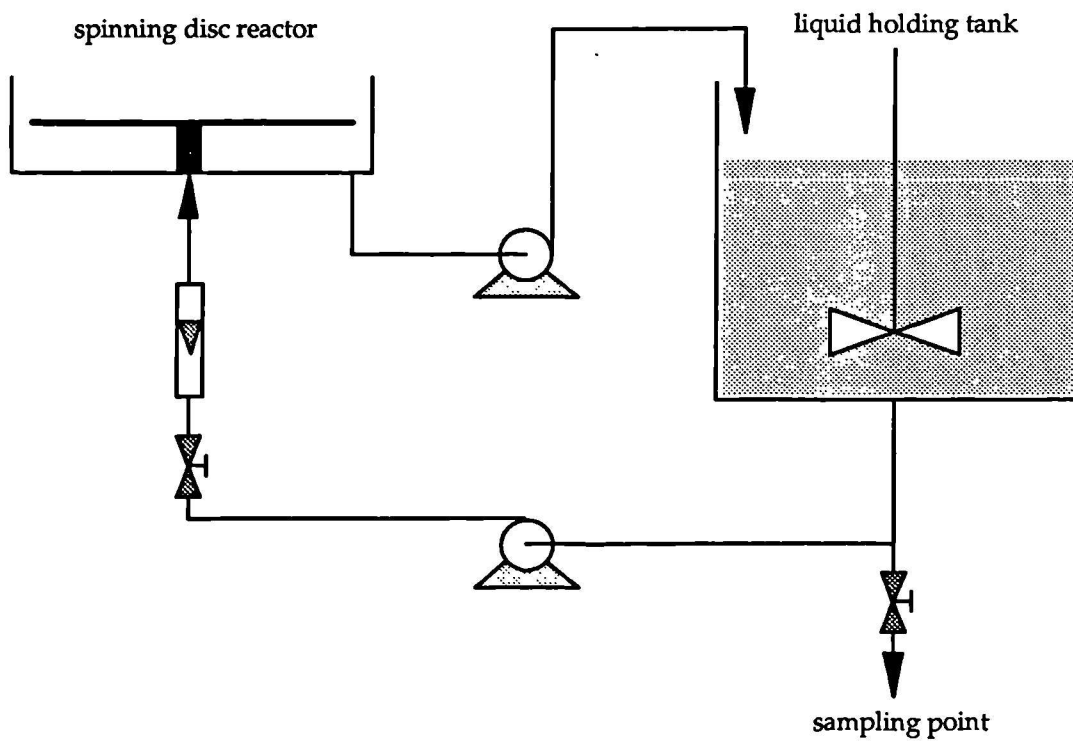
Figure 7.4 Schematic diagram of SDR process

7.3 Design of the falling film reactor (FFR)

The falling film reactor of this type was particularly designed for this work to study heterogeneous photocatalysis with TiO_2. The aim was to reach highest utilisation of light intensity and light absorbance by producing thin films within a cylindrical shape.

The main part of the reactor is a large cylindrical borosilicate glass tube. This tube is capable of accommodating a large 2.5kW medium pressure lamp (Hanovia Ltd., model UVV-2.5kW). No output data was given by the manufacturer therefore the lamp output was measured by ferrioxalate actinometry on a perspex plate under an aluminium reflector as described in section (9.2.2.1) and the total output of $4.5x10^{20}$ photon/s was obtained considering the geometry of the FFR as described in Appendix-C.

A 20lt capacity of liquid holding tank was used (Figure 7.5). A V-profiled weir was adopted to provide uniform falling film flow (Figure 7.6). A schematic diagram of the falling film reactor and the process layout are shown in Figure 7.7 and Picture 7.5.

Cooling coil : 1 cm glass pipe
total length of coil 9m - 11 coils

Air or nitrogen
to sparger

450 mm

250 mm

300 mm
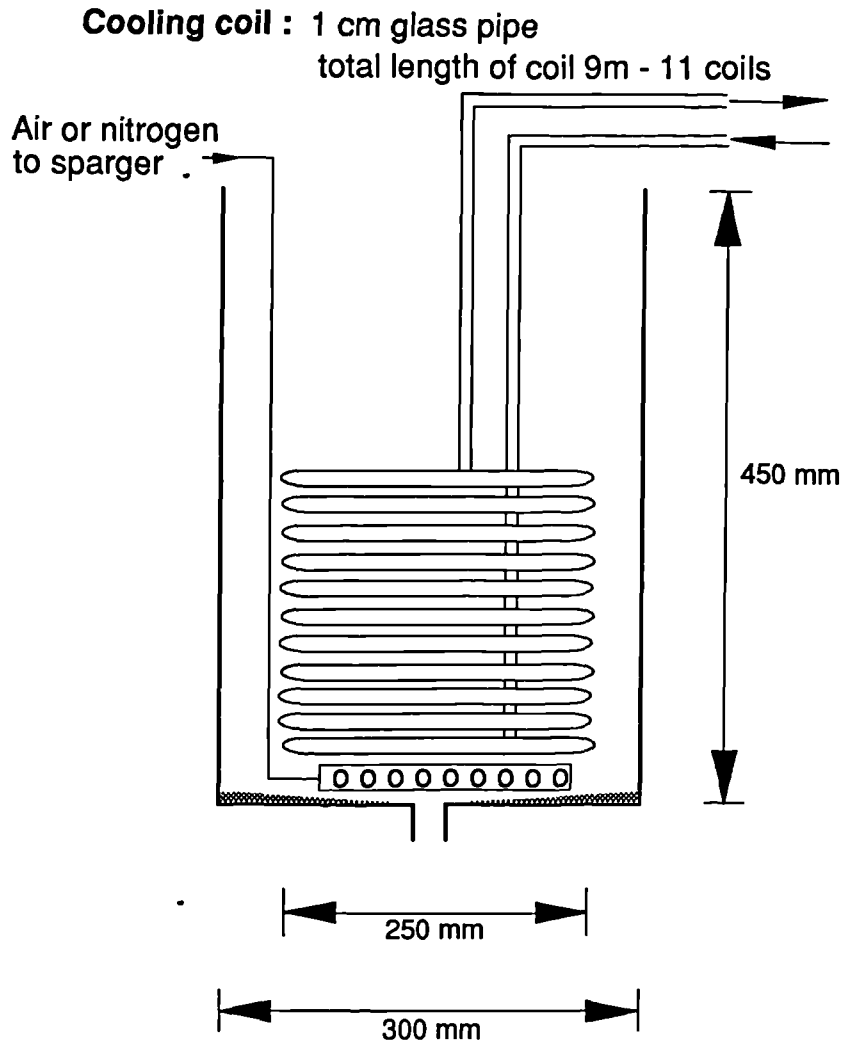
Figure 7.5 Holding tank specifications

liquid in

1 cm

6.5 cm

1 cm

1.5 cm

10 cm

15 cm
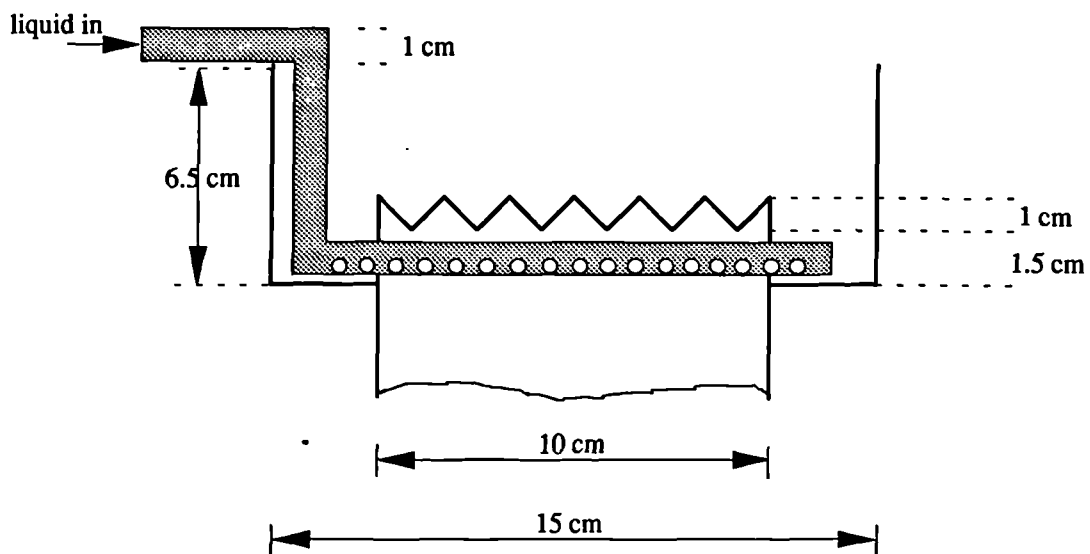
Figure 7.6 Weir section of borosilicate glass tube
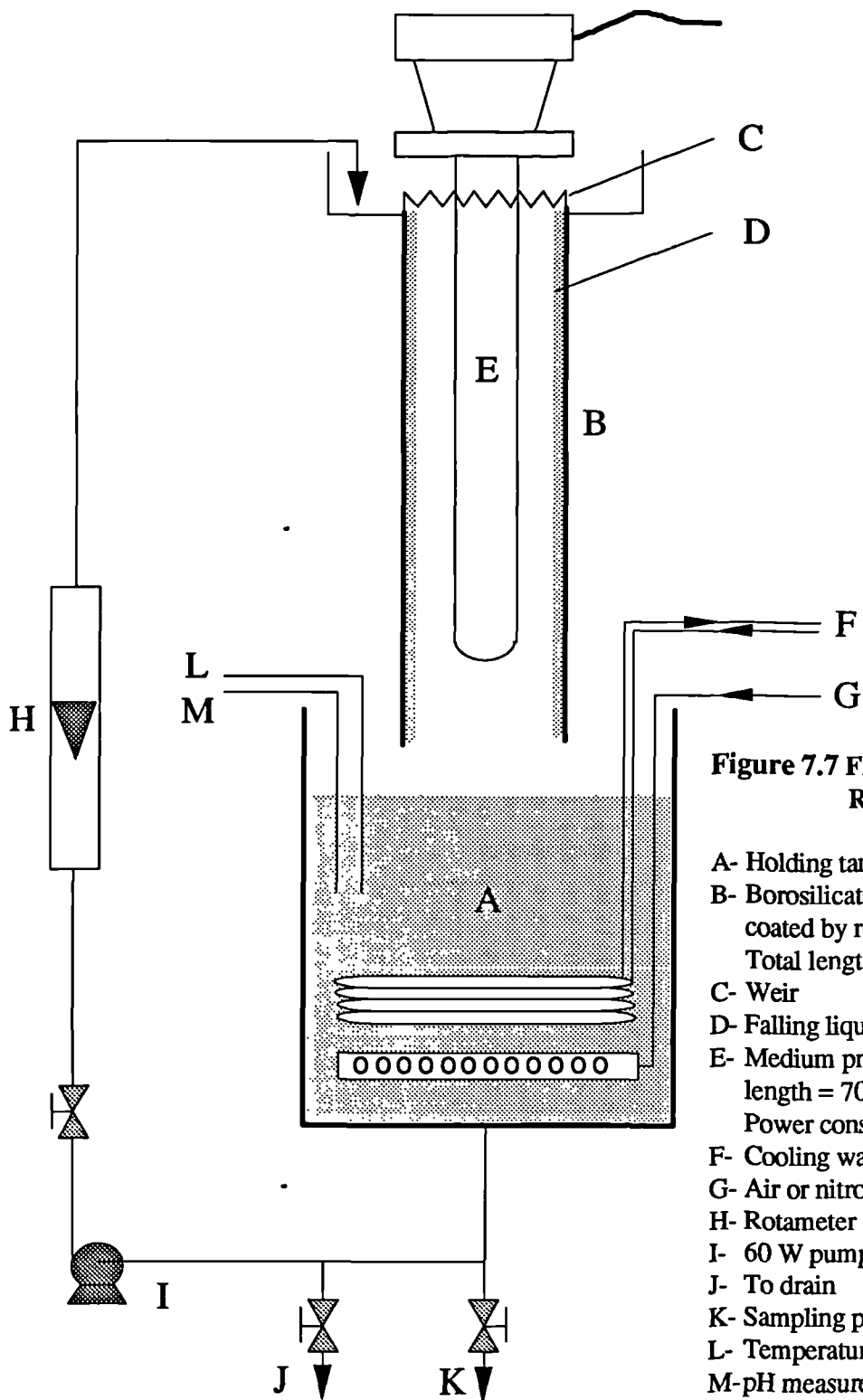
**Figure 7.7 FALLING FILM
REACTOR**

A- Holding tank
B- Borosilicate glass tube
coated by reflective aluminium
Total length = 80 cm , I.D.=10 cm
C- Weir
D- Falling liquid film
E- Medium pressure lamp
length = 70 cm, O.D.= 4.8 cm
Power consumption = 2.5 kW
F- Cooling water coil
G- Air or nitrogen to sparger
H- Rotameter to 7.5 lt/min
I- 60 W pump
J- To drain
K- Sampling point
L- Temperature measurement
M-pH measurement
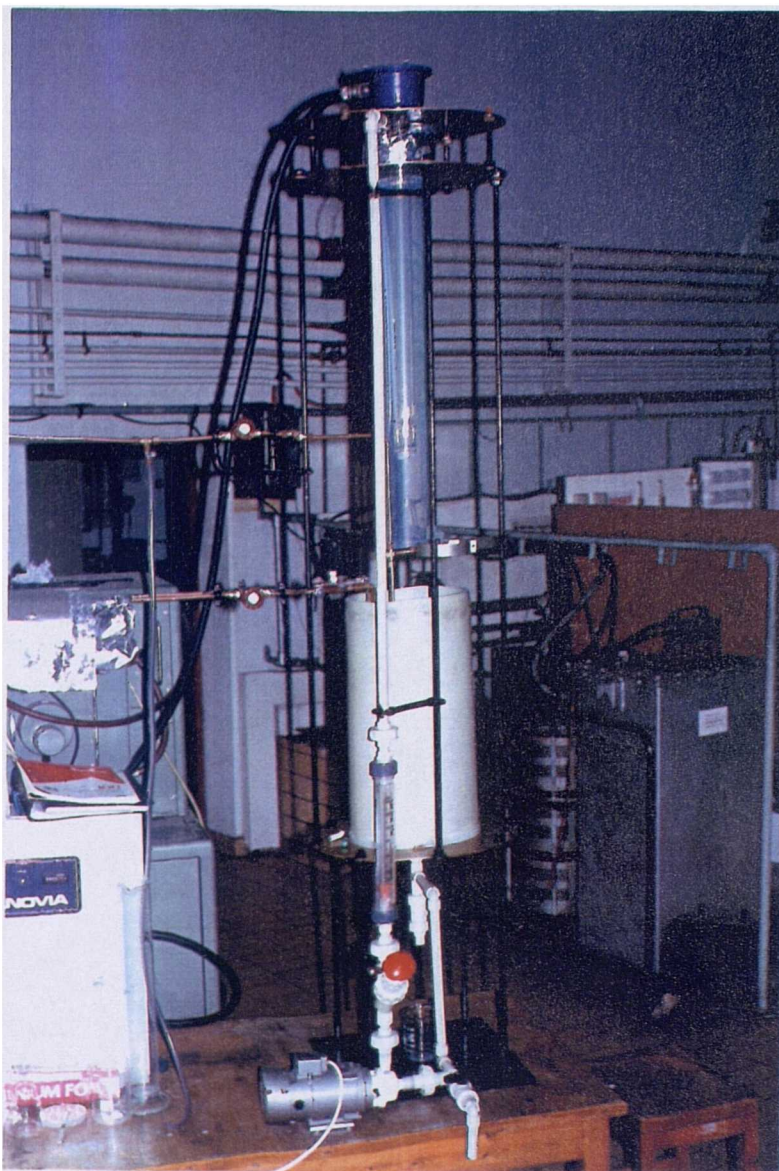
Picture 7.5 Falling film reactor

7.4   Analytical procedure and analysis

In this work, mainly two types of organic chemicals were used as model reactants. Salicylic acid was chosen because it is strongly fluorescent and hence can be measured in very low concentrations (Matthews 1987c) and 4-chlorophenol, since it represents one of the main chemicals frequently

87

found in various industrial effluent and reported in hazardous waste sites (Ellis et al. 1984).

These organic chemicals were analysed by HPLC. The HPLC unit was a Pye Unicam model (Pump PU4020, UV detector PU4010) and was fitted with a Novapak C_{18} column (Waters Ltd.). The eluent solvent (mobile phase) consisted of a mixture of water-acetonitrile-phosphoric acid (74.5:25:0.5 by volume). 20μl of samples were injected into the system with a flow rate of 1.5ml/min. The detection wavelengths were 254nm for salicylic acid and 280nm for 4-chlorophenol. HPLC results showed that these organics can be detected as accurate as possible up to 1μM levels.

Other workers also used HPLC to detect these chemicals with similar eluent and wavelengths (Al-Ekabi et al. 1989, Terzian et al. 1990, Al-Sayyed et al. 1991) and some of them used spectrofluorimeters (Matthews 1986, 1987a,b,c, Al-Ekabi 1988).

The aim of photocatalytic processes is to destroy chemicals during the process stage, hence the importance of mineralisation versus removal of contaminant is stressed. To understand the mineralisation stage several workers used different methods. Matthews (1986, 1087a,b, 1990), Barbeni et al. (1984) analysed CO_2 as one of the end products and Al-Ekabi et al. (1988) determined the end product HCl by analysing Cl⁻ concentration. The workers used HPLC for chemical detection performed intermediate analysis (Al-Ekabi et al. 1989, Terzian et al. 1990, Al-Sayed et al. 1991). Ollis et al. (1991) in their recent review revealed the use of total organic carbon (TOC) analysis and one of the utility of a photocatalytic TOC analyser was outlined by Matthews

(1992). This is suitable for the direct analysis of total organic chemicals as their organic carbon content.

In this study, apart from reactant analysis, the main intermediates were also detected to follow destruction stage. Catechol as the main intermediate of salicylic acid degradation and hydroquinone as for the 4-chlorophenol were detected. Some TOC analysis was also performed but the TOC unit was not capable of analysing low concentration of organics and the data was unreproducible, therefore the results were not useful to evaluate reaction kinetics.

CHAPTER VIII

8. Results of photocatalytic studies in the annular reactor

8.1 Absorbance variations for two different catalysts

During all experiments two different type of TiO_2 catalysts were used. They are Degussa P-25 and Tioxide PC1. Here, the effects of varying wavelength upon the absorbance of thin films of these catalysts were examined. Different quantities of catalysts were coated on quartz slides (1x4 cm) by preparing small slurry solutions of catalysts and spreading these on one side of the slide, followed by drying. The concentration was determined by weighing the slide before and after, and the effect of different concentration were examined in a UV-visible spectrophotometer (Uvikon 810). The results were shown in Figure 8.1.1, 8.1.2 and 8.2.

Comparing these figures, show that absorbance of films of Tioxide PC1 do not change by wavelength as much as those composed of Degussa P-25. But, Figure 8.2 shows that the degree of absorbance is much more dependent on concentration for Degussa P-25. This could be because the absorption coefficient is higher than Tioxide PC1 and it means more efficient utilisation of light energy hence it gives higher quantum efficiency.
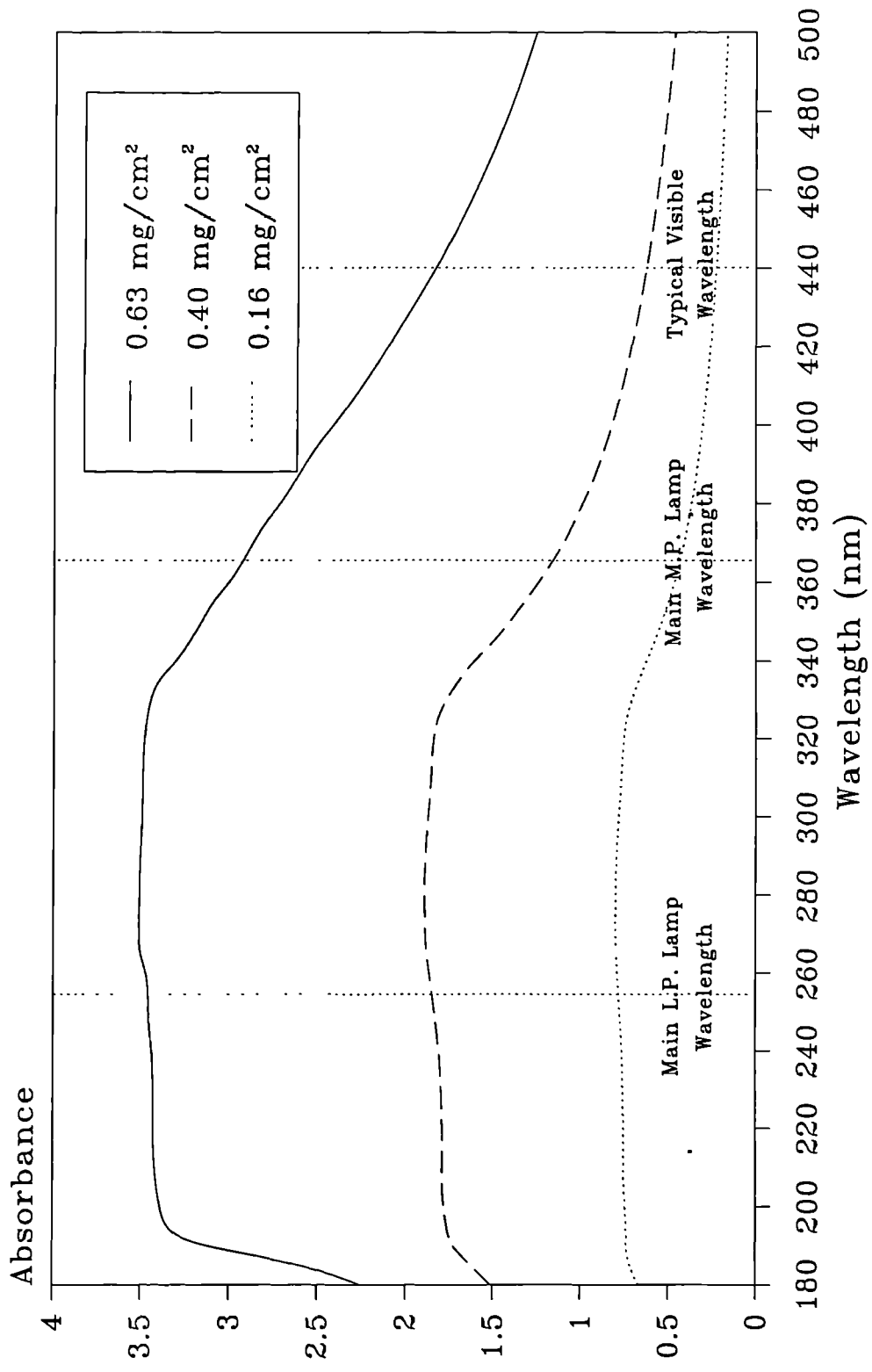
Absorbance

Figure 8.1.1 Absorbance of thin films
of Degussa P-25 catalyst
Effect of surface loading

Wavelength (nm)
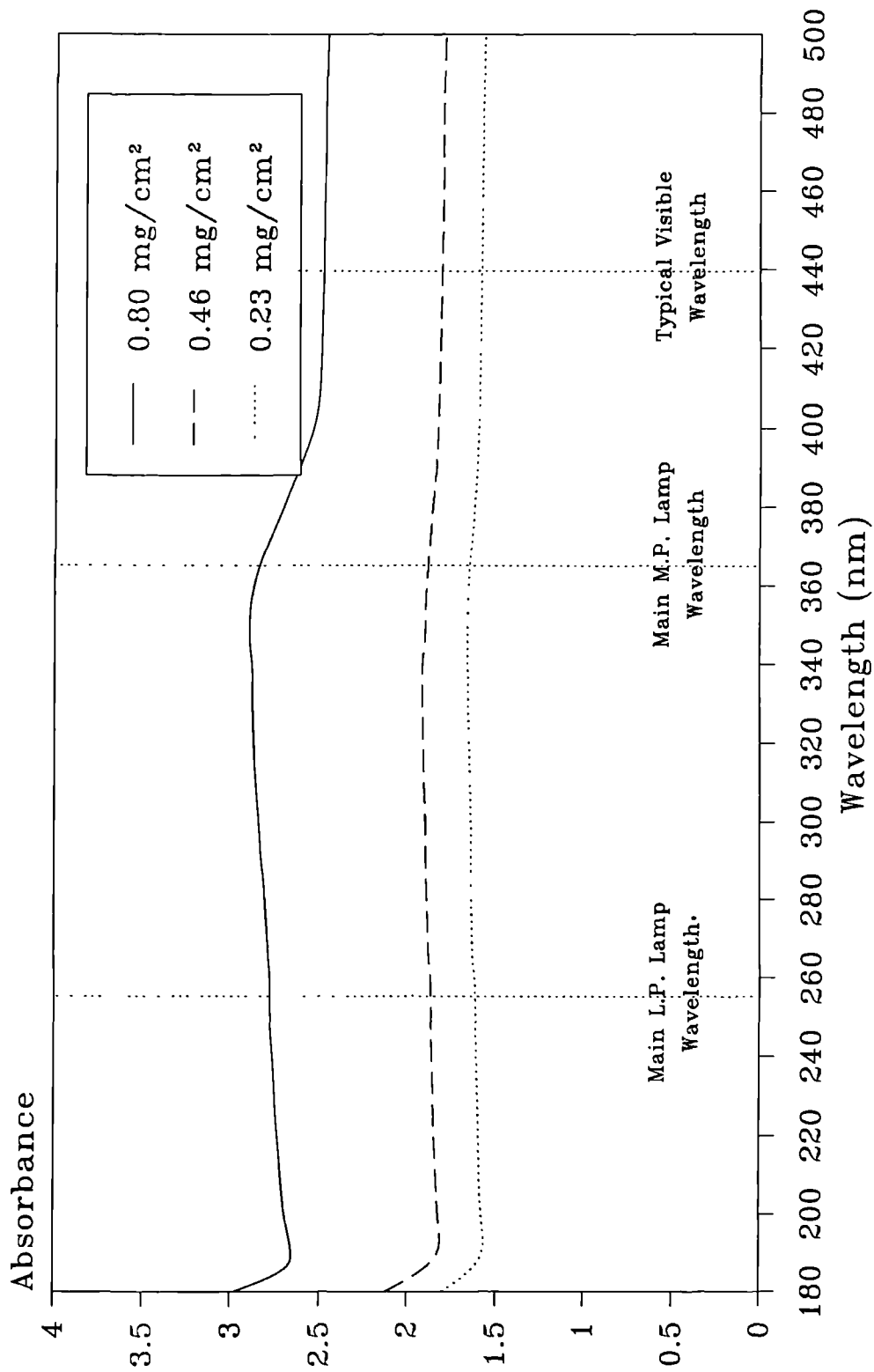
Absorbance

Figure 8.1.2 Absorbance of thin films
of Tioxide PC1 catalyst
Effect of surface loading

Figure 8.2 Absorbance of thin films of
Degussa P-25 and Tioxide PC1 catalyst
-Effect of wavelength-
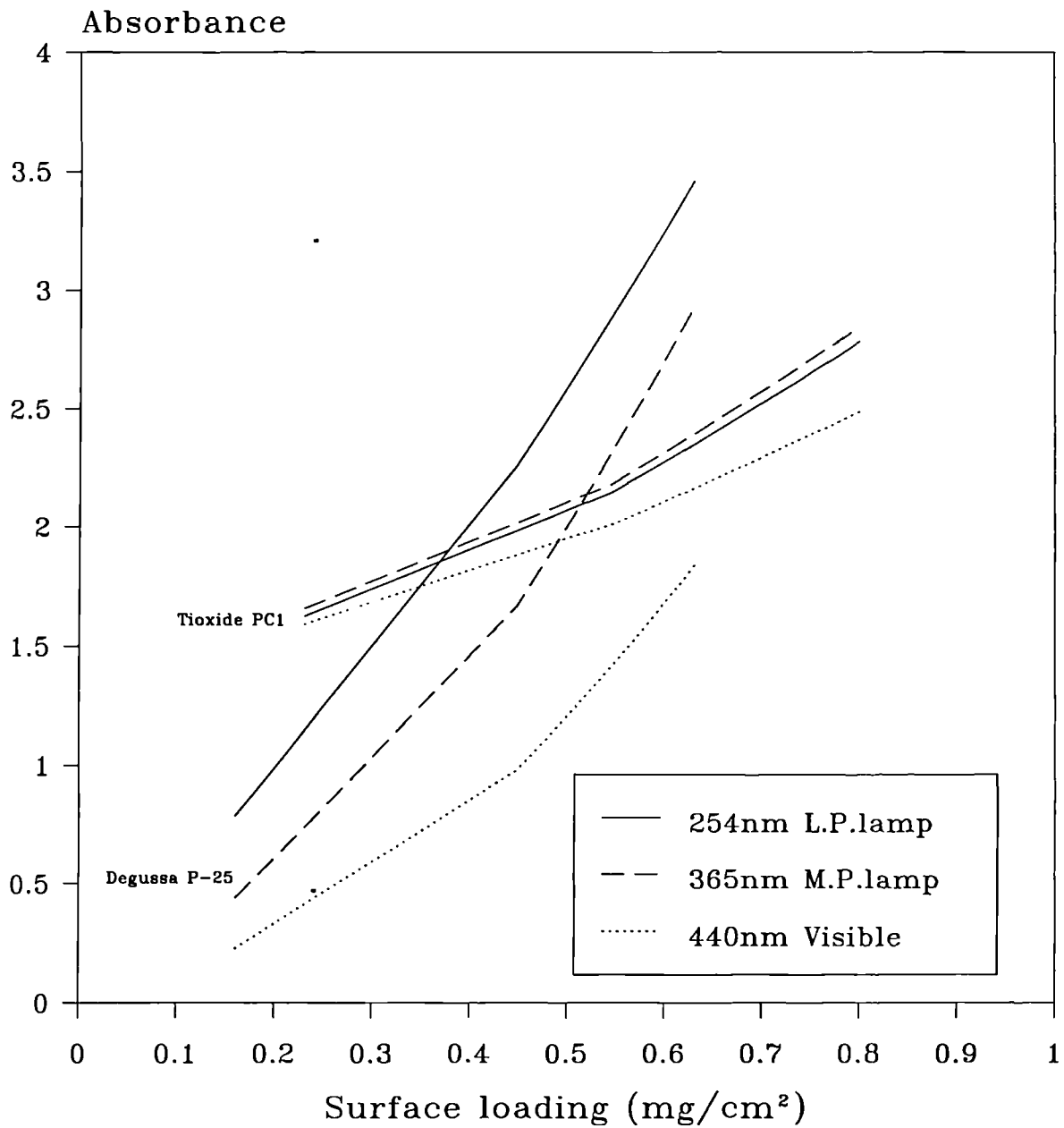
8.2 Effect of catalyst concentration in slurries

The influence of catalytic slurry concentration on the performance of the annular reactor was studied by monitoring the change in concentration of salicylic acid with time. This organic was chosen because it was used to study the same kind of effect by other workers (Matthews 1986, 1987b). The degradation rate of salicylic acid (initial concentration of 100μM of 2lt solution-Flow rate 1lt/min) was measured at various catalyst loadings. Degradation of salicylic acid concentration were analysed by HPLC. The UV source was a 400 W medium pressure lamp. Table 8.1 gives the resulting first order rate constants (k) obtained by using a linear regression analysis to fit the concentration vs time data to a first order reaction kinetics model (Equation 3.8) (r =correlation coefficient).

Table 8.1 Effect of catalytic slurry concentration upon the first order rate constant for salicylic acid degradation

Slurry conc. (g/lt)	Degussa P-25 k(min^{-1}) (r)	Tioxide PC1 k(min^{-1}) (r)
0.5	0.0865 (0.997)	0.1135 (0.993)
1.0	0.1041 (0.998)	0.1910 (0.996)
2.0	0.1038 (0.992)	0.1971 (0.995)
3.0	0.1010 (0.984)	0.0567 (0.853)

It can be seen that for this reactor the optimum catalyst concentration lies in the region of 1 g/lt for both catalyst types and Tioxide PC1 seems to have the higher rate of organic degradation. The table shows that, as the concentration of P-25 increases the rate does not fall markedly, but PC1 does, this could be explained by reference to Figure 8.2 which shows a rapid rise in absorbance with P-25 concentration, whereas PC1 does not rise rapidly. Figure 8.2 was

for a layer of catalyst and the annular work involves scattering effects due to the slurry which become more pronounced as the concentration increases so eventually the particles furthest away from the lamp will receive little radiation. If the slurry concentration is equivalent to a low surface loading then Figure 8.2 also shows that for the medium pressure lamp PC1 should be more effective.

8.3 Effect of physical adsorption

To understand the effect of adsorption affinity of the catalysts, decreases in the initial concentration of salicylic acid (SA) and also 4-chlorophenol (4-CP) (initial concentration of $100\mu M$ of a 2lt solution-Flow rate 1lt/min) were measured without any light present, with 1g/lt catalyst concentration. Results (Figure 8.3) show that Tioxide PC1 type has strong adsorption affinity for salicylic acid compared to Degussa P-25, but adsorption affinity was not as strong as for 4-CP on both catalysts surfaces. SA and 4-CP are the model organic reactants in this work. These two organics were generally used as model reactants by other workers as explained in section 2.2.1.

8.4 Effect of liquid flow rate

Other work in particular that by Matthews (1987b) had shown that increasing flow rate improved the transfer of organics to the catalyst surface with improved performance, Matthews used an immobilised surface and mass transfer effects are likely to be more important. The effect of liquid flow

Figure 8.3 Effect of physical adsorption of organic molecules on two different catalysts surfaces under no light
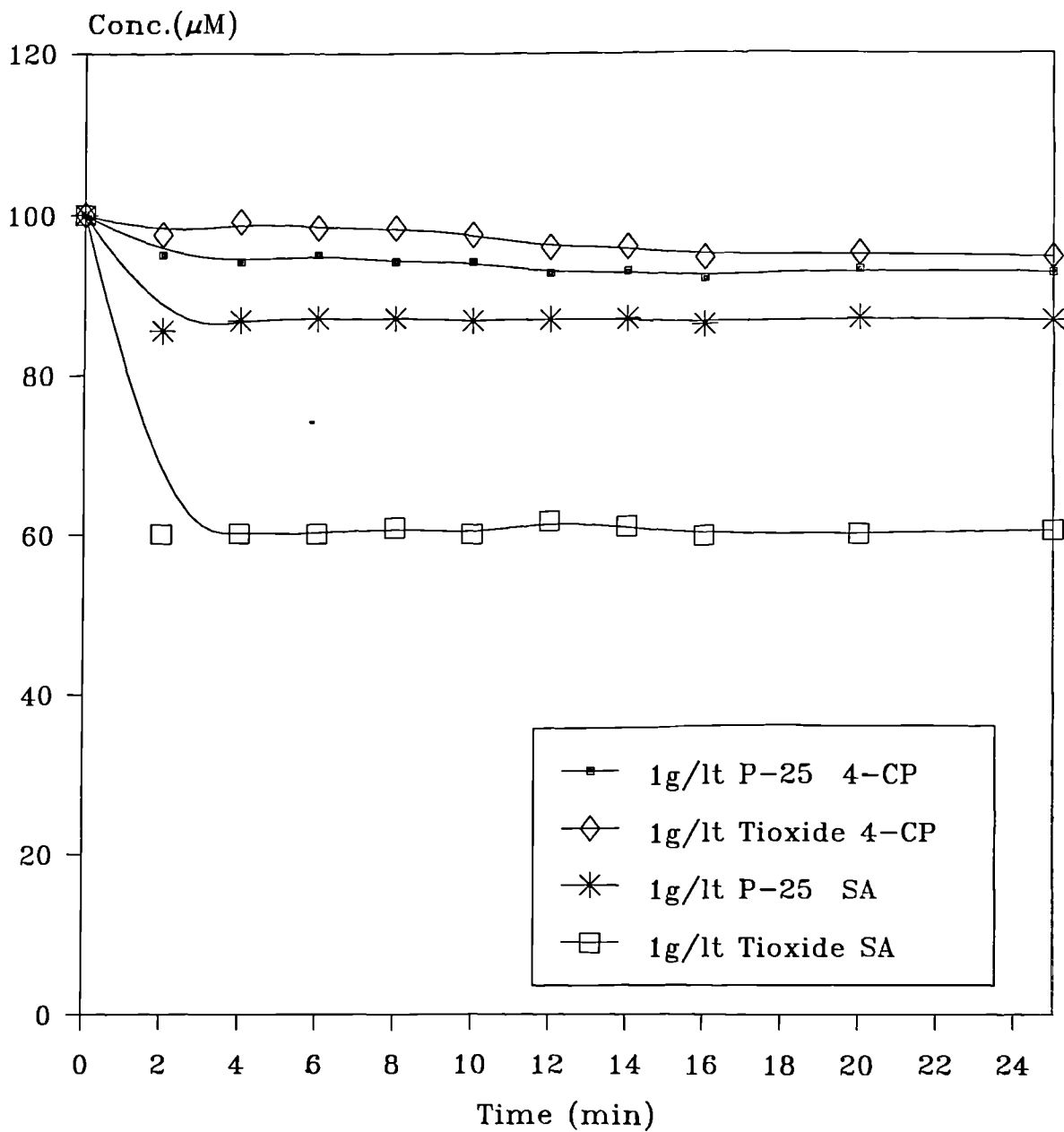
rate upon the performance of the annular reactor was assessed using slurries. The reaction used was the degradation of 100μM of a 2lt solution of salicylic acid. The catalyst used was Degussa P-25 (1g/lt) since the previous set of experiments had demonstrated that this type showed the most catalytic activity over salicylic acid. For this work the 400 W medium pressure lamp was used. Table 8.2 gives the first order reaction rate constants found from these experiments and the results are given in Figure 8.4.

Table 8.2 Effect of liquid flow rate upon the first order rate constant for salicylic acid degradation

Liquid flow rate (lt/min)	Rate constants k(min^{-1}) (r)
0.50	0.0571 (0.997)
0.75	0.0671 (0.995)
1.00	0.0810 (0.992)
1.25	0.0892 (0.994)

As can be seen from the observed rate constants, the rate of salicylic acid degradation increases with increasing liquid flow rate. When Matthews (1988) compared the aqueous solutions and immobilised surfaces of TiO_2, he concluded that no mass-transfer limitation was expected for photocatalysis using slurries of very fine catalyst particles of 1g/lt Degussa P-25 since the maximum diffusion distance was very small. It is said that differences in reaction rates observed under identical conditions in these systems have been attributed solely to the inherent surface reaction characteristics of different reactants on the photocatalyst.

Figure 8.4 Effect of liquid flow rate
upon the degradation of salicylic acid

93a
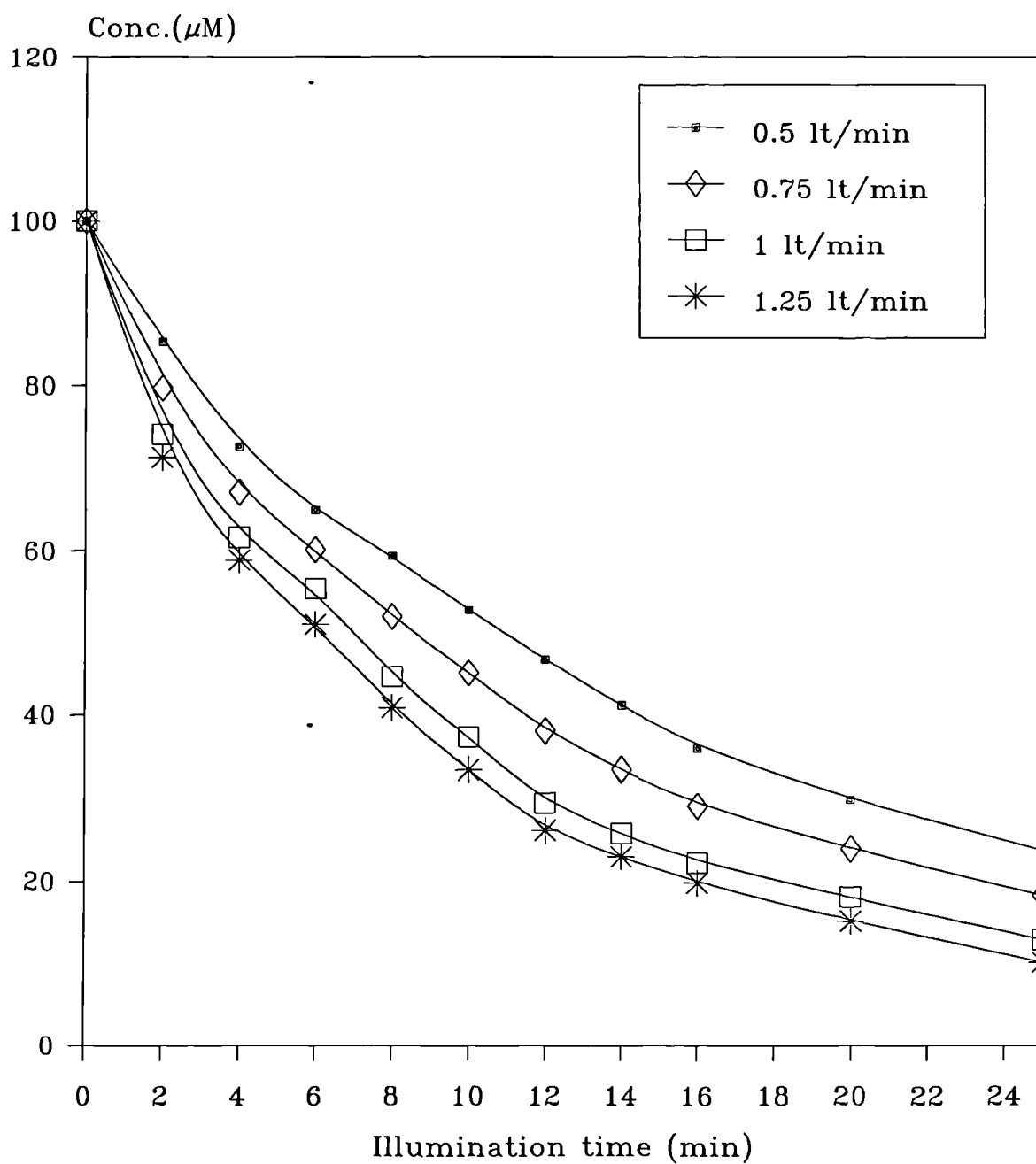
8.5 Comparison of two types of lamps

The two types of lamps produce

a) different wavelengths (Low pressure lamp emits over 90% of its radiation at 254nm, Medium pressure lamp emits predominantly 365-366nm radiation)

b) different intensities (Low pressure lamp with 3.10^{18} photon/s, Medium pressure lamp with 5.10^{19} photon/s)

in order to quantify the effect of the lamps, quantum yield was used.

Quantum yield results were calculated using Equation 5.11 (section 5.3) (Calvert and Pitts 1966, Braun et al. 1991) as explained with details in Appendix-C.

The degradation of two organic compounds (salicylic acid (SA) and 4-chlorophenol (4-CP)) was studied by using both low pressure and medium pressure lamps. Experimental conditions were as 100μM of a 2lt solution, 1g/lt of Degussa-P25 catalyst and flow rate 1lt/min. First order reaction rate constants and quantum yield results are given in Table 8.3 and Figure 8.5 shows the degradation curves.

Table 8.3 Effect of different light sources upon the first order rate constant using two organic compounds (4-CP and SA)

Lamp type	Organic compound	Rate constants $k(min^{-1})$ (r)	Quantum yield (%)
Low pressure	4-CP	0.0185 (0.990)	1.030
	SA	0.0225 (0.990)	1.418
Medium pressure	· 4-CP	0.0638 (0.970)	0.260
	SA	0.0810 (0.992)	0.293

Figure 8.5 Effect of different light
sources over two different organics
in Annular Reactor
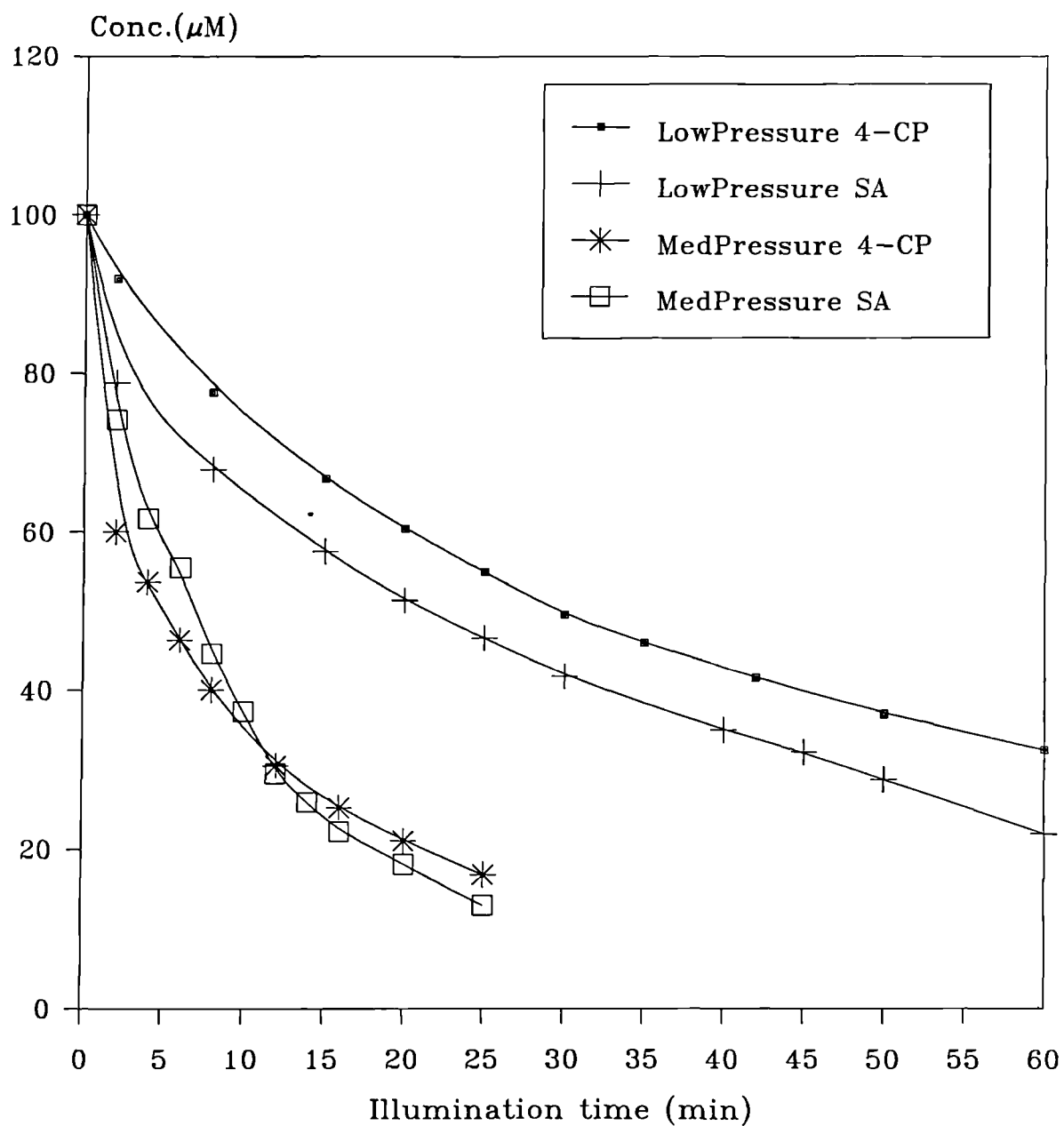
Rate constants and Figure 8.5 apparently show that the 400W medium pressure lamp has stronger photocatalytic effect due to the higher power used, whereas quantum yield results show that the 16W low pressure lamp photons were utilised more efficiently. This increase in quantum yield will also be related to the effectiveness of absorption and Figure 8.1.1 shows that P-25 absorbs more efficiently in the LP region than the MP region. This reveals the need to have more effective use of medium pressure lamp photons by improving reactor configuration and increasing chemical/catalyst/photon surface reaction efficiency or to increase the intensity of the low pressure lamp.

8.6   Effect of initial concentration

In order to perform how reaction rate changes by increasing the initial concentration of organic, the effect of initial concentration of salicylic acid was assessed with Degussa P-25 (1 g/lt) using 100, 250 and 500μM of 2lt solutions in 1lt/min flow rate. The medium pressure lamp was used for this work. Because the higher initial concentrations were used, the data obtained were fitted both first order kinetics by linear regression and Langmuir-Hinshelwood (L-H) kinetics (Equation 3.5) by non-linear regression by a multi-dimensional Newton method (see Appendix-A). The results were shown in Figure 8.6 as actual points and the both kinetics curves.

As can be seen from the observed curves (Figure 8.6), the data were fitted best to the first order kinetics model. Attempts to fit results to the L-H

Figure 8.6 Effect of initial conc. upon
the degradation of salicyliic acid
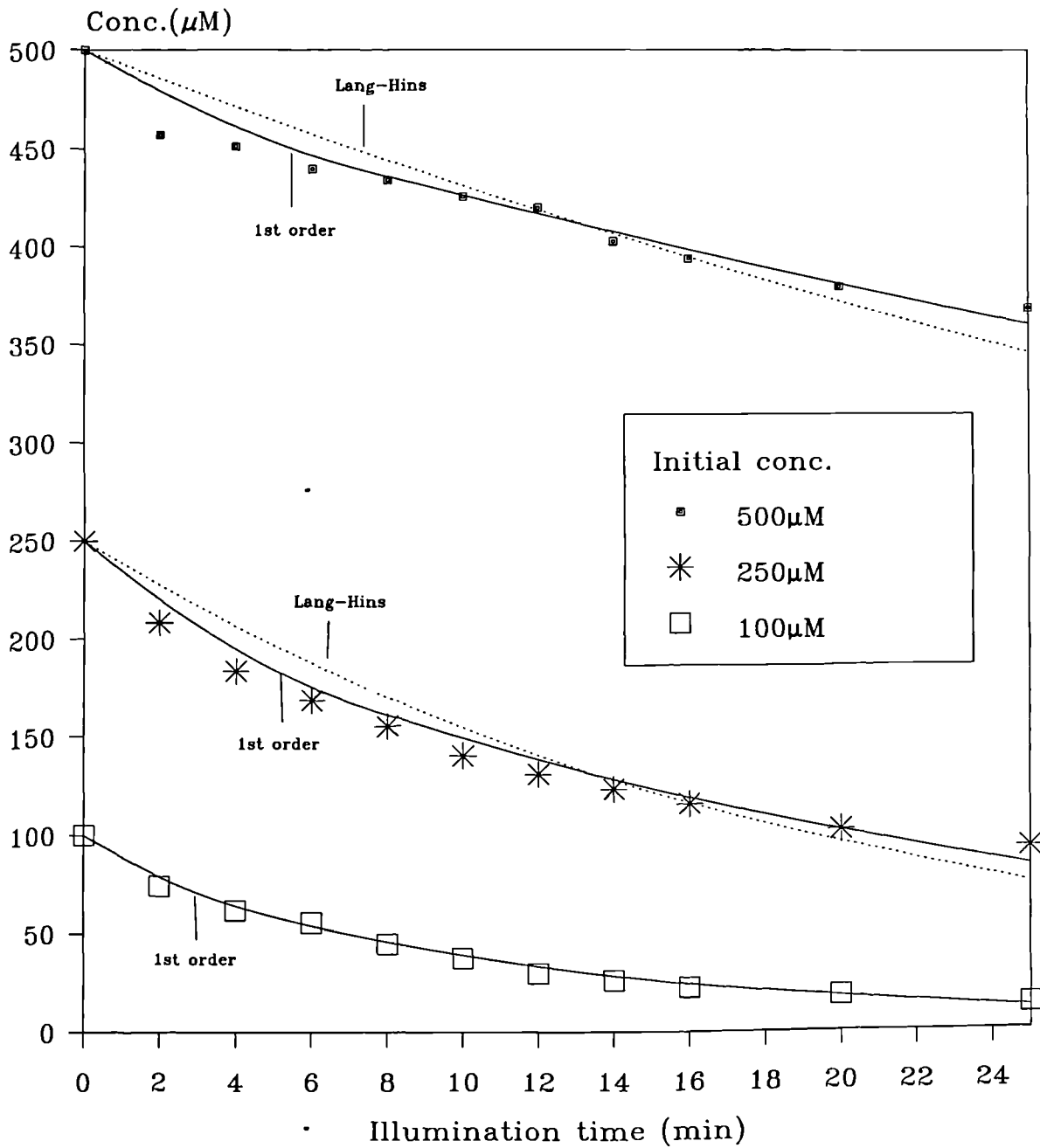
kinetics model were not as successful as the first order kinetics model due to the nature of this reactor. From this point, the first order rate constants and the calculated quantum yield results were tabulated in Table 8.4.

Table 8.4 Effect of initial concentration upon the degradation of salicylic acid by first order rate constants

Initial conc. of salicylic acid (μM)	Rate constants k(min⁻¹) (r)	Quantum yield (%)
100	0.0810 (0.992)	0.293
250	0.0385 (0.977)	0.344
500	0.0113 (0.975)	0.175

Although the reaction rate decreases by increasing the initial concentration, quantum yield results show that reaction efficiency increases to a optimum point and drops.

CHAPTER IX

9. Results of photocatalytic studies in the falling film reactor (FFR)

Experimental results based on the FFR are performed in this section and samples of some experimental data having identical conditions have been evaluated with sample standard deviation. These results are tabulated in Appendix-D.

9.1 Effect of catalyst concentration and choice of catalyst

In order to select standard operating conditions for the catalyst concentration and types, preliminary work was carried out for future experiments. The first experimental results were obtained using 100µM 10lt salicylic acid solutions to compare the efficiency of Degussa P-25 and Tioxide PC1 type catalysts and concentrations. Like the annular reactor samples (see Chapter-8), all samples from the FFR were analysed by HPLC using same eluent solution. The flow rate used was 5lt/min. The light source was a 2.5kW medium pressure lamp.

Figure 9.1 shows Degussa P-25 to be more active than Tioxide, but there is an initial rapid fall in the concentration with the Tioxide catalyst which suggests that this type has stronger physical adsorption as was seen in the annular slurry reactor results. But unlike the annular reactor, it is clear

Figure 9.1 Effect of catalyst type
on the degradation of salicylic acid
in Falling Film Reactor
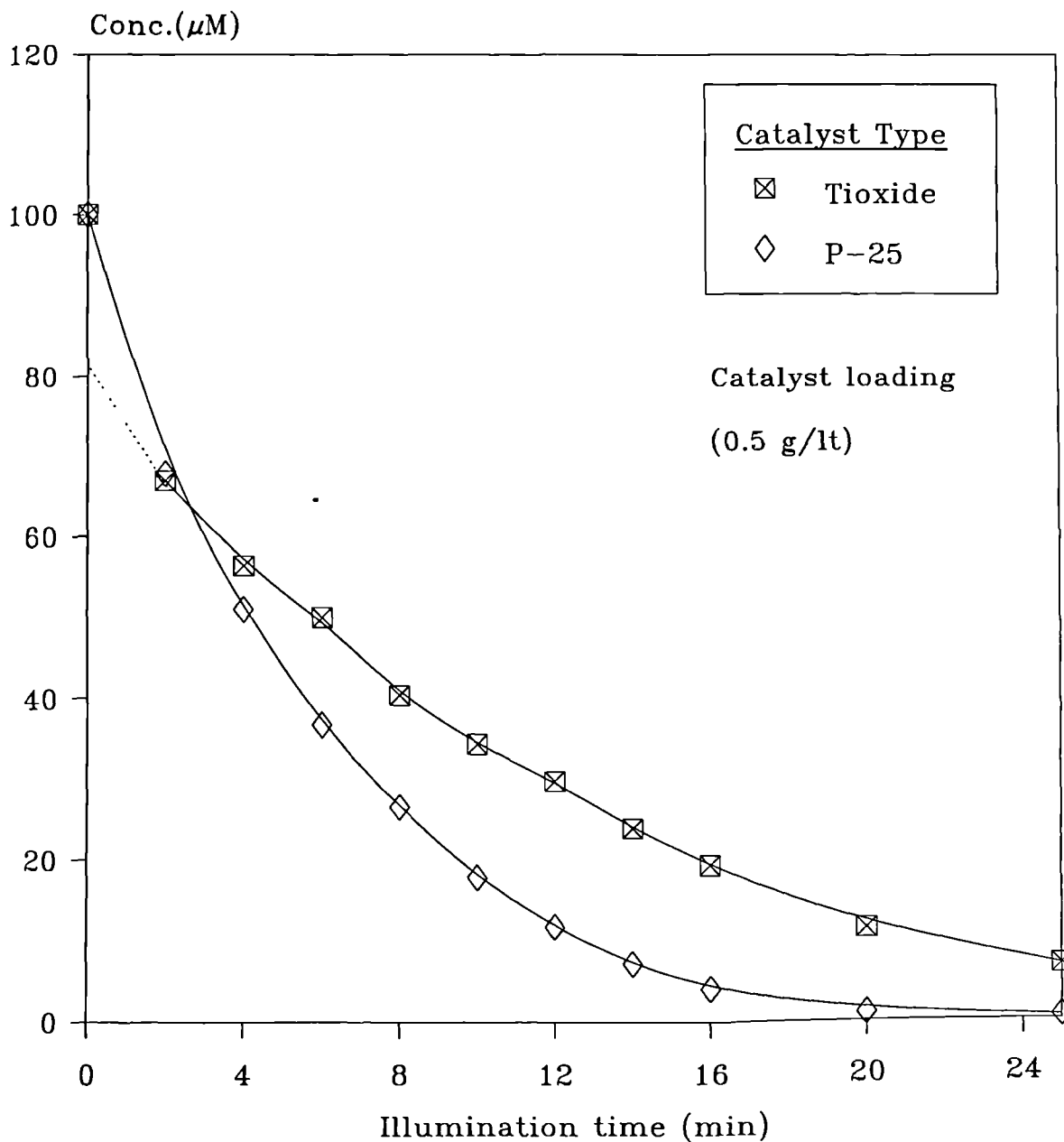
Figure 9.2 Effect of catalyst loading
in Falling Film Reactor
−Salicylic Acid−
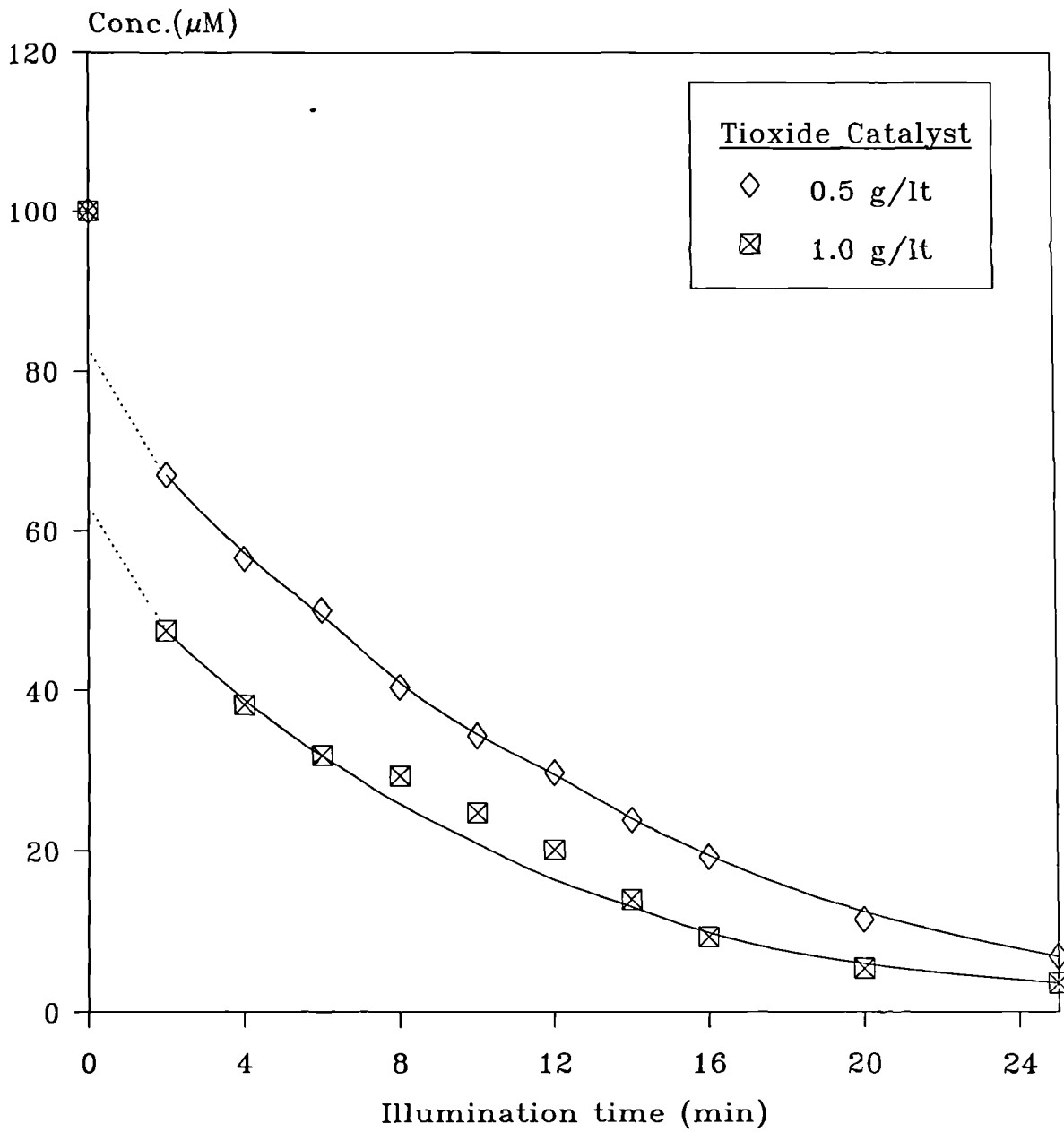
Figure 9.3 Effect of catalyst loading
in Falling Film Reactor
−Salicylic Acid−
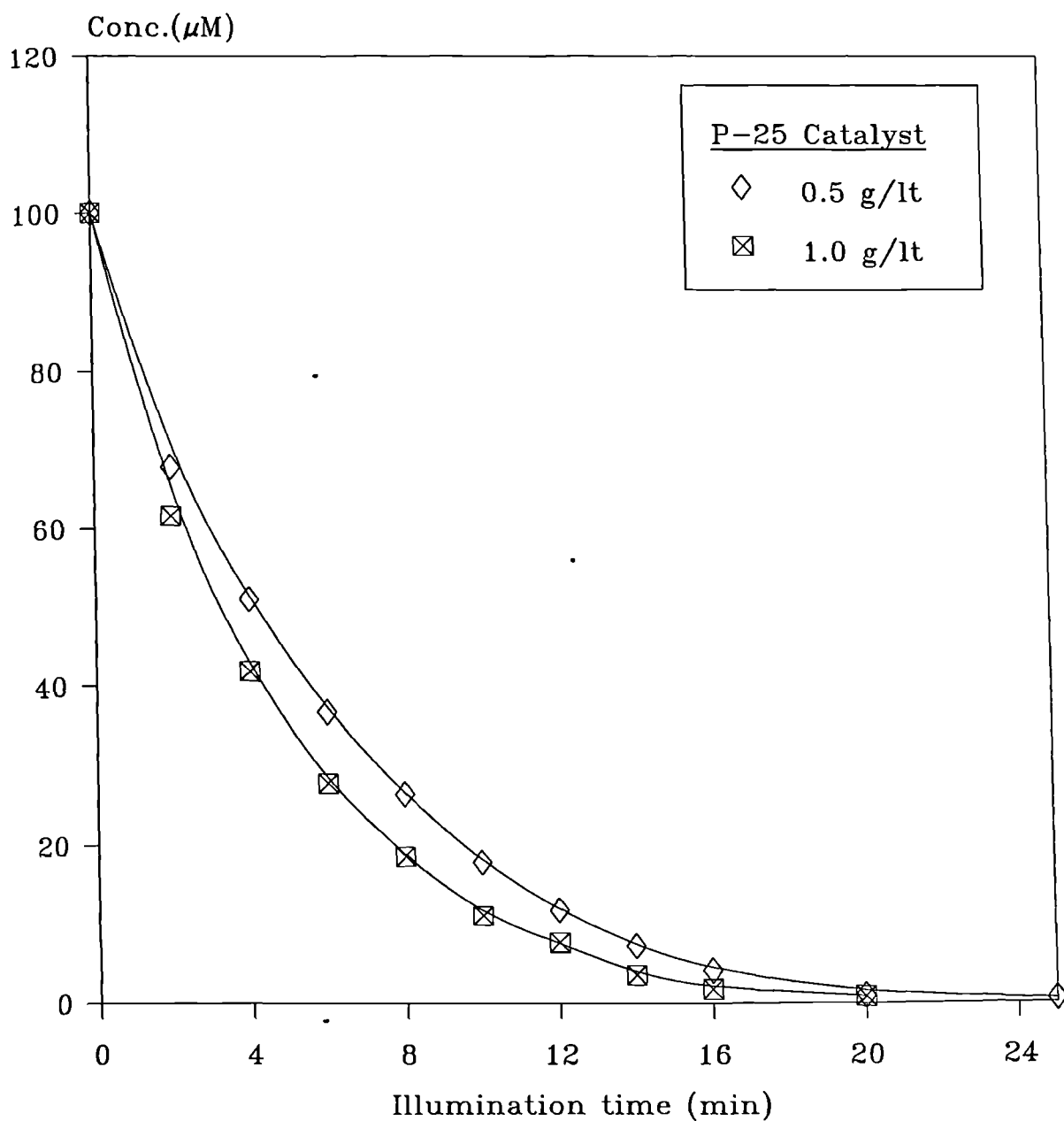
that with this type of reactor less catalyst is needed for efficient operation (Figure 9.2 and 9.3). One of the main reasons for less catalyst requirement could be attributed to the thin film characteristics of FFR, such as effective oxygen take up at gas/liquid interface and/or effective photon absorption on catalyst surface.

In the light of these results all further experiments were carried out using P-25 type catalyst of 0.5g/lt concentrations.

Using 10lt of 100μM initial concentrations Figure 9.4 shows a rapid rate of destruction for salicylic acid (SA) and 4-chlorophenol (4-CP) and the rates obtained were fitted both Langmuir-Hinshelwood (L-H) and pseudo-first order kinetic models, the results are shown in Table 9.1 for both reactants.

Table 9.1 Kinetic rates for 100μM initial concentration

Organic chemical	L-H kinetic rates				First order rates	
	$k_1(\mu M^{-1})$	$k_2(\mu Mmin^{-1})$	(SSE)	$t_{1/2}$	$k(min^{-1})$	(r)
SA	$7.07*10^{-3}$	33.53	(0.82)	4.41	0.194	(0.995)
4-CP	$2.40*10^{-3}$	126.03	(0.67)	2.68	0.284	(0.997)

(SSE=sum of squared errors, data fits best if SSE is as less as zero; r=correlation coefficient, data fits best if r is as near as to 1)

As can be seen from Table 9.1, a very good fit was obtained from both pseudo-first order and L-H kinetic rates for 100μM initial concentration.

Figure 9.4 Destruction of reactants
with 100μM initial concentration
in Falling Film Reactor
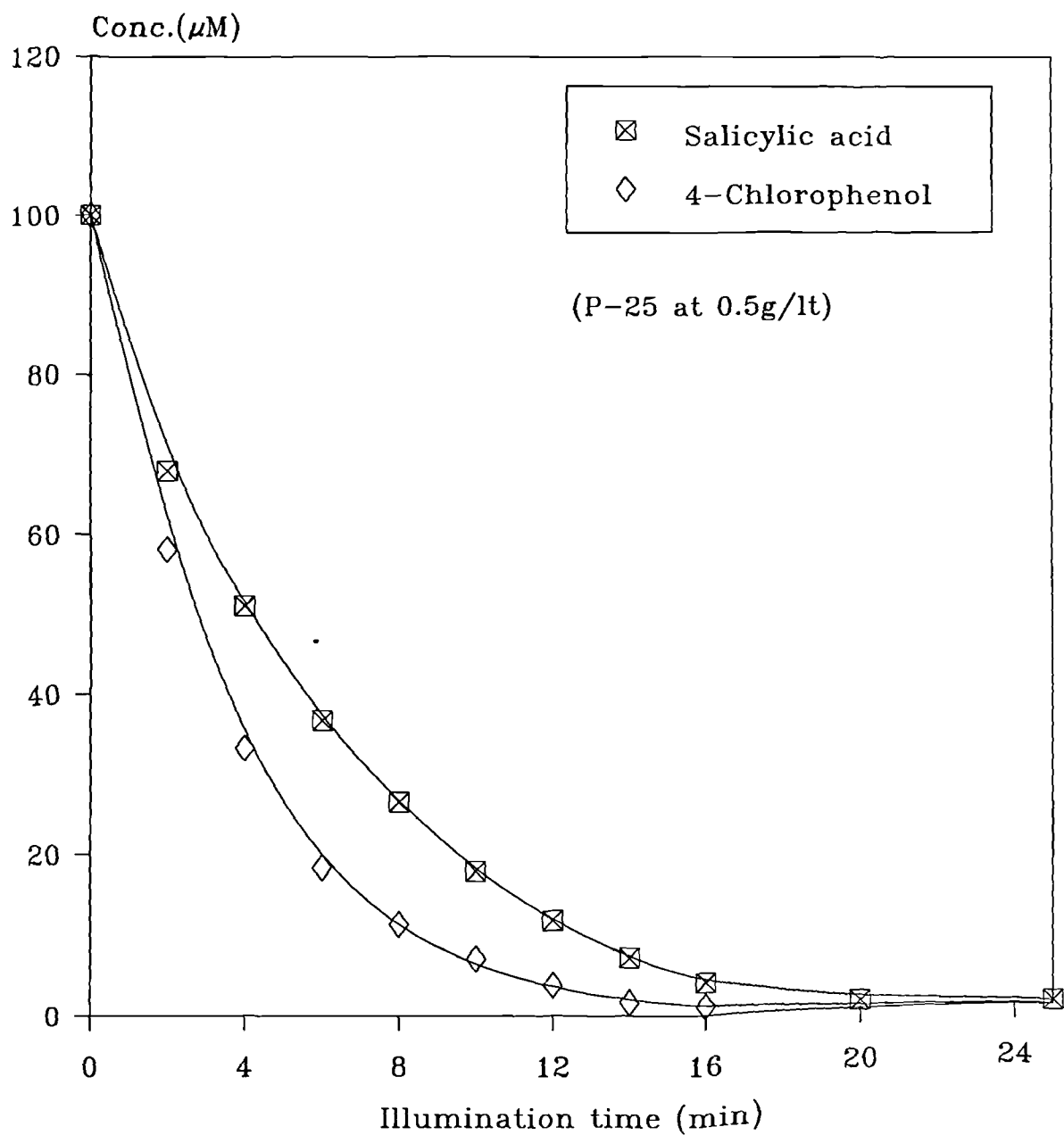
9.2   Effect of initial concentration

9.2.1   Rate constants

Further results were obtained at 10lt of 250μM concentrations and other reactants were used namely catechol (CA) and hydroquinone (HQ). These two organics were determined by HPLC as the main intermediate products of salicylic acid and 4-chlorophenol degradation, respectively. Flow rate was 5lt/min. Both kinetic rates are shown in Table 9.2.

Figure 9.5 shows the experimental data points and the curves obtained from pseudo-first order kinetic model, meanwhile Figure 9.6 shows the same experimental data points but the curves obtained from L-H kinetic model.

Table 9.2   Kinetic rates for 250μM initial concentration

Organic chemical	L-H kinetic rates				First order rates	
	$k_1(\mu M^{-1})$	$k_2(\mu Mmin^{-1})$	(SSE)	$t_{1/2}$	$k(min^{-1})$	(r)
CA	$3.13*10^{-3}$	17.47	(0.65)	19.83	0.0357	(0.998)
HQ	$3.43*10^{-4}$	148.29	(1.09)	14.47	0.0479	(0.999)
SA	$3.07*10^{-3}$	26.70	(1.56)	13.13	0.0551	(0.995)
4-CP	$2.98*10^{-4}$	752.26	(0.13)	3.25	0.2212	(0.999)

As can be seen from both figures (9.5 and 9.6) and Table 9.2, both kinetic models fit the experimental data perfectly for 250μM initial concentrations, similar fit was also obtained for 100μM initial concentrations (Table 9.1).

Figure 9.5 Destruction of reactants with 250μM initial concentration in 1st order kinetic model curves (FFR)
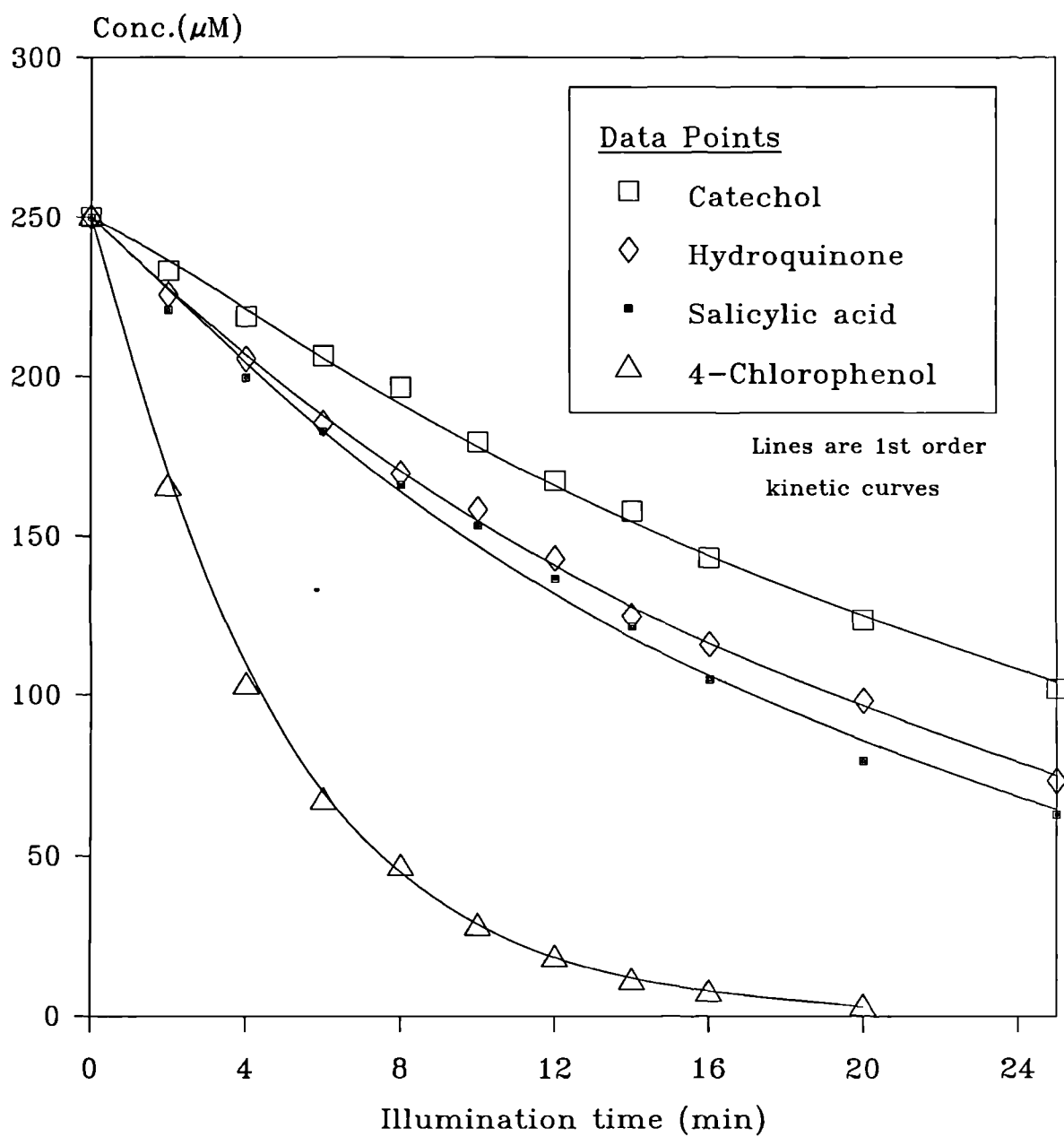
Figure 9.6 Destruction of reactants
with 250μM initial concentration
in L-H kinetic model curves (FFR)

Conc.(μM)

Illumination time (min)

Data Points

□ Catechol

◇ Hydroquinone

■ Salicylic acid

△ 4-Chlorophenol

Lines are L-H
kinetic curves
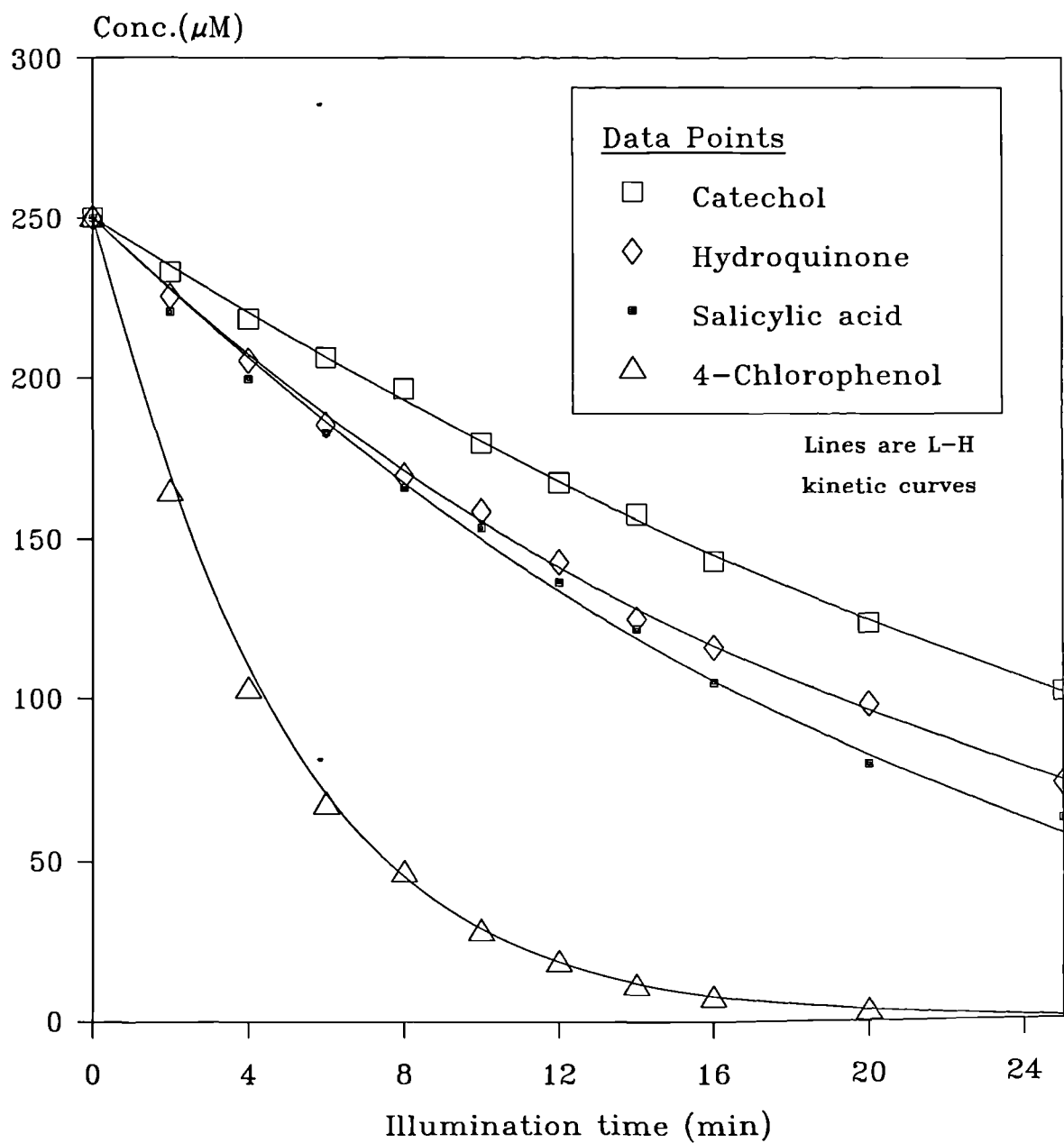
9.2.2 The effects of intensity and quantum yields

In order to calculate the quantum yield the output from the lamp is needed. Unlike the medium-pressure and low-pressure lamps used in the annular reactor (Chapter-7), the output power of the medium-pressure lamp used in the FFR is not given by the manufacturer. Therefore it was necessary to assess the intensity of this high power medium-pressure lamp. In order to do this, a convenient method was chosen and a measuring system was devised considering the geometry of falling film reactor. The procedure and the equipment are given as follows:

9.2.2.1 Light intensity measurements of medium-pressure lamp with potassium-ferrioxalate actinometer system

Chapter-5 discussed methods of determining light intensity, thus in order to relate conversion to intensity, the medium-pressure lamp used in the falling film reactor is investigated for light intensity measurements by using potassium-ferrioxalate actinometer solution (Chapter-5, Calvert and Pitts 1966). The equipment to measure the intensity of the light is devised to get the light distribution as uniform as possible. The input power of this medium pressure lamp by the manufacturer is reported to be 2.5kW. Because of this high power output, it makes difficult to devise such an equipment to measure the light intensity by an actinometer solution since the solution is even very sensitive to low light outputs, but it gives more reliable results. Figure 9.7 shows the schematic layout of measurement equipment from front and side positions. An aluminium reflector in 1.0x1.0m size is concaved inwards to make uniform light distribution. A perspex plate with eight separated V-

shaped sections is used and each one is filled with 40*ml* actinometer solution. For this a 0.006*M* solution of $K_3Fe(C_2O_4)_3$ (potassium-ferrioxalate BDH grade) was used. To prepare the 0.006*M* solution of $K_3Fe(C_2O_4)_3$, 2.947 grams of the solid are dissolved in 800*ml* of H_2O, 100*ml* 1.0*N* H_2SO_4 are added, and the solution is diluted to 1 litre and mixed. As indicated by Hatchard and Parker (1956), a 0.006*M* solution of $K_3Fe(C_2O_4)_3$ can be used conveniently for wavelengths up to 430nm and a standard calibration graph for analysis of the Fe^{2+} complex is prepared according to their recommended procedure for use with the UV-visible spectrophotometer (Uvikon 810). A linear plot of molar concentration of Fe^{2+} complex versus $\log(I_0/I)$ which is the measured optical density of the solution at 510nm gives the apparent molar extinction coefficient ε (slope of plot), it was found as $ε = 1.1137*10^4$ *liters/mole-cm*. To determine the light intensity distribution of the medium-pressure lamp, the 40*ml* 0.006*M* ferrioxalate solution is added to each section of perspex plate and irradiated for 5 seconds. This is repeated for different lamp positions (*a* and *b cm*) and the different positions of perspex plate to analyse the light intensity distribution. The qualitative notion of the intensity of the light beam is experienced by regulating the time of exposure in order to produce about $5*10^{-8}$ mole of Fe^{2+}/ml (Hatchard and Parker-1956), and is best found as 5 seconds.
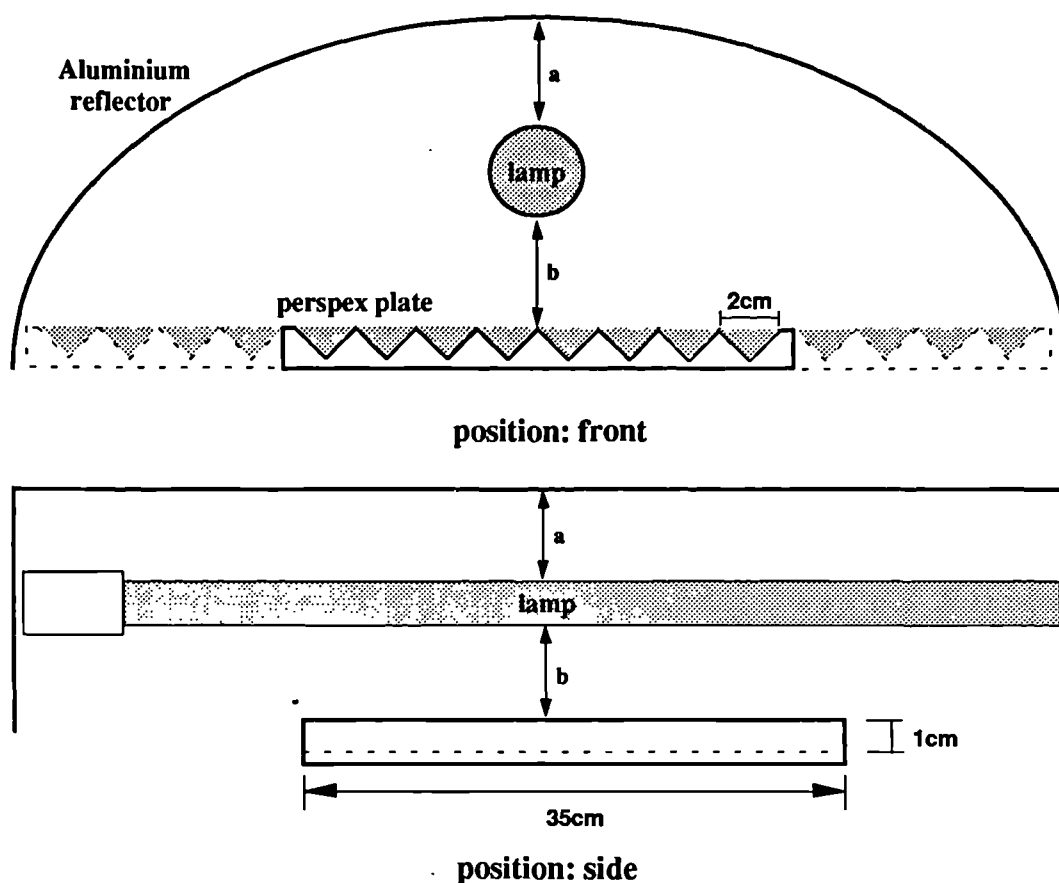
Figure 9.7 Light intensity measurement of medium-pressure lamp with potassium ferrioxalate actinometer solution using perspex plate under aluminium reflector

Experimental procedure. After an irradiation of 5 seconds of 40*ml* ferrioxalate solution in each section of perspex plate, 1*ml* sample of solution from each is taken into a 100*ml* volumetric flask; 2*ml* of the phenanthroline solution (containing 0.1% (by weight) 1,10-phenanthroline in water) and a volume of buffer solution (600*ml* of 1N sodium acetate and 360*ml* 1N H_2SO_4 diluted to 1 liter) equal to half the volume of photolyte (1*ml*) are added to the flask, diluted to 100*ml* and mixed well allowing to stand for 1 hr in the dark. The same procedure is also prepared for an identical but unirradiated solution for use as the blank in the reference beam and is allowed to stand as before. The transmission of the each solution is measured in the spectrophotometer at 510nm in a 1*cm* path-length cell, using the blank solution in the reference

beam. The number of ions of Fe^{2+} formed during the photolysis $(n_{Fe^{2+}})$ is calculated by using (Calvert and Pitts 1966):

$$n_{Fe^{2+}} = \frac{6.023 \times 10^{20} V_1 V_3 \log_{10}(I_o/I)}{V_2 l \varepsilon}$$

(9.1)

where;

$V_1 =$ the volume of actinometer solution irradiated (ml)

$V_2 =$ the volume of aliquot taken for analysis (ml)

$V_3 =$ the final volume to which the aliquot V_2 is diluted (ml)

$\log_{10}(I_o/I) =$ the measured optical density of the solution at 510nm

$l =$ the path length of the spectrophotometer cell used (cm)

$\varepsilon =$ the experimental value of the molar extinction coefficient of the Fe^{2+}

complex as determined from the slope of the calibration plot

$(1.1137 \times 10^4 \ liters/mole\text{-}cm)$

The light intensity incident can be calculated using the modified form of Eq. (5.11), (Chap. 5.3):

$$I_i = \frac{n_{Fe^{2+}}}{\Phi_{Fe^{2+}} A t} \ quanta / s.cm^2$$

(9.2)

where;

$n_{Fe^{2+}} =$ the number of ions of Fe^{2+} formed during the photolysis

$\Phi_{Fe^{2+}} =$ quantum yield of Fe^{2+} in the ferrioxalate actinometer at 366nm given

by Hatchard and Parker (1956) as 1.21

$A =$ the area of the each section of perspex plate $(70cm^2)$

$t =$ the time of exposure (5 $seconds$)

103

Intensity (quanta/s.cm^2)*10^{17}

Distance
a=lamp-reflector
b=lamp-surface

a=1cm b=15cm
a=6cm b=10cm
a=11cm b=5cm

1.9 1.7 1.5 1.3 1.1 0.9 0.7 0.5 0.3

-25 -20 -15 -10 -5 0 5 10 15 20 25

Distance from centre (cm)
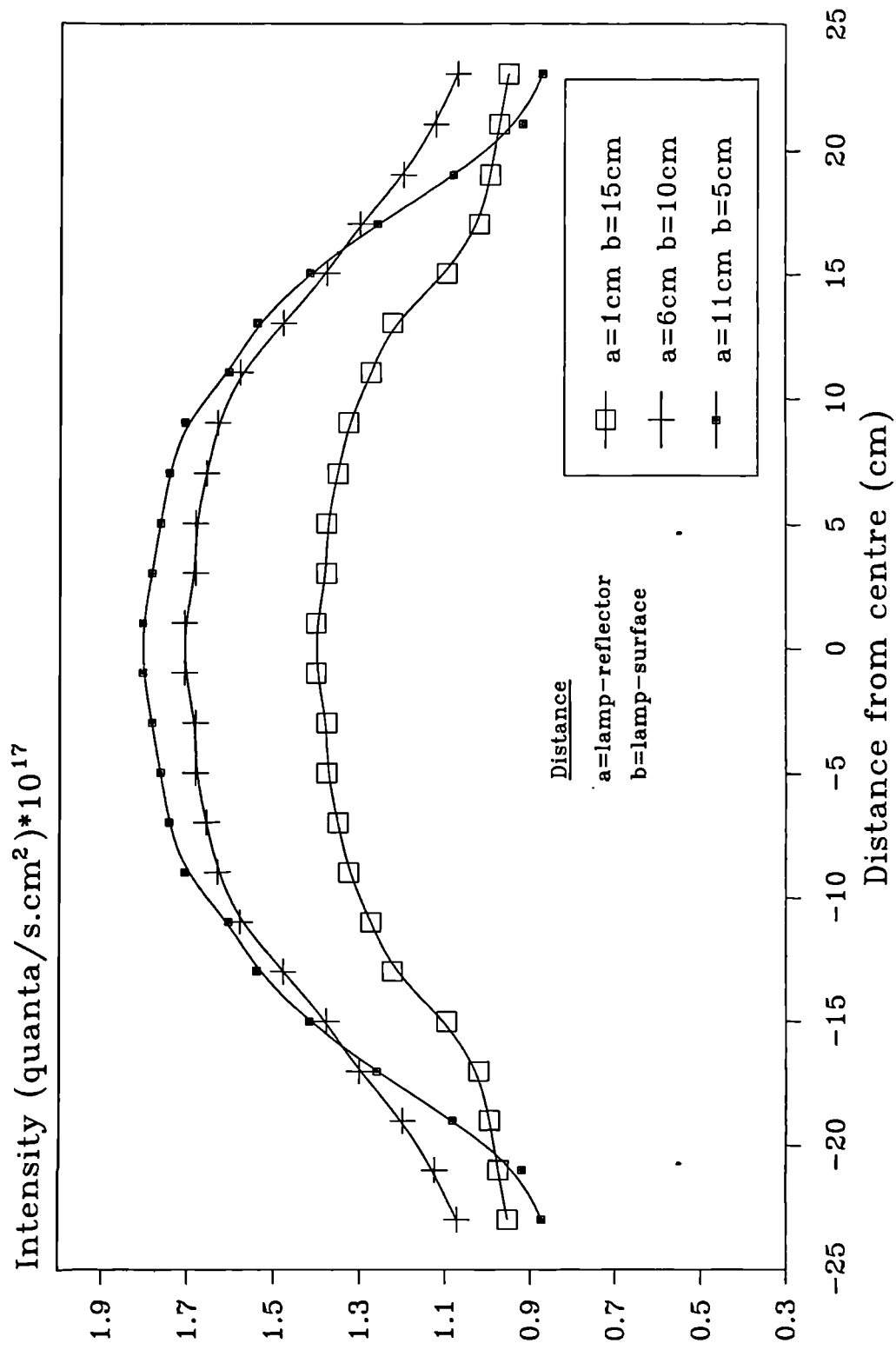
Figure 9.8 Light intensity distribution
of medium-pressure lamp used in FFR

The experimental results with different positions of lamp under the aluminium reflector are shown in Figure 9.8. The maximum value of intensity is obtained as $I_i = 1.8 \times 10^{17}$ quanta/s.cm^2 at 5cm distance from the lamp.

Using the destruction rate and the intensity, it is possible to calculate the quantum yield as in Appendix-C.

For both initial concentrations quantum yield results were tabulated to evaluate the initial concentration effect of SA and 4-CP in falling film reactor (Table 9.3).

Table 9.3 Quantum yields and first order rates for 100 and 250µM initial concentrations based on SA and 4-CP

Organic chemical	Initial conc. (µM)	First order rates			Quantum yield (%)
		k(min^{-1})	(r)	t$_{1/2}$	
SA	100	0.194	(0.995)	4.41	0.253
	250	0.055	(0.995)	13.13	0.212
4-CP	100	0.284	(0.997)	2.68	0.416
	250	0.221	(0.999)	3.25	0.858

9.2.3 Intermediate formation

If the falling film reactor performance is to be fully understood, it is necessary to consider whether total mineralisation occurs. Figure 9.9 shows that intermediates are formed with salicylic acid and 4-chlorophenol, as catechol and hydroquinone respectively. Intermediate detection was made by HPLC during the main reactant analysis. As seen from the figure intermediate formation and degradation occurs simultaneously with primary reactants.

Figure 9.9 Salicylic acid, 4-CP
removal with intermediates (FFR)

104a
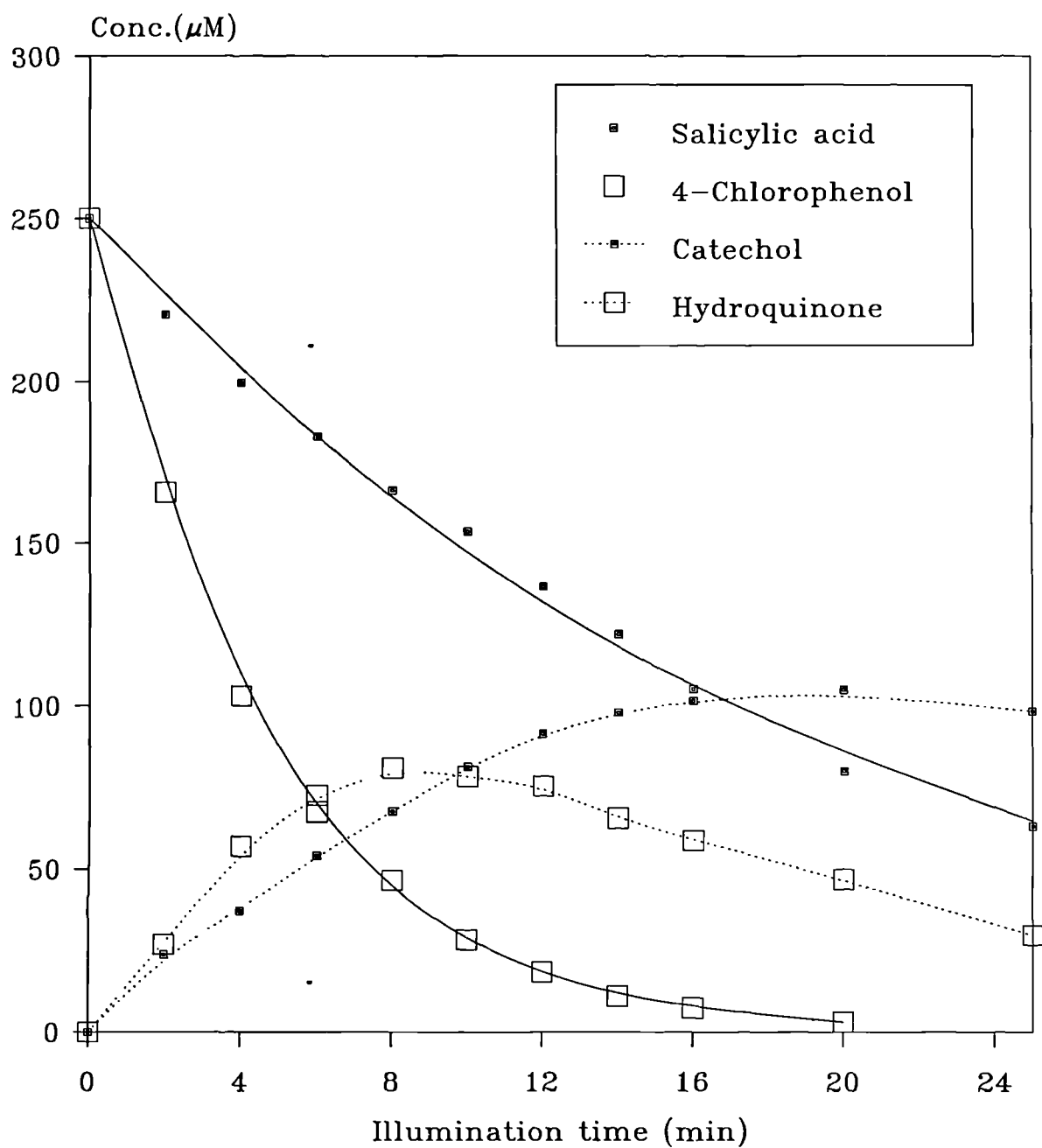
9.3   Effect of liquid flow rate

9.3.1   Film thickness and flow type in FFR

Because it is useful to assess the degree of conversion as a function of flow rate, it is necessary to relate this to both thickness and flow regime. The mathematical model for an average velocity of vertical flow of a falling film is indicated as following in Chapter-6, Eq. (6.20) (Bird et al. 1960):

$$V_{Z_{Av}} = \frac{\rho g \delta^2}{3\mu} \qquad (9.3)$$

and Re number as in Eq. (6.23),

$$Re = \frac{4\delta \rho V_{Z_{Av}}}{\mu} \qquad (9.4)$$

where ρ is density ($997.08 kg/m^3$ at $25°C$) of the liquid, δ is the average film thickness and μ is viscosity ($0.893.10^{-3} kg/m.s$ at $25°C$). The values of ρ and μ *are assumed as near to water.*

Meanwhile volumetric flow rate can be obtained by multiplying the average velocity and the cross sectional area:

$$Q = W\delta V_{Z_{Av}} = \pi D \delta V_{Z_{Av}} \qquad (9.5)$$

$\pi D \delta$ is cross-sectional area of a falling film in a vertical tube.

105

When equations (9.3) and (9.5) are combined, the film thickness is defined in terms of the average velocity and the volumetric flow rate as in Eq. (6.22):

$$\delta = \left(\frac{3\mu Q}{\rho g \pi D}\right)^{1/3} \tag{9.6}$$

and from equations (9.4) and (9.5), Re number can also be defined as,

$$Re = \frac{4\rho Q}{\pi D \mu} \tag{9.7}$$

Table 9.4 shows the film thicknesses and Re numbers for different flow rates.

Table 9.4 Film thicknesses and Re numbers based on different flow rates

Flow rate Q (lt/min)	Average film thickness δ (mm)	Re number
5	0.417	1185.2
7.5	0.478	1776.9

9.3.2 Results and discussion

The effect of liquid flow rate in the falling film reactor was assessed using salicylic acid slurries of 10lt-100µM and pseudo-first order rates were tabulated in Table 9.5.

Table 9.5 Effect of liquid flow rate and residence time upon the first order
rate constant

Flow rate (Q) (*lt/min*)	Residence time (RT) inside the reactor (s) $(V=\pi D\delta L)$ $(RT=V/Q)$	Rate constants	
		$k(min^{-1})$	(r)
5.0	1.26	0.194	(0.994)
7.5	0.96	0.206	(0.985)

As the rate constants results show, flow rate increase has no significant effect on salicylic acid degradation. However, the flow rate and the residence time must be assessed to set the reactor configurations properly. Residence time is an important parameter in continuous flow through reactor systems. In this falling film reactor, increased flow rate has given shorter residence time, but the results showed that degradation rates did not drop with shorter residence time but were slightly increased. The question of why this occurs is not clear, the increase in flow rate produces a thicker film but a shorter residence time. It also increases the Re number as shown in Table 9.4 thus more turbulence is expected. The balance of increased turbulence hence better mass transfer together with increased film thickness with more light absorption against reduced residence time is difficult to assess. It is likely that an optimum condition can be arrived at for different reactor geometries.

It is interesting to note that Sczechowski et al. (1993) did arrive at optimum illumination times. In their work, they performed the periodic illumination of the photocatalyst to increase the photoefficiency in heterogeneous photocatalysis. They claimed that the periodic illumination generates the electron/hole pairs that drive the oxidation process, however, the actual decomposition reaction can take place during the dark intervals. They, therefore, carried out experiments to determine the most effective

illumination time as well as the dark recovery time and using optimal illumination and dark recovery times, the photoefficiency was increased 500% compared to the continuous illumination experiment. Shoffner et al. (1993) also performed similar work and agreed that electron/hole pairs generated by UV light initiate the oxidation of organics and this oxidation process continues to occur without illumination for short time periods. They worked out optimal light and dark periods and the increase in quantum efficiency for ethylene glycol in a continuous flow channel reactor.

These studies reveal the importance and the advantage of the optimal light and dark periodic times and hence could explain the increase of degradation with increased flow rate and decreased residence time in this work. Once the aqueous solution picks up the photons inside the falling film reactor, degradation reaction still continues inside the holding tank and increased flow rate improves the periodic illumination time. This might be the advantage of using continuous flow through reactors.

9.4   Effect of oxygen mass transfer

Efficient oxygen transfer is important in photocatalytic reactor design and with a high intensity lamp it was necessary to determine whether the reaction was oxygen limited in the falling film reactor. Oxygen diffusion in a laminar falling film is assessed theoretically in Chapter-6 and a model equation is derived, Eq. (6.34). Based on this equation the following compilation is made:

$$M_A = (LW)c_{Ao}\sqrt{\frac{4D_{AB}v_{max}}{\pi L}} \qquad (9.8)$$

Using Eq. (6.17) for $v_{max} = \rho g \delta^2 / 2\mu$ and $W = \pi D$;

$$M_A = (L\pi D)c_{Ao}\delta\sqrt{\frac{2D_{AB}\rho g}{\mu \pi L}} \qquad (9.9)$$

and using the values; $D_{AB} = 24 \ 10^{-6} \ cm^2 s^{-1}$, diffusivity of oxygen in water at 25°C (Brodkey and Hershey 1988), $c_{Ao} = 2.53 \ 10^{-7} \ mol \ cm^{-3}$, solubility of oxygen from air in water at 25°C (Linke and Seidell 1965), the rate of oxygen mass transfer (M_A) to the liquid surface is tabulated in Table 9.6 for different film thicknesses.

Table 9.6 Oxygen mass transfer rate to laminar falling film

Film thickness δ (mm)	Mass transfer rate M_A (mol/s)	No of moles O_2 transferred (M_A*RT)
0.417	3.79*10^{-6}	4.77*10^{-6}
0.478	4.35*10^{-6}	4.18*10^{-6}

Because of the high rate degradation, 4-CP and its intermediate hydroquinone was used for the experimental investigation. In order to establish that the falling film reactor could provide good oxygen transfer at the film/air interface, the holding tank and the bottom of the reactor were sparged and blanketed with nitrogen. Using 10lt of 250μM 4-CP slurry solution, Figure 9.10 clearly shows that sufficient oxygen is supplied within the reactor to carry out the primary destruction stage, but the intermediate removal appears to be oxygen deficient. The flow rate was 5lt/min.

Figure 9.10 Effect of oxygen
transfer within reactor (FFR)

109a
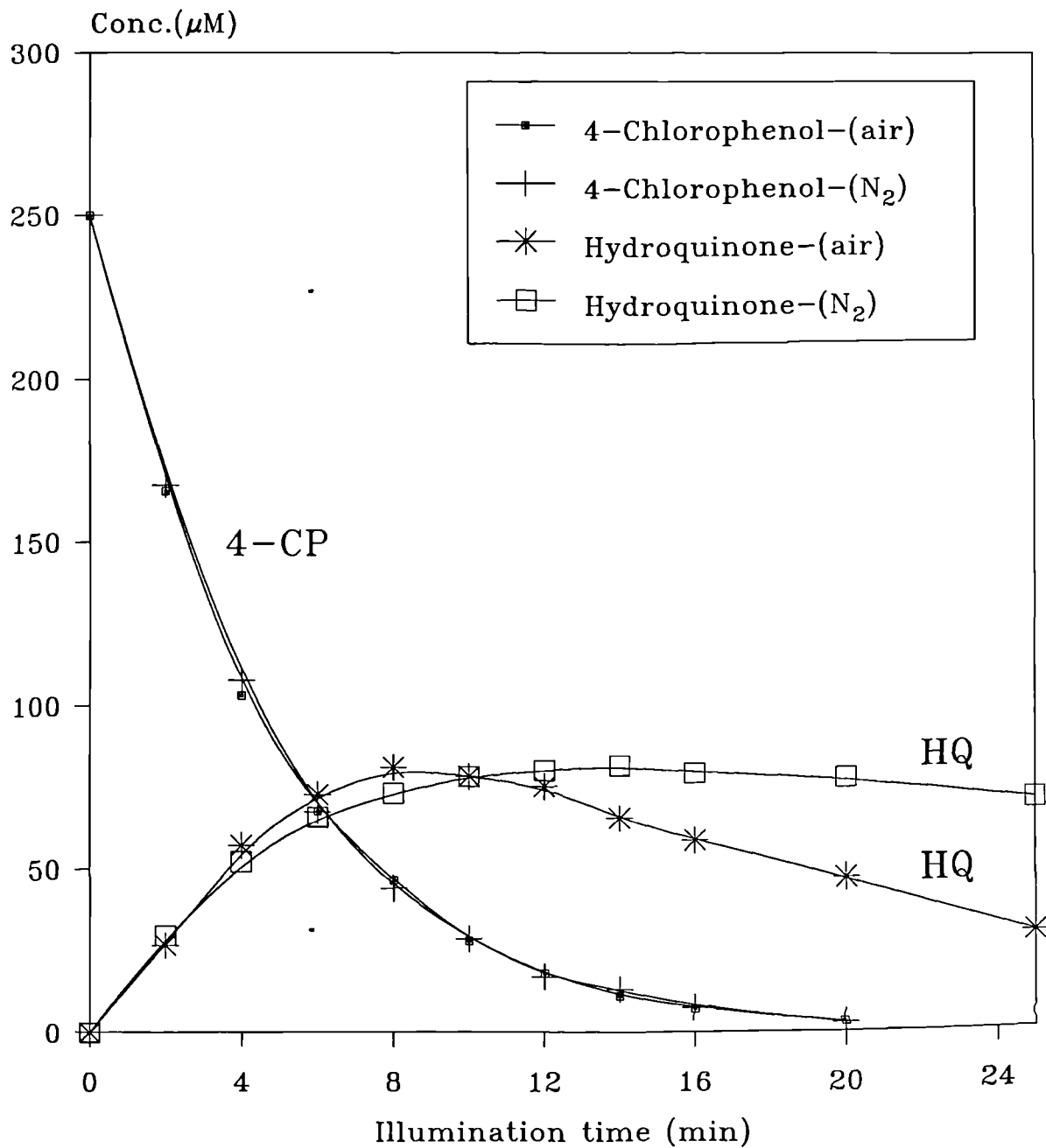
Figure 9.11 pH variation for four organics in slurry system (FFR)

109b
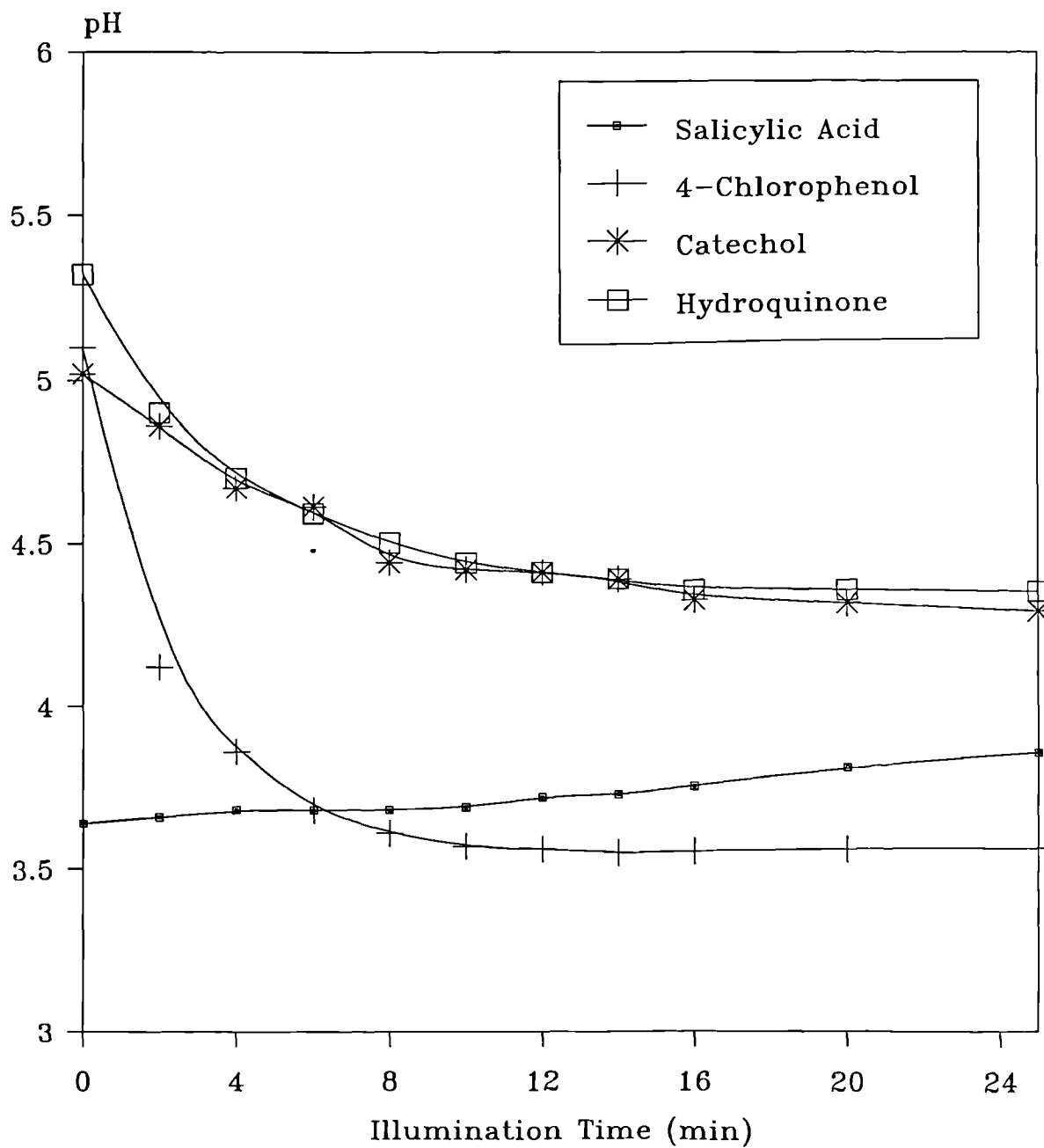
Matthews (1987a) also supplied external oxygen to his system which was essential by a long plug flow reactor without any oxygen transfer as the reaction proceeded. He found 77% higher efficient degradation in TiO_2 suspensions.

9.5 Change in pH levels due to degradation

With the high intensity lamp used in the FFR it was noted that the pH changed due to higher rate of degradation therefore these changes were monitored. During the experiments, temperature of liquid was kept constant at around 25±2°C depending on the tap water temperature inside the cooling coil and the air temperature sparged into the liquid holding tank.

pH variations during the degradation process for four organics in slurry system (10lt of 250µM solutions) were shown in Figure 9.11. Results show that pH for salicylic acid degradation was almost constant (~3.7). For hydroquinone and catechol degradation, it followed a slight initial drop from ~5 to 4.5, but for 4-chlorophenol degradation there was a significant initial drop compare to others (from ~5 to 3.5). This could be explained by high rate degradation of 4-chlorophenol to the final products CO_2 and HCl. In their study with 4-chlorophenol, Al-Ekabi et al. (1989) reported the same pH drop and suggested the formation of some acidic intermediates which was subsequently converted to the final products CO_2 and HCl.

Figure 9.12 Salicylic acid, 4-CP removal
with intermediates using Nutech
catalyst coated fibre glass gauze (FFR)

110a
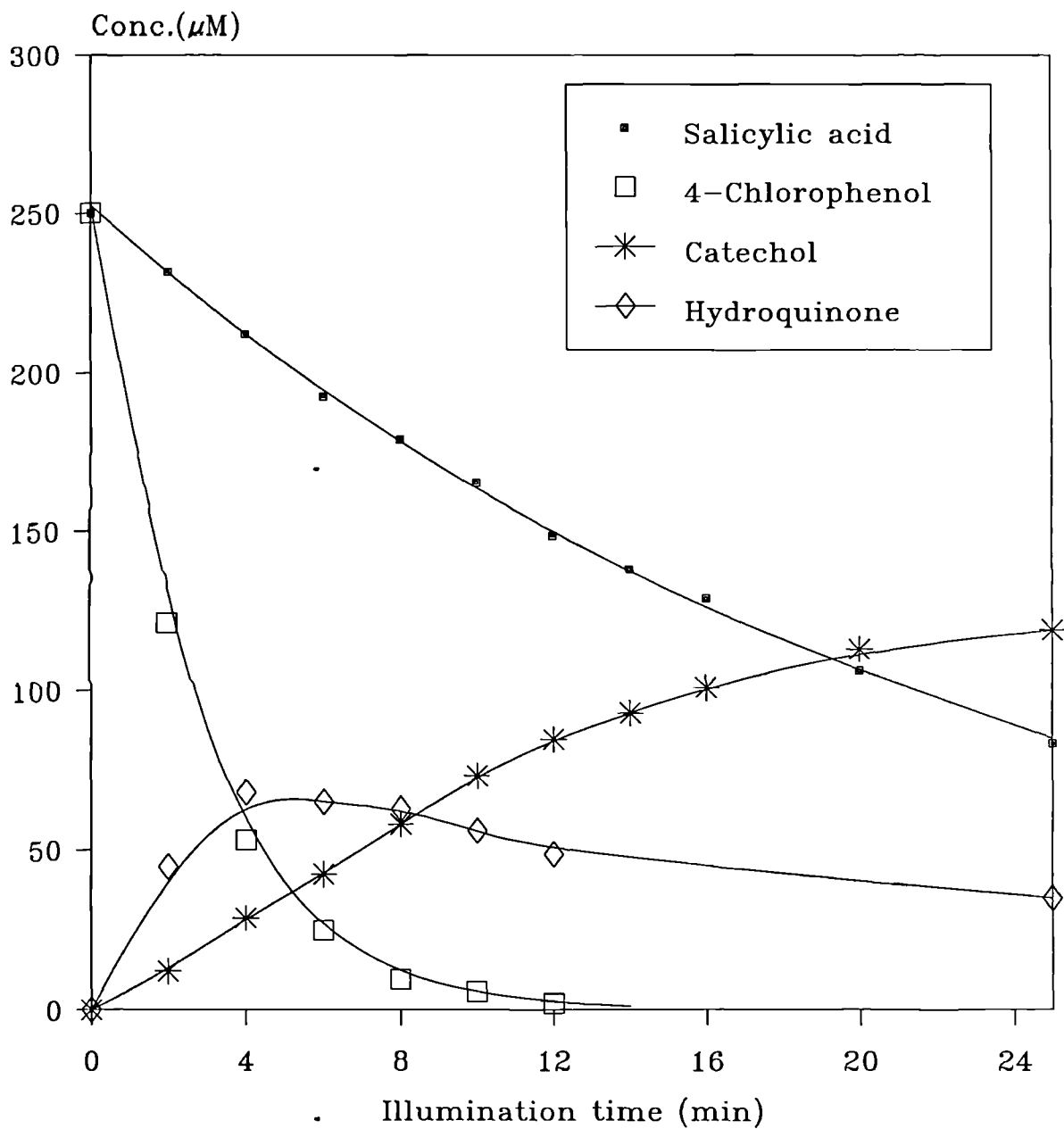
9.6 Photocatalysis with immobilised catalyst system

The characteristics of the FFR were studied because it was felt that this type of reactor was simple to design as an immobilised catalyst type of reactor provided the inner surface could be coated by a robust catalyst. Unfortunately the parallel work carried out by the Chemistry Department to generate robust surfaces was not completed in time, therefore a commercial catalyst coated fibre glass gauze was placed inside the reactor surface for use as a supported system. The fibre glass gauze was commercially supplied from Nutech Environmental (Ontario-Canada) and carefully surrounded inside the reactor attaching from each end as one layer.

10lt of 250μM salicylic acid and 4-chlorophenol solutions were used and flow rate was 5lt/min. Results were shown in Figure 9.12 and kinetic rates were tabulated in Table 9.7.

Table 9.7 Kinetic rates for immobilised catalyst with 250μM initial concentration

Organic chemical	L-H kinetic rates				First order rates	
	$k_1(\mu M^{-1})$	$k_2(\mu M\ min^{-1})$	SSE	$t_{1/2}$	$k(min^{-1})$	(r)
SA	$8.79*10^{-4}$	56.29	(0.48)	14.46	0.0435	(0.999)
4-CP	$2.55*10^{-4}$	1559.78	(0.27)	1.82	0.3905	(0.998)

On handling the catalyst coated gauze it was noticed that catalyst came off, therefore to test the stability and the efficiency of the supported catalyst a second run was made with 4-chlorophenol solution and compared results were shown in Figure 9.13.

111

Figure 9.13 4–CP removal with intermediates using Nutech catalyst coated fibre glass gauze (FFR)

111a
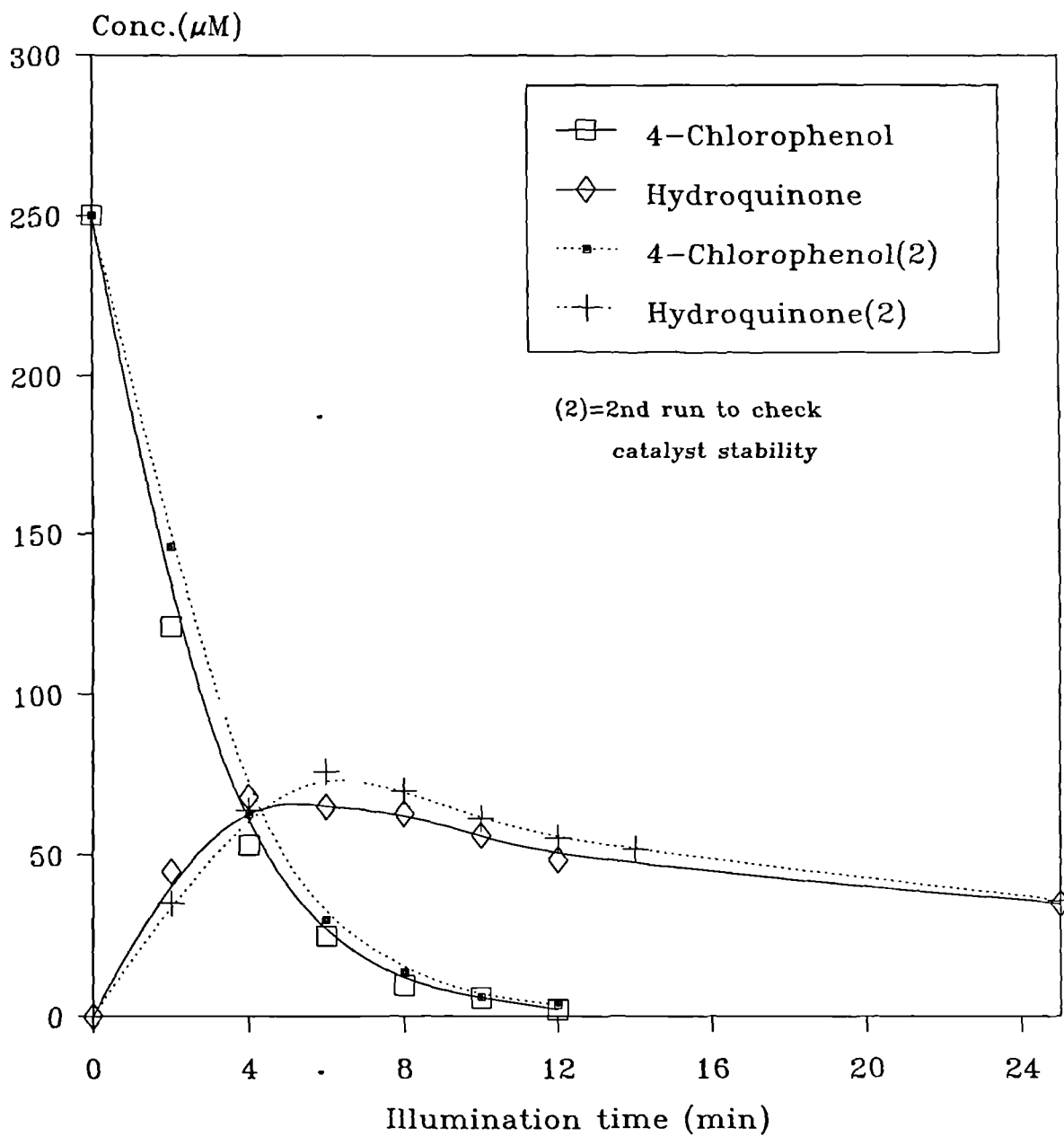
Figure 9.14 Salicylic acid, 4-CP removal with intermediates on both slurry based and coated system (FFR)

111b
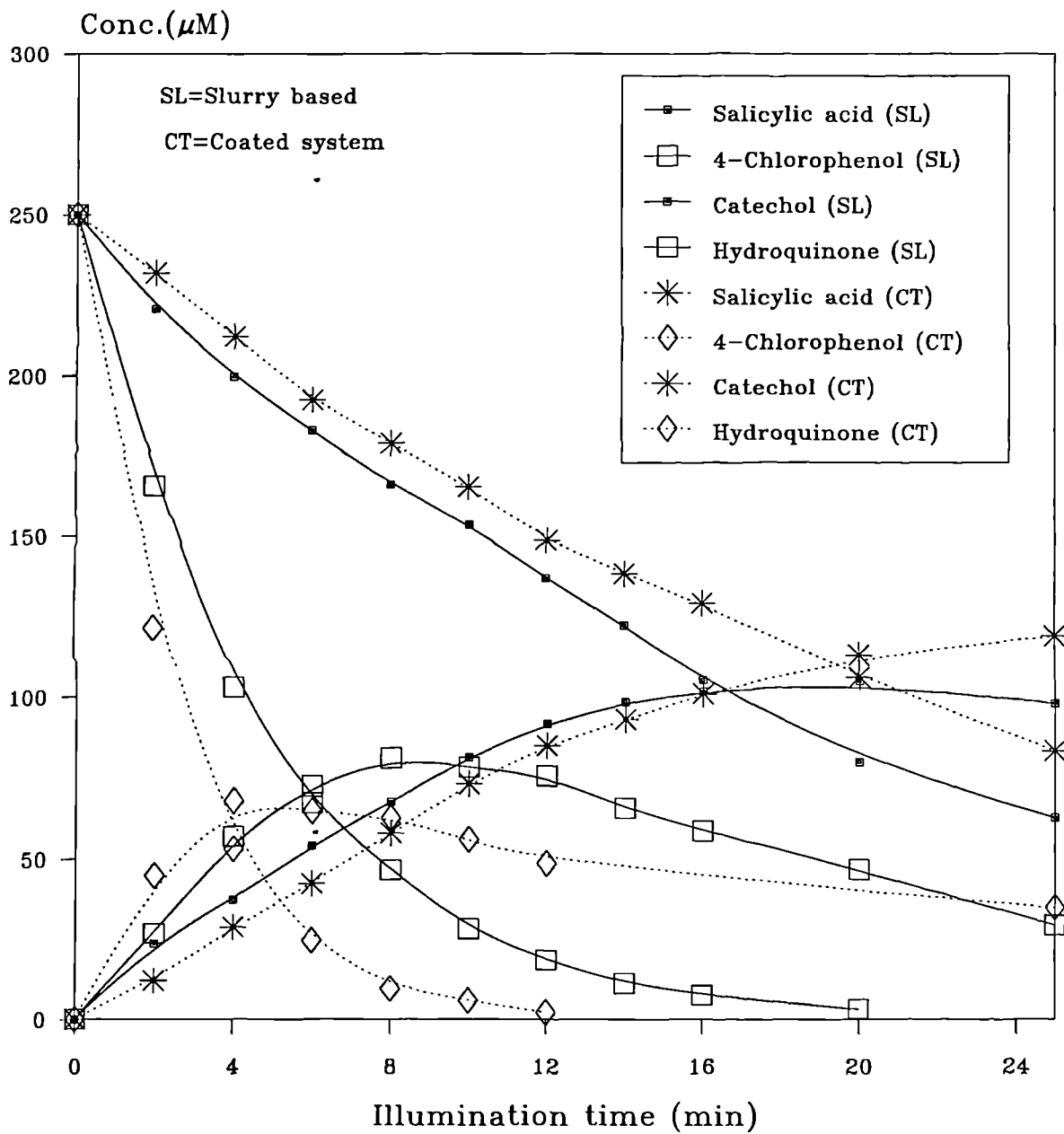
As seen from the figure, the efficiency of coated catalyst does not diminish rapidly.

For salicylic acid and 4-chlorophenol degradation, slurry based and coated systems in falling film reactor were compared with $250\mu M$ initial concentration and the results based on the pseudo-first order kinetics were tabulated in Table 9.8 and shown in Figure 9.14.

Table 9.8 SA and 4-CP degradation in slurry system and coated system based on the first order kinetic rates

Organic chemical	Slurry based reaction rates				Supported system reaction rates			
	$k(min^{-1})$	(r)	$\Phi(\%)$	$t_{1/2}$	$k(min^{-1})$	(r)	$\Phi(\%)$	$t_{1/2}$
SA	0.0551	(0.995)	0.212	13.13	0.0435	(0.999)	0.193	14.46
4-CP	0.2212	(0.999)	0.858	3.25	0.3905	(0.998)	1.531	1.82

(Φ=quantum yield)

As seen from both Table 9.8 and Figure 9.14 degradation increases for 4-CP and decreases for SA on supported catalyst compared with slurry systems. Clearly the use of a supported catalyst in the FFR is a more practical option and further work is necessary.

CHAPTER X

10.   Results of photocatalytic studies in the spinning disc reactor (SDR)

Spinning disc reactors (SDR) have been studied in the past in connection with gas-liquid reactions in different modifications (Barberis 1987, Wallis 1991). They produce a thinner and more controllable liquid film than the falling film reactor and the thin liquid films produced in these reactors possess a high degree of turbulence and hence correspondingly high values for their gas-liquid mass transfer coefficients. In the work considered here a borosilicate glass disc was fitted and TiO_2 catalyst was supported upon the surface of this rotating disc, across which the liquid containing the organic reactants was passed forming a thin radially flowing film. It is believed that the physical phenomena responsible for enhancing gas-liquid mass transfer rates under these conditions will have a similar effect upon the rate of transfer of organic reactant to the surface of the supported catalyst.

10.1   Experimental procedure and results

Two type of organics used as 10lt of 100μM initial concentrations were 4-chlorophenol and salicylic acid, and concentration measurements were performed by HPLC as explained previously. Liquid flow rate through the reactor was 50cc/s, and the disc rotational speed was 350 rpm. The average liquid film thickness was found 0.079mm based on these values by Wallis (1991).

Glass surfaces have been shown that they could be coated. Small size glass tubes which catalyst coated inside and coiled around the lamp source (Matthews 1987b,c, 1988, 1989, Al-Ekabi and Serpone 1988, Al-Ekabi et al. 1989) and catalyst coated glass beads in small vessels (Serpone et al. 1986, Minero et al. 1992) have been used as immobilised catalyst surfaces. Therefore the disc fitted to the SDR was a borosilicate glass sheet and had been coated previously with TiO_2. However smooth and grooved metal (aluminium) surfaces were also coated but the catalyst was unstable and washed off with time.

The coating procedure was as follows. A 10g/lt slurry was prepared, in which the glass disc was immersed for 5 minutes. The disc was then removed from the slurry and placed in an oven operating at 90°C for one hour. This procedure was repeated 10 times in total. Prior to fitting the disc to the SDR, it was washed thoroughly in order to remove any loose TiO_2 particles from the surface. Two TiO_2 powders were used to produce the coating slurries: Degussa P-25 and Tioxide PC1. The disc was washed with distilled water between experiments.

The type of lamps and their features were described previously and mounting procedure was shown in the figures. The two different low pressure lamp intensities were obtained by switching on only one of the lamps and both at the same time. In order to obtain different UV intensities with the medium pressure lamp, the depth that the lamp was inserted under the photographic reflector into the reactor chamber was varied as 8cm, 16cm, 25cm and full, 38cm.

Figure 10.1 shows the variation of 4-chlorophenol concentration when the SDR was operated with different UV lamp types and intensities. The catalyst used was Degussa P-25. It can be seen that the best results were achieved when the low pressure lamps were used. Even when the medium pressure lamp was utilised at its full output intensity (240 Wm^{-2} at 365nm), the rate of degradation of 4-chlorophenol was inferior to that produced by the low pressure lamps. This phenomenon is only specific to 4-CP with other chemicals the low pressure lamp produces no degradation and it could be the absorption coefficient of 4-CP. It is possible that a photochemical reaction may occur at the wavelength emitted by the low pressure lamps (254nm), but not at that produced by the medium pressure lamp (365nm) (D'Oliveira et al. 1990). However when a solution of 4-chlorophenol was exposed to UV-irradiation of wavelength 254nm in the SDR without the presence of catalyst, as Figure 10.2 shows, very little photochemical decomposition was observed. No photochemical decomposition was observed with the medium pressure lamp. Hence the improvement in performance observed for the low pressure lamps does appear to be photocatalytic in nature for this particular system and geometry. This may be due to the efficiency of light transmission to the surface.

Figure 10.3 shows the effect of catalyst type upon the performance of the SDR. For both types of lamp, Degussa P-25 showed the higher rates of organic degradation. It is not possible to conclude from these results whether this was due to a more efficient photocatalytic performance by this catalyst compared to that of Tioxide PC1, or whether the former was more suitable for the disc coating technique used, however as the annular reactor and the falling film reactor results both gave better Degussa P-25 performance this

115

Figure 10.1 Effect of UV lamp type and
intensity upon the degradation
of 4-chlorophenol
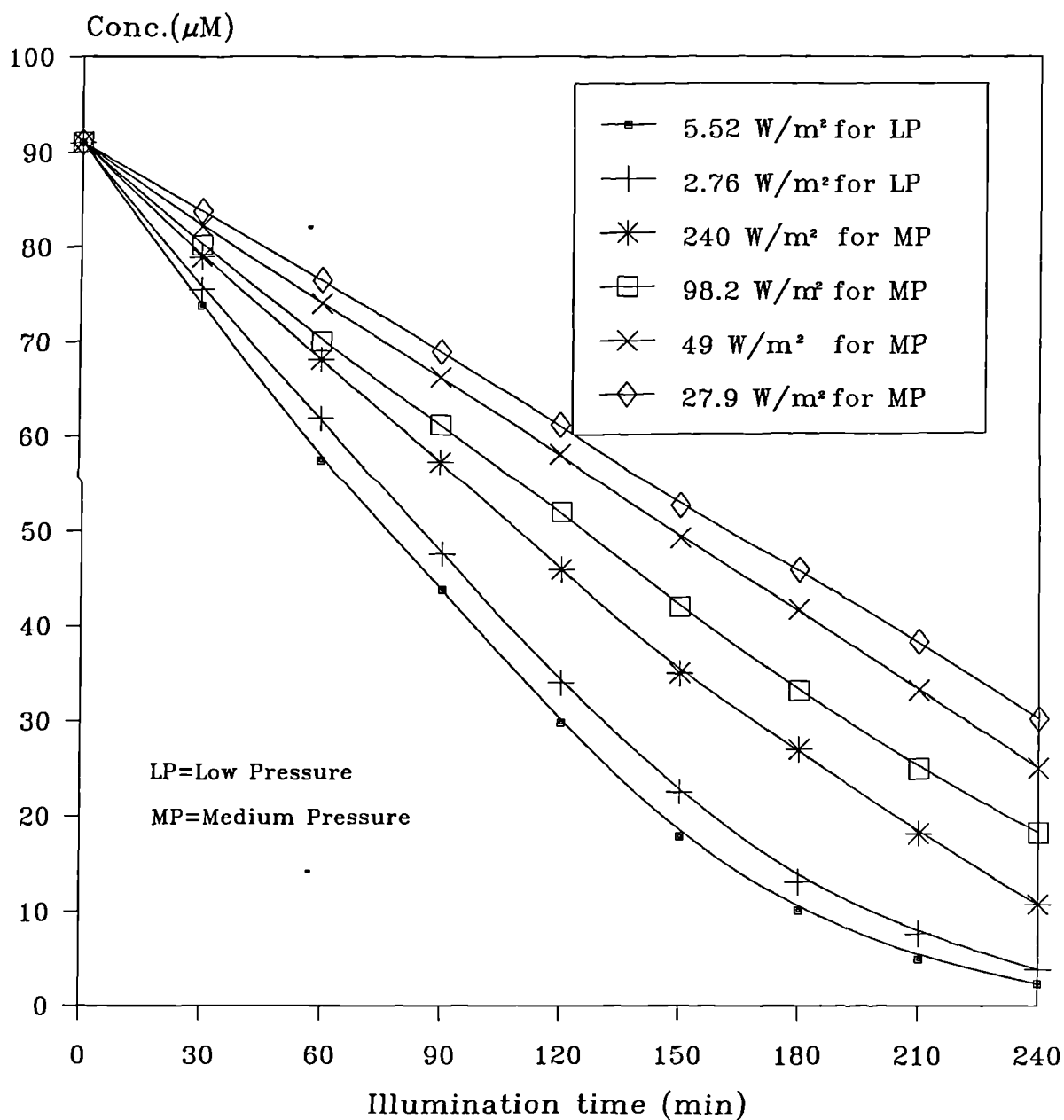
Figure 10.2 Photochemical decomposition
of 4−chlorophenol
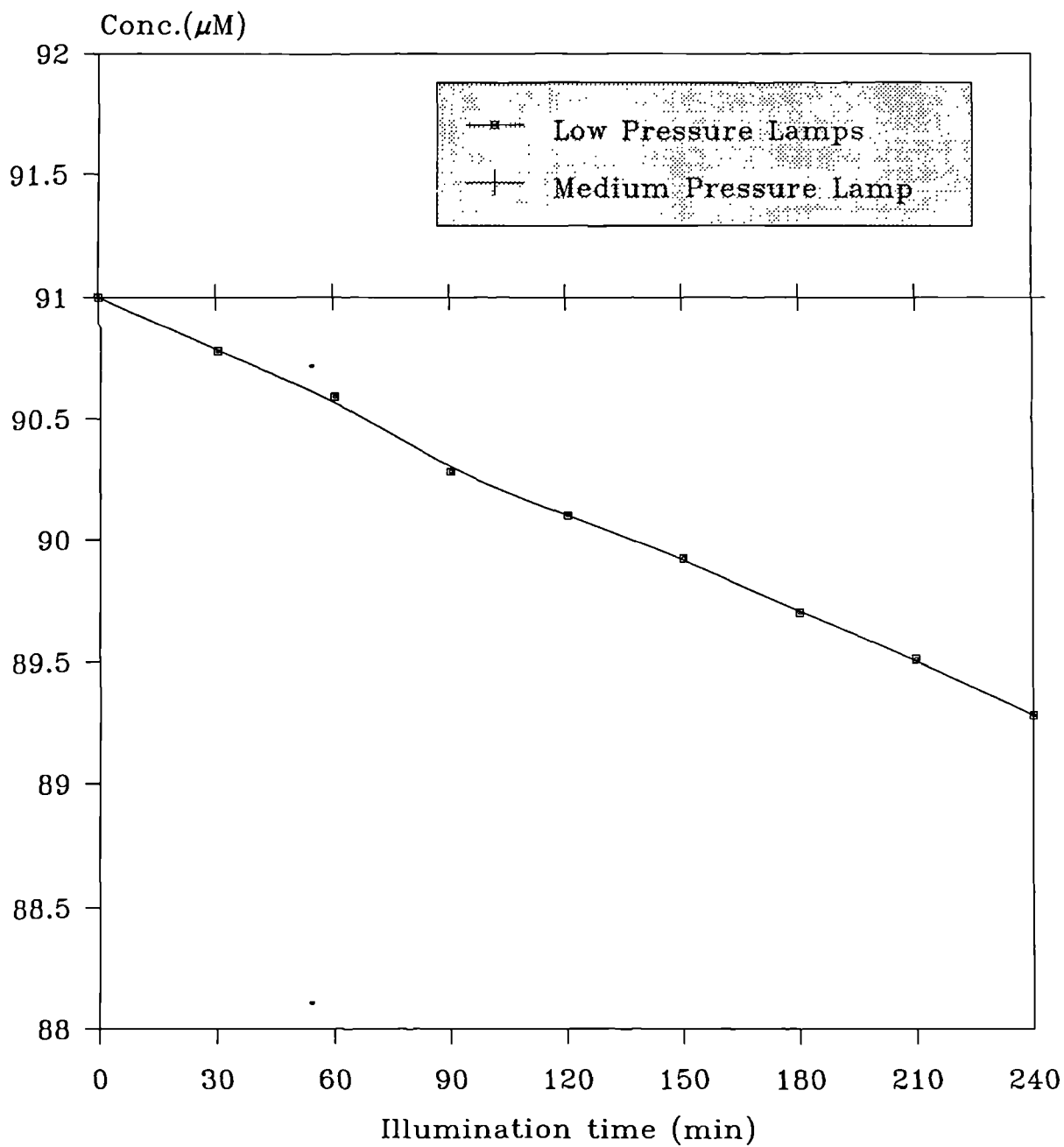
Figure 10.3 Effect of catalyst type upon
the performance of the SDR
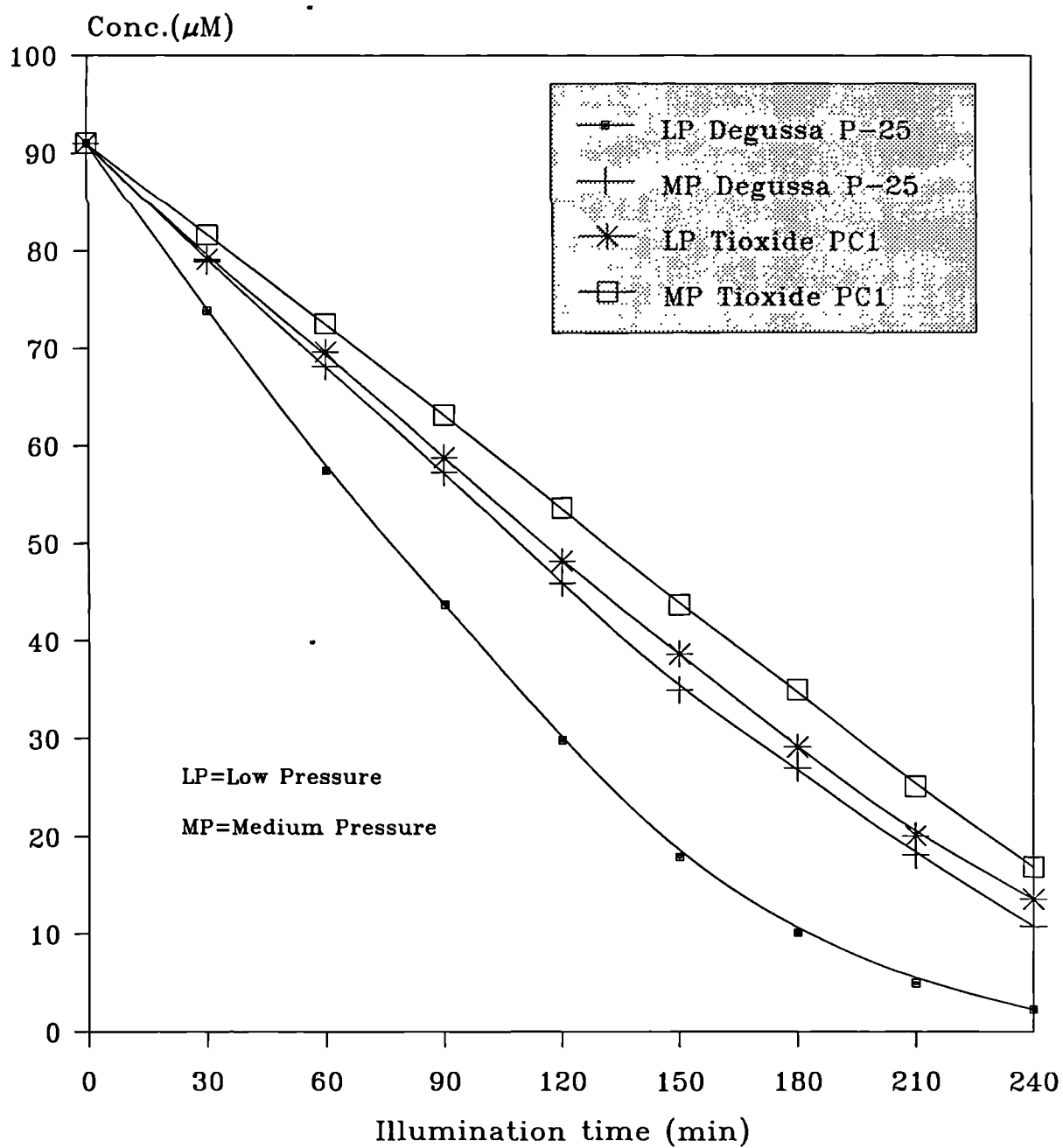
suggests that the coating technique is not the major cause for the improvements.

The results presented so far suggest that the 254nm radiation produced by the low pressure lamps is efficiently utilised by the catalyst than the longer wavelengths emitted by the medium pressure lamp when 4-CP is used. In order to see if this phenomenon is true of organic degradation in general, rather than being solely associated with the photocatalytic oxidation of 4-chlorophenol, a pair of experiments were performed in which the oxidation of salicylic acid were studied. Figure 10.4 shows that, again, the low pressure lamps produced a higher degree of photocatalytic behaviour and that this effect appears to be independent of the nature of the organic being treated. This again could be the effect of light transmission of the low pressure lamps in this reactor geometry.

The reasons why the shorter wavelength radiation should produce a higher degree of photocatalytic activity are not obvious in SDR. In theory the emissions of both the types of lamp produce photons which possess an energy level greater than the band gap of anatase TiO_2, which lies at 3.23 eV (Goodenough and Hamnett 1987). Only photons which possess energy exceeding the band gap may initiate the photocatalytic process. However, anatase would be expected to absorb photons much more strongly at the shorter wavelength. Since the TiO_2 is only present in a thin layer on the surface of the disc, the relative difference in its ability to absorb photons at the two different wavelengths is likely to have a significant effect upon the photocatalytic process. Absorption experiments also showed the wide spectral absorption characteristics of TiO_2 (Figure 8.1.1 and 8.1.2).

116

Figure 10.4 Effect of lamp type upon
the degradation of salicylic acid
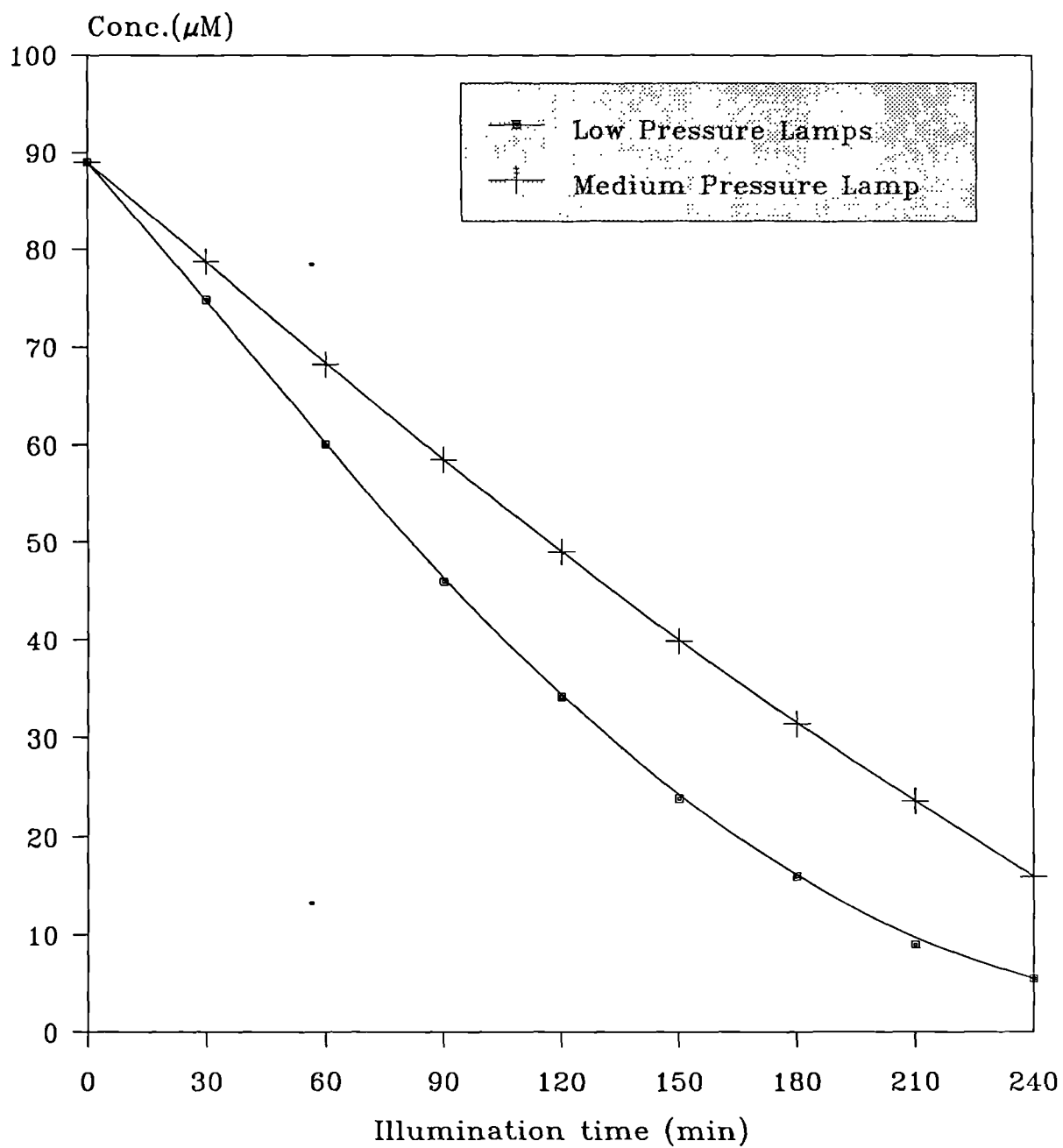
The data sets obtained from the experiments performed in order to assess the effect of UV intensity and wavelength variation were fitted to pseudo-first order kinetics by linear regression and results are presented in Table 10.1.

Table 10.1 Variation in the values of the first order rate constants with lamp type and illumination intensity for the degradation of 4-chlorophenol

Lamp type	UV intensity (Wm^{-2})	k (min^{-1}) (r)
LP	5.52	0.0151 (0.976)
LP	2.76	0.0130 (0.977)
MP	240	0.0085 (0.977)
MP	98.2	0.0066 (0.985)
MP	49	0.0052 (0.984)
MP	27.9	0.0045 (0.987)

(LP=Low Pressure Lamp, MP=Medium Pressure Lamp)

As can be seen, doubling the intensity of the low pressure radiation only has a noticeable but small effect upon the reaction rate. A similar trend is observed for the reaction rate in the case of the medium pressure lamp intensities.

Similar reaction rates for the degradation of salicylic acid are also given in Table 10.2.

Table 10.2 First order reaction rate constants for the degradation of salicylic acid

Lamp type	UV intensity (Wm^{-2})	k (min^{-1}) (r)
LP	5.52	0.0117 (0.976)
MP	240	0.0069 (0.983)

As seen from both tables reaction rates are much lower than those obtained in annular and falling film reactors. This possibly indicates that the coating technique used in this study is not suitable for the SDR and that a supported catalyst with better mechanical properties is required. Although the collection of the photons in the annular and falling film reactor is much more efficient than in the SDR and this may account for the differences.

CHAPTER XI

11. Discussions and conclusions

11.1 Discussions and conclusions derived from the annular reactor

11.1.1 Effect of catalyst concentration

Table 8.1 shows that a 1g/lt catalyst concentration was found to be the optimum loading for slurry system in the annular reactor. Ollis et al. (1991) in their recent review of photocatalysis stated that most photocatalysis studies have used ~0.1 wt% slurries of titanium dioxide particles which mean concentrations of about 1g/lt. Matthews (1987a) earlier discussed the possible effects of increasing catalyst concentration and stated that if the reaction occurs at the surface of the TiO_2 particles and other factors remain the same, increasing catalyst concentration should increase reaction rate linearly but this was not borne out by experiments. They concluded that the following factors should also be considered:

    a) Aggregation of the particles may occur at high loadings.

    b) The distribution of light to the particles which limits the reaction.

Because of their opacity and light-scattering properties, increasing particle loadings will result in a decreasing penetration of light into the suspension. Thus the photoactivated volume shrinks as the TiO_2 loading increases and the increased surface area is offset by a decreasing access of the

particles to the exciting light. It is evident that increased oxidation rates will not be achieved by simply increasing the TiO_2 loading. Maximum surface area is required but it must be accessible to the photoactivating light. There needs to be a compromise between the inner and outer cylinder separation (pathlength) in annular reactors and particle loading for a given particle type. Obviously these two variables will change as particle size changes. In addition, a deposit of TiO_2 builds up on the surfaces of reactor and this blocks the transmission of light, therefore it was suggested that thin film reactors would probably give the most efficient energy use and also improved oxygen transfer (see section-9.4).

11.1.2 Effect of physical adsorption

Results (Figure 8.3) showed that Tioxide PC1 type catalyst had strong adsorption affinity compare to Degussa P-25 for salicylic acid, but for both catalyst types adsorption affinity was not significant for 4-chlorophenol. This factor was generally not considered by other workers but Ollis et al. (1991) concluded from recent experimental studies that active oxygen has been identified at the titanium dioxide surface and in solution, the reaction therefore may proceed at either or both locations. Hence, strong adsorption of organic reactants at the surface of catalyst will have the negative effect of the reaction in solution. Considering the reaction occurs on both locations - catalyst surface and solution- optimum result was obtained using P-25 with salicylic acid which suggests that the surface reaction is not much effected by the catalyst surface area. This was conferred by Sakata and Kawai (1983) who argued that the catalytic activity of TiO_2 is independent of catalyst surface area since the overall rate of the process is limited by the supply of positive holes to the surface. In this case it is the light intensity which controls the rate

reaction rather than surface area of the catalyst. Farin (1989) also observed that there was a non-linear relationship between surface area and reaction rate rather than the linear one expected.

11.1.3 Effect of liquid flow rate

The first order rate constants for different flow rates (Table 8.2) showed that salicylic acid degradation rate increased with increased liquid flow rate. Little work on the effect of flow rate has been reported for slurries, however using immobilised catalysts, other workers found that increasing flow rate improved the transfer of organics to the catalyst surface with improved performance hence mass-transport limitations were believed to be responsible for the observed dependence of reaction rate on flow rate in the immobilised system (Matthews 1988, Turchi and Ollis 1988). But no mass-transfer limitation was expected for photocatalysis using slurries of very fine catalyst particles of 1g/lt Degussa P-25 since the maximum diffusion distance was very small. Differences in reaction rates in slurries have been attributed solely to the inherent surface reaction characteristics of different reactants on the photocatalyst (Matthews 1988).

11.1.4 Comparison of two types of lamps

When both low pressure and medium pressure lamps used (Figure 8.5) in the annular reactor, reaction rates (Table 8.3) were higher with the medium pressure lamp. This is because the medium pressure lamp used had a stronger light intensity and increased intensity always results in an increase in volumetric reaction rate, until the mass transfer limit is encountered (Ollis et al. 1991). Another effect could be attributed to the wide spectral absorption

121

characteristics of TiO_2 (Figure 8.1.1 and 8.1.2) allowing its excitation in the UV-C(below 280nm), UV-B (280-315nm) and UV-A(315-400) domain (Braun et al. 1992) since the medium pressure lamp emits its photons over a wider range wavelengths than the low pressure lamp (section 7.1). Braun et al. (1992) also found that the use of preferentially doped medium pressure mercury arcs of high electrical power is of considerable interest. However the annular reactor quantum yield results show that low pressure lamp photons range UVC were utilised more efficiently and therefore the power costs should be lower. But medium pressure lamps are more compact and hence more useful in reactor design, therefore if their full spectrum of UVC, UVB, UVA are to be usefully used and the quantum efficiency increased, it will be necessary to produce catalysts which match these characteristics. There is also an important physical factor of these lamps used in the annular reactor that their actual discharge lengths are different. Although both lamps fit inside the annular reactor (overall length 390mm-Figure 7.1) perfectly, the low pressure lamp has 380mm overall length and 275mm discharge length whereas the medium pressure lamp has 375mm overall length and only 90mm discharge length (section 7.1). This means that the low pressure lamp photons reach more reaction areas directly inside the annular reactor than medium pressure ones.

11.1.5 Effect of initial concentration

This effect is important to understand the efficiency of photocatalytic processes and the photocatalytic reactor used. Rate constants of salicylic acid (Table 8.4) showed that reaction rates decreased with increased initial concentration but quantum yield results indicated that reaction efficiency increased with increasing initial concentration to a optimum point and

dropped. Matthews (1987a) in his study with salicylic acid obtained similar results and reported that the existence of an additional reaction involving salicylate which competes with the CO_2 forming reaction at high concentrations effected the reaction rate negatively. It is clear that the concentration required for optimum efficiency needs to be matched to the type of reactor used.

11.1.6 Comparison of rates with other workers

Other workers used different reactor types, lamp types with different intensities, different liquid volumes and different initial concentrations of different reactants. This makes the direct comparisons of different processes difficult. The quantum yield is one of the factors to make comparisons effective, but the evaluation of quantum yield values was hardly touched by most workers. For instance, Matthews (1988b) defined a quantum yield of 0.06 molecules of CO_2 per photon based on the maximum rate of oxidation to CO_2 of the several different reactants. Braun et al. (1992) in their preview found the quantum yield of TiO_2/UV process is relatively low ($\Phi<0.05$).

Unable to compare quantum efficiencies, the alternative is to make some rate comparisons to give some performance evaluations of different processes. The first order rate constants (k min^{-1}) with the medium pressure lamp obtained in the annular reactor (2lt of 100μM solutions) were 0.0638 and 0.0810 for 4-chlorophenol and salicylic acid respectively, and the degradation half times were 7.70 and 6.85min. Matthews (1987b) obtained 0.0519 as a first order constant and 13.35min as a half time for salicylic acid (0.5lt of 100μM solution) and 0.0793-8.73min for 4-chlorophenol (0.5lt of 10μM solution) in his immobilised system. Al-Ekabi et al. (1988) obtained 0.0095 and 73min as a

123

first order kinetic constant and a half time respectively for 4-chlorophenol (250ml of 13μM). It can be seen that the rate for salicylic acid is higher than the one obtained by Matthews, however the rate for 4-chlorophenol is lower because the low initial concentration was used by Matthews for this chemical, and the rate obtained by Al-Ekabi is well below the rate obtained for 4-chlorophenol in the annular reactor.

11.2 Discussions and conclusions derived from the falling film reactor

11.2.1 Catalyst concentration, choice of catalyst and flow rate

<u>Effect of concentration:</u>

In annular reactor 1g/lt catalyst concentration (Table 8.1) was found optimum whereas in falling film reactor it was 0.5g/lt (Figure 9.2 and 9.3) and this was attributed to the thin film characteristics of FFR coupled with 'reflection' from the metal walls. Because the film thickness (5lt/min-0.417mm) in the falling film reactor was much lower than the annular reactor (~8mm). In the annular reactor this considerably effects the light scattering inside the reactor and eventually the particles furthest away from the lamp will receive little radiation. Another important factor is that in the falling film reactor oxygen transfer is efficient (Figure 9.10), whereas the annular reactor is a closed system and there is no direct connection with air and oxygen transfer is an important factor in photocatalysis.

<u>Effect of catalyst type:</u>

Degussa P-25 type catalyst showed more effective degradation than Tioxide PC1 type (Figure 9.1) although the latter seemed to have higher rates

124

in annular reactor (Table 8.1). This indicates that these rates were effected by the strong adsorption of reactants on this type of catalyst. In the falling film reactor, photon distribution and oxygen transfer were more effective and so this improves the reaction on the catalyst surface rather than the physical adsorption itself which is more pronounced in the annular reactor which has a larger volume of catalyst and in particular a large proportion of catalyst which is not receiving radiation and thus pure absorption is important.

Effect of flow rate:

Unlike the annular reactor, increasing flow rate did not show any significant effect on the degradation rate (Table 9.5) in the falling film reactor. As explained in section 11.1.3, in slurry systems differences in reaction rates have been attributed to the surface reaction characteristics of different reactants, but in the falling film reactor it seems the flow rate increase has no significant effect on the surface reaction characteristics. Increasing flow rate in the FFR does not increase the residence time (Table 9.5), it merely increases the film thickness (Table 9.4). This suggests that one should use the highest flow rate possible until the film thickness reaches a value which prevents light reaching all the particles (section 11.1.5). Therefore an optimum flow rate is likely. However if a immobilised system is used then thinner liquid films are likely to be more beneficial.

11.2.2 Effect of initial concentration

Like the annular reactor results (Table 8.4), rate constants obtained from the falling film reactor (Table 9.3) showed the similar effect as reaction rates decreased with increased initial concentration, but the decrease in the reaction rate of 4-chlorophenol was not as strong as salicylic acid. The reason

for this was suggested by Matthews (1988b) that the intermediate decomposition products compete with the original reactant for the photogenerated radical oxidising species. The quantum yield results (Table 9.3) showed that degradation efficiency increased for 4-chlorophenol with increased initial concentration because of its higher reactive efficiency with improved photon distribution and effective oxygen transfer which induces effective reaction on the catalyst surface. Another factor could be higher intermediate degradation for 4-chlorophenol (Figure 9.9) which means a more direct conversion to CO_2 and less competition with the original reactants.

11.2.3 Assessing the kinetic models

The Langmuir-Hinshelwood kinetic treatment model has been widely used to quantitatively describe solid-gas heterogeneous catalytic reactions. As described in Chapter 3, this model has been selected to evaluate the reaction kinetics in heterogeneous photocatalysis and especially investigated, as required by this model, whether the degradation reaction proceeds on the semiconductor particle surface (Al-Ekabi et al. 1988, 1989). Al-Ekabi et al. (1989) therefore reported that when saturation coverage of the TiO_2 surface active sites is achieved, no further increase in the rate of degradation is obtained with further increase in 4-CP concentration and they concluded that the L-H kinetic model is appropriate and, the degradation reaction proceeds on the TiO_2 catalyst surface.

In this work L-H kinetic model was also found quite appropriate to assess reaction kinetics, especially in the falling film reactor a good fit was achieved compare to the annular reactor results in which the first order

126

kinetics model was fitted better. This can also be attributed to the thin film characteristics and efficient photon distribution in the falling film reactor indicating the better surface reaction on the TiO_2 catalyst.

The integrated form of L-H kinetics (Equation 3.4, Chap. 3) comprises two separate terms:

$$k_1 k_2 t = \ln \frac{C_0}{C_t} + k_1 (C_0 - C_t) \qquad (9.1)$$

Matthews (1987b) and Al-Ekabi et al. (1988) reported that at low initial concentrations of C_0, the second term in the expression (9.1) becomes small compared with the first term and small values of k_1 also makes the second term small $[\ln(C_0 / C_t) >> k_1 (C_0 - C_t)]$, under this conditions equation becomes first order. In the falling film reactor k_1 values were smaller enough ($k_1 < 10^{-2}$), so that the experimental values also obeyed first order kinetics, that explains the very good approximation of both kinetic models.

11.2.4 Use of immobilised catalyst

Falling film reactor results with TiO_2 slurries already showed much higher performance compare to annular reactor and this performance was even much more effective for 4-chlorophenol (Table 11.1). Using commercial TiO_2 coated fibre glass gauze increased the 4-chlorophenol degradation rate still further but a slight decrease was obtained for salicylic acid compare to slurry system (Table 9.8). Matthews (1988) also reported that chlorophenols had reaction rates greater than benzoic acid in the immobilised system but lower in the free suspension and attributed the reason due to mass-transport

limitations and differences in diffusion coefficients of reactants. Therefore this suggests that a FFR with a better immobilised film geometry could be more successful (section 11.4).

It is obvious that the rates obtained by other workers (section 11.1.6) are much lower than the rates obtained in the falling film reactor.

11.3   Discussions and conclusions derived from the spinning disc reactor

The efficiency of the photocatalytic process in SDR appeared to be effected by the wavelength of the UV light supplied to the reactor. Light provided by low pressure mercury lamps, whose peak emission occurs at a wavelength of 254nm was found to more effective than that supplied by a medium pressure lamp, its peak emission being at 365nm. This behaviour was observed for both the catalyst types used and also was found not to be dependent upon the nature of the organic material being degraded. On the other hand low pressure lamps showed a little photochemical effect (Figure 10.2).

The coating technique used for attaching the TiO_2 catalyst to the surface of the borosilicate glass disc was found unsuitable for use in combination with the SDR. Work is underway in which different coating techniques are being examined. Matthews (1987b) used a spiral tube reactor whose inner surface had been coated with TiO_2 using a similar technique to that given here. It is clear that for both chemicals Matthews (section 11.1.6) obtained much higher rates than here (Table 10.1, 10.2), it could be because author was more successful in obtaining a stable catalytic coating and more

128

efficient light distribution in his reactor. Increased light intensity had small effect upon the reaction rate for both type of lamps (Table 10.1), this also shows the lack of effective catalyst surface.

The rates obtained in SDR for both chemicals were found much lower than those obtained in annular and falling film reactors, beside the poor coating technique, this could also be attributed to the lack of effective photon distribution compare to the annular and falling film reactors.

11.4   Reactor comparisons

11.4.1 Slurry systems

The rates obtained in the falling film reactor were much higher than the annular reactor. However, unlike the annular reactor results, the rates obtained with 4-chlorophenol were higher than salicylic acid, whereas in annular reactor the rates were higher for salicylic acid (Table 11.1).

Table 11.1 Comparison of two reactor performances based on slurry system with 100μM initial organic concentration

Organic chemical	Annular reactor				Falling film reactor			
	$k(min^{-1})$	(r)	$\Phi(\%)$	$t_{1/2}$	$k(min^{-1})$	(r)	$\Phi(\%)$	$t_{1/2}$
SA	0.0810	(0.992)	0.293	6.85	0.194	(0.995)	0.253	4.41
4-CP	0.0638	(0.970)	0.260	7.70	0.284	(0.997)	0.416	2.68

These results clearly shows that with slurry systems, the thin film characteristics of the falling film reactor have had much stronger effect on the degradation of 4-chlorophenol than salicylic acid and the quantum efficiency

increased for 4-chlorophenol. The most important different factors between these reactor designs are the use of higher intensity lamp and the effective oxygen transfer inside the falling film reactor since the annular reactor is a closed system, it seems these have the most influence for higher degradation rates, however quantum efficiency results show that each organic has different film characteristics hence it effects the reactions on the catalyst surface.

11.4.2 Immobilised systems

Table 11.2 shows the results for the falling film and spinning disc reactors with different designs and different immobilised systems. These differences make the performance comparisons difficult, but at least give some evaluations about immobilised systems.

Table 11.2 Comparison of the FFR and SDR based on the immobilised system

Organic chemical	SDR P-25 coated				FFR Nutech gauze			
	$k(min^{-1})$	(r)	$\Phi(\%)$	$t_{1/2}$	$k(min^{-1})$	(r)	$\Phi(\%)$	$t_{1/2}$
SA	0.0068	(0.984)	0.075	119.2	0.0435	(0.999)	0.193	14.46
4-CP	0.0085	(0.977)	0.088	104	0.3905	(0.998)	1.531	1.82

It can be seen from the Table 11.2 that because of poor coating technique and much less effective photon distribution with less intensity, the SDR performance is low compared to FFR.

11.4.3 Optimum reactor

The results show that light intensity with effective photon distribution, mass transfer with thin film characteristics and effective oxygen transfer inside the reactor are the most important factors for photocatalytic reactor systems. Under these circumstances falling film reactors with a cylindrical shape produce the optimum conditions for suitable photocatalytic reactors, but the light intensity effect should be assessed more effectively for economic reasons considering different reactants and especially different catalyst coating systems.

It is also important to note that falling film reactors with higher light intensity are capable of handling larger amounts of contaminated liquid and therefore more suitable for industrial purposes.

CHAPTER XII

12. Major conclusions and recommendations for future work

12.1 Major conclusions

Catalyst type:

For two types of reactors namely the annular and the falling film;

1.   Degussa P-25 showed more effective photocatalytic performance than Tioxide PC1 which showed strong physical adsorption affinity.

2.   With slurry systems the catalyst concentration depends on reactor type and light intensity distribution, thus the optimum catalyst concentration was 1g/lt in the annular reactor and 0.5g/lt in the falling film reactor because of its thinner film characteristics.

Lamps:

1.   Using different types of lamps in the annular reactor showed that the medium pressure lamp produced higher degradation rates because of its high intensity and wide range of wavelength emission. However this reactor configurations did not allow the effective use of medium pressure lamp photons and the quantum efficiency for the low pressure lamp photons was higher. In order to get the best compromise between quantum efficiency and degradation rate it is necessary to match the reactor characteristics of

irradiated length and slurry depth to the emission characteristics of each lamp used.

Kinetics:

1. Different initial reactant concentrations showed that increased concentration resulted in a decrease in the rate of degradation for salicylic acid and 4-chlorophenol in the annular and falling film reactors.

2. The overall rate of removal is an important design criteria matching the chemical to the reactor is also important. Much higher rates were obtained for 4-chlorophenol in the falling film reactor than salicylic acid. This indicates the different surface reaction characteristics for both chemicals. 4-Chlorophenol showed more effective degradation with the thin film characteristics of the falling film reactor and more effective use of light photons (Table 11.1).

3. A Langmuir-Hinshelwood kinetic model was found more appropriate to assess reaction kinetics in the falling film reactor since this model indicates the surface reaction on catalyst surface, therefore thin film characteristics shows effective surface reactions on catalyst surface. Meanwhile in the annular reactor first order kinetics model followed better fit which indicates less surface reaction and less efficient degradation.

Immobilised catalyst:

1. When commercial TiO_2 coated fibre glass gauze was used in the falling film reactor, it resulted in a successful degradation especially for 4-chlorophenol.

133

2.   The poor coating technique and the lack of effective photon distribution resulted in low degradation rates in the spinning disc reactor.

Reactor comparisons:

General outlined comparison of three different reactor performances according to the quantum yield results was made in Table 12.1 and 12.2.

Table 12.1 Comparison of the slurry based systems with quantum
yield results (Φ) based on two different chemicals

Organic chemical	Annular reactor Φ(%)	Falling film reactor Φ(%)
SA	0.293	0.253
4-CP	0.260	0.416

Table 12.2 Comparison of the immobilised systems with quantum
yield results (Φ) based on two different chemicals

Organic chemical	SDR P-25 coated Φ(%)	FFR Nutech gauze Φ(%)
SA	0.075	0.193
4-CP	0.088	1.531

These quantum efficiency results show that optimum reactor design should be falling film reactors with a cylindrical shape but the economics of using high light intensity lamps should be assessed considering different reactants and reactant combinations.

12.2 Recommendations for future work

The following recommendations for further study are made:

• As a catalyst type Degussa P-25 showed the most effective performance especially in slurry systems and can be very effective as immobilised catalyst if it is coated with strong surface features. Therefore this type of catalyst can be used in a supported system with improved coating technique.

• The thin film characteristics of the falling film reactor showed effective reactant-catalyst interaction and good oxygen mass transfer with effective photon utilisation therefore it is the best possible simple design to achieve optimum results within a cylindrical shape, however these thin film characteristics and effective photon utilisation can be improved by further modification. Rotation of cylindrical tube can give more effective and homogeneous flow distribution inside the tube hence it can improve the thin film characteristics.

• One of the main problems in photocatalysis and photoreactor design is to use immobilised catalyst, therefore an effective robust catalyst surface should be created and a parallel work is under progress to create such a surface and it should be incorporated in a falling film reactor.

• Because of different surface reaction characteristics of different chemicals degradation reactions and mineralisation can be extended to other possible contaminating chemicals including the combination of them with improved analysing techniques.

- In order to make progress in photoreactor design, the optimum combination of all characteristics in photocatalysis and further modelling must be considered. In particular this will need more detailed work on the effect of intensity and the output per unit surface area of lamp of different wavelength.

NOMENCLATURE

θ = surface coverage

b = apparent binding constant

C = concentration (μM)

C_0 = initial concentration (μM)

C_t = concentration after a reaction period of time (μM)

C_1 = concentration of a second reactant (μM)

k = first order rate constant (min^{-1})

k_1 = L-H binding constant (μM^{-1})

k_2 = L-H rate constant (μM min^{-1})

t = time (min)

r = rate (μM min^{-1})

R = radius of a sphere (cm)

S = UV power from source in μWatts

P = total UV power (watts)

I = light intensity at a distance (photon s^{-1}) or (μWatts cm^{-2})

I_o = light intensity from the source (photon s^{-1}) or (μWatts cm^{-2})

I_o^i = light intensity just inside the front cell window (photon s^{-1})

I_a = light intensity absorbed by the reactant A (photon s^{-1})

α = absorbance coefficient (cm^{-1})

ε = molar extinction coefficient (lt mole^{-1} cm^{-1})

β = apex angle between the detector and the axis of the emitting lamp

φ = rotational angle of the light source versus the axis of the emitting lamp

n_B = number of molecules of product B

n_f = number of quanta of fluorescence light

Φ = quantum efficiency or yield

Φ_B = quantum yield of product B

φ_f = fluorescence quantum yield

D = inside diameter cylinder (cm)

W = distance in the y direction or round of cylinder (πD) (cm)

L = length of cylinder (cm)

V = volume of liquid (cm^3) or (lt)

δ	=	average liquid film thickness (cm)
$V_{z_{av}}$	=	average velocity of liquid (cm s^{-1})
V_z	=	velocity of liquid (cm s^{-1})
v_{max}	=	maximum velocity of liquid (cm s^{-1})
ρ	=	liquid density (g cm^{-3})
g	=	gravity (cm s^{-2})
μ	=	liquid viscosity (g cm^{-1} s^{-1})
v	=	kinematic viscosity (cm^2 s^{-1})
Q	=	liquid flow rate (cm^3 s^{-1}) or (lt min^{-1})
Re	=	Reynolds number
Ta	=	Taylors number
D_{AB}	=	diffusivity coefficient (cm^2 s^{-1})
M_A	=	mass transfer rate (mol s^{-1})
r_e	=	outer radius of the disc (cm)
r_i	=	distributor radius of the disc (cm)
t_r	=	mean residence time (s)
u_r	=	radial velocity of the liquid (cm s^{-1})
u_θ	=	angular velocity of the liquid (cm s^{-1})
w	=	angular velocity of the disc (cm s^{-1})
$\bar{u}_r$	=	average velocity of liquid on disc (cm s^{-1})

REFERENCES

Ahmed S., Ollis D.F., "Solar Photoassisted Catalytic Decomposition of the
Chlorinated Hydrocarbons Trichloroethylene and Trichloromethane",
Solar Energy 32(5):597, 1984.

Al-Ekabi H., Serpone N., "Kinetic Studies in Heterogeneous Photocatalysis
1. Photocatalytic Degradation of Chlorinated Phenols in Aerated
Aqueous Solutions over TiO_2 Supported on a Glass Matrix", *Journal of
Physical Chemistry* 92:5726, 1988.

Al-Ekabi H., Serpone N., Pelizzetti E., Minero C., Fox M.A., Draper R.B.,
"Kinetic Studies in Heterogeneous Photocatalysis 2. TiO_2-Mediated
Degradation of 4-Chlorophenol Alone and in a Three Component
Mixture of 4-Chlorophenol, 2,4-Dichlorophenol and 2,4,5-
Trichlorophenol in Air Equilibrated Aqueous Media", *Langmuir* 5:250,
1989.

Al-Sayyed G., D'Oliveira J-C., Pichat P., "Semiconductor-Sensitized
Photodegradation of 4-Chlorophenol in Water", *Journal of
Photochemistry and Photobiology A:Chemistry* 58:99, 1991.

Anpo M., "Photocatalytic activity of TiO_2 Species in Various Oxide Catalysts",
Proceedings of the Electrochemical Society 88(14):34, 1988.

Anpo M., Tomonari M., Fox M.A., "In Situ Photoluminescence as a Probe of Photocatalytic Reactions", *Journal of Physical Chemistry* 93:7300, 1989.

Ashton R.C., Killick E.G., Shama G., Smith A.J., "A Wetted Wall Ultraviolet Photoreactor for the Disinfection of Liquids", *Environmental Technology Letters* 9:853, 1988.

Augugliaro V., "Current Problems in the Modelling of Photochemical Reactors", *Photoelectrochemistry, Photocatalysis and Photoreactors*, M. Schiavello, Ed., Reidel Publishing, 1985.

Barbeni M., Pramauro E., Pelizzetti E., Borgarello E., Gratzel M., Serpone N., "Photodegradation of 4-Chlorophenol Catalyzed by Titanium Dioxide Particles", *Nouveau Journal de Chimie* 8:547, 1984.

Barbeni M., Pramauro E., Pelizzetti E., Borgarello E., Serpone N., "Photodegradation of Pentachlorophenol Catalyzed by Semiconductor Particles", *Chemosphere* 14:195, 1985.

Barberis K., 1987, "Ozone and the Spinning Disc Reactor in Water and Wastewater Treatment", PhD thesis, University of Newcastle upon Tyne, Great Britain.

Bickley R.I., Jayanty R.K.M., "Photo-Adsorption and Photo-Catalysis on Titanium Dioxide Surfaces", *Faraday Discussions of the Chemical Society* 58:194, 1974.

Bird R.B., Stewart W.E., Lightfoot E.N., <u>Transport Phenomena</u>, John Wiley & Sons, USA, 1960.

Blatt E., Furlong D.N., Mau A.W-H., Sasse W.H.F., Wells D., "Photooxidation of m-Phenoxytoluene at Colloidal Titanium Dioxide/Non-Aqueous Solution Interfaces", *Australian Journal of Chemistry* 42:1351, 1989.

Bockelmann D., Goslich R., Weichgrebe D., Bahnemann D., "Solar Detoxification of Polluted Water: Comparing the Efficiencies of a Parabolic Trough Reactor and a Novel Thin-Film-Fixed-Bed Reactor", *The First International Conference on TiO$_2$ Photocatalytic Purification and Treatment of Water and Air, Proceedings,* London-Ontario, Canada, November 8-13, 1992.

Bond, G.C., <u>Heterogeneous Catalysis</u> Principles and Applications, Clarendon Press, Oxford-UK, 1990.

Braun A.M., "Technical Development and Industrial Prospects of Preparative Photochemistry", <u>Photocatalysis and Environment</u>, M. Schiavello, Ed., Kluwer Academic Publishers, 1988.

Braun A.M., Maurette M-T., Oliveros E., <u>Photochemical Technology</u>, Translated by: D.F. Ollis, N. Serpone, John Wiley & Sons, 1991.

Braun A.M., Jacob L., Legrini M., Oliveros E., "TiO$_2$ Photocatalytic Treatment of Water Reactor Design and Optimization Experiments", *The First International Conference on TiO$_2$ Photocatalytic Purification and Treatment*

of Water and Air, Abstracts, London-Ontario, Canada, November 8-13, 1992.

Brodkey R.S., Hershey H.C., Transport Phenomena, A Unified Approach, McGraw-Hill, 1988.

Calvert J.G., Pitts J.N., Photochemistry, John Wiley & Sons, 1966.

Campbell, I.M., Catalysis at Surfaces, Chapman and Hall-UK, 1988.

Che M., Tench A.J., "Characterization and Reactivity of Molecular Oxygen Species on Oxide Surfaces", Advances in Catalysis, Volume 32, Academic Press, 1983.

Childs L.P., Ollis D.F., "Is Photocatalysis Catalytic?", *Journal of Catalysis* 66:383, 1980.

Cundall R.B., Rudham R, Salim M.S., "Photocatalytic Oxidation of Propan-2-ol in the Liquid Phase by Rutile", *Faraday Transactions 1*, 72:1642, 1976.

D'Oliveira J-C., Al-Sayyed G., Pichat P., "Photodegradation of 2- and 3-Chlorophenol in TiO_2 Aqueous Suspensions", *Environmental Science and Technology* 24:990, 1990.

Ellis W.D., Payne J.R., Tafuri A.N., Freestone F.J., "The Development Chemical Countermeasures for Hazardous Waste Contaminated Soil", 1984 Hazardous Material Spill Conference, J Ludwigson, Ed., p118, Government Institutes, Inc. MD, 1984.

Emmert R.E., Pigford R.L., "A study of Gas Absorption in Falling Liquid Films", *Chemical Engineering Progress* 50(2):87, 1954.

Farin D., Kiwi J., Avnir D., "Size Effects in Photoprocesses on Dispersed Catalysts", *Journal of Physical Chemistry* 93:5851, 1989.

Fox M.A., Chen C-C., "Mechanistic Features of the Semiconductor Photocatalyzed Olefin-to-Carbonyl Oxidative Cleavage", *Journal of the American Chemical Society* 103:6757, 1981

Fujihira M., Satoh Y., Osa T., "Heterogeneous Photocatalytic Oxidation of Aromatic Compounds on TiO_2", *Nature* 293(17):206, 1981.

Fujihira M., Satoh Y., Osa T., "Heterogeneous Photocatalytic Reactions on Semiconductor Materials III. Effect of pH and Cu^{2+} ions on the Photo-Fenton Type Reactions", *Bulletin of the Chemical Society of Japan* 55:666, 1982.

Goodenough J.B., Hamnett A., "Titanium Oxide (TiO_2)", Physics of Non-Tetrahedrally Bonded Binary Compounds III, Semiconductors subvolume g, Volume 17, Group III, Landolt-Bornstein, 1987.

Harvey P.R., Rudham R., Ward S., "Photocatalytic Oxidation of Liquid Propan-2-ol by Titanium Dioxide", *Faraday Transactions 1*, 79:1381, 1983.

Hatchard C.G., Parker C.A., "A New Sensitive Chemical Actinometer, II. Potassium Ferrioxalate as a standard Chemical Actinometer" *Proceedings of the Royal Society of London*, A235:518, 1956.

Herrmann J-M., Mozzanega M-N., Pichat P., "Oxidation of Oxalic Acid in Aqueous Suspensions of Semiconductors Illuminated with UV or Visible Light", *Journal of Photochemistry* 22:333, 1983.

Hsiao C-Y., Lee C-L., Ollis D.F., "Heterogeneous Photocatalysis: Degradation of Dilute Solutions of Dichloromethane, Chloroform and Carbon Tetrachloride with Illuminated TiO_2 Photocatalyst", *Journal of Catalysis* 82:418, 1983.

Izumi I., Dunn W., Wilbourn K.O., Fan F-R.F., Bard A.J., "Heterogeneous Photocatalytic Oxidation of Hydrocarbons on Platinized TiO_2 Powders", *Journal of Physical Chemistry* 84:3207, 1980.

Jacob S.M., Dranoff J.S., "Light Intensity Profiles in a Perfectly Mixed Photoreactor" *Journal of AIChE* 16(3):359, 1970.

Kalyanasundaram K., "Semiconductor Particulate Systems for Photocatalysis and Photosynthesis: An Overview", Chapter 7, <u>Energy Resources through Photochemistry and Catalysis</u>, M. Gratzel, Ed., Academic Press, 1983.

Kraeutler B., Bard A.J., "Heterogeneous Photocatalytic Decomposition of Saturated Carboxylic Acids on TiO_2 Powder. Decarboxylative Route to

Alkanes", _Journal of the American Chemical Society_ 100(19):5985, 1978.

Lim S.T., 1980, Hydrodynamics and Mass Transfer Processes Associated with the Absorption of Oxygen in Liquid Films Flowing Across a Rotating Disc", Ph.D. thesis, University of Newcastle-upon-Tyne, Great Britain.

Linke W.F., Seidel A., Solubilities of Inorganic and Metal-Organic Compounds, A Compilation of Solubility Data from the Periodical Literature, Fourth Edition, Volume-II, American Chemical Society, Washington, D.C. 1965.

Masschelein W.J., Denis M., Minon G., "Light Intensity in UV-Reactors", _Ozone: Science and Engineering_, The Journal of the International Ozone Association, 13(2):221, 1991.

Matthews R.W., "Near UV Light Induced Competitive Hydroxyl Radical Reactions in Aqueous Slurries of Titanium Dioxide", _Journal of Chemical Society-Chemical Communications_ 177, 1983.

Matthews R.W., "Hydroxylation Reactions Induced by Near-ultraviolet Photolysis of Aqueous Titanium Dioxide Suspensions", _Journal of Chemical Society Faraday Transactions 1_, 80:457, 1984.

Matthews R.W., "Photocatalytic Oxidation of Chlorobenzene in Aqueous Suspensions of Titanium Dioxide", _Journal of Catalysis_ 97:565, 1986.

Matthews R.W., "Photo-oxidation of Organic Material in Aqueous Suspensions of Titanium Dioxide", *Water Research* 20(5):569, 1986b.

Matthews R.W., "Carbon Dioxide Formation from Organic Solutes in Aqueous Suspensions of Ultraviolet-Irradiated TiO_2. Effect of Solute Concentration", *Australian Journal of Chemistry* 40:667, 1987a.

Matthews R.W., "Phofooxidation of Organic Impurities in Water using Thin Films of Titanium Dioxide", *Journal of Physical Chemistry* 91:3328, 1987b.

Matthews R.W., "Solar-Electric Water Purification Using Photocatalytic Oxidation with TiO_2 as a Stationary Phase", *Solar Energy* 38(6):405, 1987c.

Matthews R.W., "Response to the Comment 'Photocatalytic Reactor Design: An Example of Mass Transfer Limitations with an Immobilized Catalyst'", *Journal of Physical Chemistry* 92:6853, 1988.

Matthews R.W., "Kinetics of Photocatalytic Oxidation of Organic Solutes over Titanium Dioxide", *Journal of Catalysis* 111:264, 1988b.

Matthews R.W., "Photocatalytic Oxidation and Adsorption of Methylene Blue on Thin Films of Near Ultraviolet Illuminated TiO_2", *Faraday Transactions 1*, 85(6):1291, 1989.

Matthews R.W., "Purification of Water with Near UV Illuminated Suspensions of Titanium Dioxide", *Water Research* 24(5):653, 1990.

Matthews R.W., "Photooxidative Degradation of Coloured Organics in Water Using Supported Catalysts. TiO$_2$ on Sand", *Water Research* 25(10):1169, 1991.

Matthews R.W., "Photocatalysis in Water Purification: Possibilities, Problems and Prospects", *The First International Conference on TiO$_2$ Photocatalytic Purification and Treatment of Water and Air, Abstracts*, London-Ontario, Canada, November 8-13, 1992.

Minero C., Catozzo F., Pelizzetti E., "Role of Adsorption in Photocatalyzed Reactions of Organic Molecules in Aqueous TiO$_2$ Suspensions", *Langmuir* 8:481, 1992.

Ollis D.F., Hsiao C-Y., Budiman L., Lee C-I., "Heteroogeneous Photocatalysis: Conversions of Perchloroetylene, Dichloroethane, Chloroacetic Acids and Chlorobenzenes", *Journal of Catalysis* 88:89, 1984.

Ollis D.F., "Contaminant Degradation in Water", *Environmental Science and Technology* 19(6):480, 1985.

Ollis D.F., Pelizzetti E., Serpone N., "Heterogeneous Photocatalysis in the Environment: Application to Water Purification", Chapter 18, Photocatalysis: Fundamentals and Applications, Serpone N., Pelizzetti E., Eds.;Wiley:New York, 1989.

Ollis D.F., Turchi C., "Heterogeneous Photocatalysis for Water Purification: Contaminant Mineralization Kinetics and Elementary Reactor Analysis", *Environmental Progress* 9(4):229, 1990.

Ollis D.F., Pelizzetti E., Serpone N., "Photocatalyzed Destruction of Water Contaminants", *Environmental Science and Technology* 25(9):1522, 1991.

Pacheco J.E., Tyner C.E., "Enhancement of Processes for Solar Photocatalytic Detoxification of Water", *The Twelfth Annual ASME International Solar Energy Conference*, Miami-Florida, April 1-4, 1990.

Pelizzetti E., Maurino V., Minero C., Sclafani A., Serpone N., Hidaka H., "Photocatalytic Degradation of Nonylphenol Etoxylated Surfactants", *Environmental Science and Technology* 23:1380, 1989.

Pelizzetti E., Minero C., "Mechanism of the Photo-oxidative Degradation of Organic Pollutants over TiO_2 Particles", *Electrochimica Acta* 38(1):47, 1993.

Pichat P., "Photocatalytic Reactions", Photoelectrochemistry, Photocatalysis and Photoreactors, M. Schiavello, Ed., Reidel Publishing, 1985.

Pruden A.L., Ollis D.F., "Photoassisted Heterogeneous Catalysis: The Degradation of Trichloroethylene in Water", *Journal of Catalysis* 82:404, 1983.

Qualls R.G., Johnson J.D., "Bioassay and Dose Measurement in UV Disinfection", *Applied and Environmental Microbiology*, 45:872, 1983.

X

Rizzuti L., "Absorption of Light Energy in Photoreactors"
Photoelectrochemistry, Photocatalysis and Photoreactors, M.
Schiavello, Ed., Reidel Publishing, 1985.

Rizzuti L., Brucato A., "Photochemical Reactors Engineering Fundamentals",
Photocatalysis and Environment, M. Schiavello, Ed., Kluwer Academic
Publishers, 1988.

Sakata T, Kawai T, "Photosynthesis and Photocatalysis with Semiconductor
Powders", Chapter 10, Energy Resources through Photochemistry and
Catalysis, M. Gratzel, Ed., Academic Press, 1983.

Schenck G.O., "Ultraviolet Sterilization", Chapter 16, Handbook of Water
Purification, W. Lorch, Ed., Ellis Horwood Limited, 1987.

Sclafani A., Palmisano L., Schiavello M., "Influence of the Preparation
Methods of TiO_2 on the Photocatalytic Degradation of Phenol in
Aqueous Dispersion", *Journal of Physical Chemistry* 94:829, 1990.

Sclafani A., Palmisano L., Davi E., Photocatalytic Degradation of Phenol in
Aqueous Polycrystallinne TiO_2 Dispersions: The Influence of Fe^{3+}, Fe^{2+}
and Ag^+ on the Reaction Rate", *Journal of Photochemistry and
Photobiology A: Chemistry* 56:113, 1991.

Sczechowski J.G., Koval C.A., Noble R.D., "Increasing the Photoefficiency in
Heterogeneous Photocatalysis", *Book of Abstracts, 205th ACS National
Meeting*, Denver, Colorado, March 28-April 2, 1993.

Serpone N., Borgarello E., Harris R., Cahill P., Pelizzetti E., "Photocatalysis over TiO_2 Supported on a Glass Substrate", *Solar Energy Materials* 14:121, 1986.

Serpone N., Lawless D., Terzian R., "Heterogeneous Photocatalysis with TiO_2 Semiconductor Particles in Aqueous Media", *Abstracts of Papers Fourth Chemical Congress of North America*, New York, NY, August 25-30, 1991.

Sherwood T.K., Pigford R.L., Wilke C.R., Mass Transfer, McGraw-Hill, 1975.

Shoffner G.D., Koval C.A., Noble R.D., "Improving the Quantum Yield of Aqueous Photocatalytic Systems", *Book of Abstracts, 205th ACS National Meeting*, Denver, Colorado, March 28-April 2, 1993.

Tanguay J.F., Suib S.L., Coughlin R.W., "Dichloromethane Photodegradation Using Titanium Catalysts", *Journal of Catalysis* 117:335, 1989.

Teichner S.J., Formenti M., "Heterogeneous Photocatalysis", Photoelectrochemistry, Photocatalysis and Photoreactors, M. Schiavello, Ed., Reidel Publishing, 1985.

Terzian R., Serpone N., Minero C., Pelizzetti E., Hidaka H., "Kinetic Studies in Heterogeneous Photocatalysis 4. The Photomineralization of a Hydroquinone and a Catechol", *Journal of Photochemistry and Photobiology A: Chemistry* 55:243, 1990.

Terzian R., Serpone N., Minero C., Pelizzetti E., "Photocatalyzed
    Mineralization of Cresols in Aqueous Media with Irradiated Titania",
    Journal of Catalysis 128:352, 1991.

Tseng J.M., Huang C.P., "Removal of Chlorophenols from Water by
    Photocatalytic Oxidation", *Water Science and Technology* 23:377, 1991.

Tunesi S., Anderson M.A., "Photocatalysis of 3,4-DCB in TiO_2 Aqueous
    Suspensions: Effects of Temperature and Light Intensity; CIR-FTIR
    Interfacial Analysis", *Chemosphere* 16:1447, 1987.

Turchi C.S., Ollis D.F., "Photocatalytic Reactor Design: An Example of Mass-
    Transfer Limitations with an Immobilized Catalyst", *Journal of Physical
    Chemistry* 92:6852, 1988.

Turchi C.S., Ollis D.F., "Mixed Reactant Photocatalysis: Intermediates and
    Mutual Rate Inhibition", *Journal of Catalysis* 119:483, 1989.

Turchi C.S., Ollis D.F., "Photocatalytic Degradation of Organic Water
    Contaminants: Mechanisms Involving Hydroxyl Radical Attack",
    Journal of Catalysis 122:178, 1990.

Venkataraman R.S., 1966, "Mass Transfer to an Expanding Interface", Ph.D.
    thesis, University of Leeds, Great Britain.

Wallis C., 1991, "The Ozone Disinfection Performance of Rotary Contactors",
    PhD thesis, University of Newcastle upon Tyne, Great Britain.

Yoneyama H., Haga S., Yamanaka S., "Photocatalytic Activities of

   Microcrystalline TiO_2 Incorporated in Sheet Silicates of Clay", *Journal of*

   Physical Chemistry 93:4833, 1989.

Yue P.L., "Introduction to the Modelling and Design of Photoreactors",

   Photoelectrochemistry, Photocatalysis and Photoreactors, M.

   Schiavello, Ed., Reidel Publishing, 1985a.

Yue P.L., "Studies of Photoreactions in Homogeneous Photoreactors",

   Photoelectrochemistry, Photocatalysis and Photoreactors, M.

   Schiavello, Ed., Reidel Publishing, 1985b.

Yue P.L., "Studies of Photoreactions in Heterogeneous Photoreactors",

   Photoelectrochemistry, Photocatalysis and Photoreactors, M.

   Schiavello, Ed., Reidel Publishing, 1985c.

Yue P.L., "Modelling and Design of Photochemical Reactors for Water

   Purification", Photocatalysis and Environment, M. Schiavello, Ed.,

   Kluwer Academic Publishers, 1988.

APPENDIX A

Computer Programs

This program is to find out k_1 and k_2 coefficients using experimental values and L-H kinetic model written by Ebert et al. (1989) and modified here for L-H kinetic model. The programming language used is Qbasic.

(Ref. K. Ebert, H. Ederer, T.L. Isenhour Computer Applications in Chemistry, VCH, Germany, 1989)

```
0  REM "NL-REGR "          EBERT/EDERER          881212
1  REM **************************************************
2  REM *** Nonlinear regression by a multi-        ***
3  REM *** dimensional Newton method. The function ***
4  REM *** of regression has to be programmed in   ***
5  REM *** line # 50000, the number of parameters  ***
6  REM *** in line # 20100 and the data input      ***
7  REM *** section starts in line # 60000.         ***
9  REM **************************************************
100    DIM A(20,20), B(20,20), U(20,20)
110    DIM V(20,20), W(20,20)
200    DIM X(20), X9(20), F(20), F9(20)
210    DIM F0(20), H(20), K(20)
220    DIM XX(100), YY(100)
250    GOTO 20000   :   REM jump to the MAIN program
300    REM **********************************************
305    REM *** Subroutine: INVERS                    ***
310    REM *** Input Matrix    in A()                ***
315    REM *** Inverted Matrix in W()                ***
320    REM **********************************************
400    FOR I=1 TO N
420      FOR J=1 TO N
460        B(I,J) = 0
480        V(I,J) = 0
500        IF I<>J THEN GOTO 600
520        B(I,J) = 1
540        V(I,J) = 1
600      NEXT J
620    NEXT I
1000   FOR Z=1 TO N
1050     S=0
1100     REM *******************************************
1105     REM *** Searching for the pivot element.   ***
1110     REM *******************************************
1120     FOR I=Z TO N
1150       IF S>ABS(A(I,Z)) THEN GOTO 1300
1200       S=ABS(A(I,Z)) : T=I
1300     NEXT I
```

```
2000    REM ********************************************
2001    REM *** Lines Z and T will be exchanged.   ***
2005    REM ********************************************
2050    FOR I = 1 TO N
2100       S=A(Z,I) : A(Z,I)=A(T,I) : A(T,I)=S
2200    NEXT I
2300    IF ABS(A(Z,Z))>1E-30 THEN GOTO 2400
2350    PRINT "No inversion is possible " : END
2400    V(Z,Z)=0 : V(T,T)=0
2450    V(Z,T)=1 : V(T,Z)=1
3000    REM ********************************************
3020    REM *** Gauss-Jordan elimination            ***
3040    REM ********************************************
3100    FOR I=1 TO N
3200      FOR J=1 TO N
3300         IF I=Z THEN GOTO 4000
3350         IF J=Z THEN GOTO 4500
3400         U(I,J)=A(I,J)-A(Z,J)*A(I,Z)/A(Z,Z)
3500         GOTO 5000
4000         IF I=J THEN GOTO 4350
4050         U(I,J)=-A(I,J)/A(Z,Z)
4100         GOTO 5000
4350         U(Z,Z)=1/A(Z,Z)
4400         GOTO 5000
4500         U(I,Z)=A(I,Z)/A(Z,Z)
5000    NEXT J : NEXT I
5100    REM ********************************************
5102    REM *** Multiplication  B=V*B               ***
5110    REM ********************************************
5200    FOR I=1 TO N
5250      FOR J=1 TO N
5300        W(I,J)=0
5350        FOR K=1 TO N
5400           W(I,J)=W(I,J)+V(I,K)*B(K,J)
5450    NEXT K : NEXT J : NEXT I
5500    FOR I=1 TO N : FOR J=1 TO N
5550        B(I,J)=W(I,J)
5600    NEXT J : NEXT I
6000    FOR I=1 TO N
6050      FOR J=1 TO N
6100        A(I,J)=U(I,J) : V(I,J)=0
6250        IF I=J THEN V(I,J)=1
6300    NEXT J : NEXT I
6500    NEXT Z
7000    REM ********************************************
7005    REM *** The result is obtained by multiplying***
7010    REM *** matrix A with the permutation        ***
7020    REM *** matrix B.                            ***
7030    REM ********************************************
7100    FOR I=1 TO N
7200      FOR J=1 TO N
7300        W(I,J)=0
7400        FOR K=1 TO N
7500           W(I,J)=W(I,J)+A(I,K)*B(K,J)
7600    NEXT K : NEXT J : NEXT I
7700    RETURN : REM end of INVERS
```

```
12000 REM **************************************************
12010 REM *** Subroutine: FUNCTIONS                    ***
12020 REM *** The functions, whose roots have to        ***
12030 REM *** be calculated, are programmed here.       ***
12040 REM ***    dS/dK(J)                               ***
12060 REM **************************************************
12100 FOR J=1 TO N : K(J)=X(J) : NEXT J
12200 GOSUB 30000 : F0=SS
12300 FOR J=1 TO N : DJ=ABS(X(J)/10000!)+1E-08
12400   K(J)=K(J)+DJ : GOSUB 30000
12410   F(J)=SS : K(J)=K(J)-2*DJ : GOSUB 30000
12500   F(J)=(F(J)-SS)/2/DJ
12600   K(J)=X(J) : NEXT J
12999 RETURN
15000 REM **************************************************
15010 REM *** Subroutine: PARTIAL                      ***
15020 REM *** The partial derivatives at the po-        ***
15030 REM *** sition X9() are calculated and            ***
15035 REM *** stored in matrix A().                     ***
15040 REM ***    d (dS/dK(J) ) / dK(I)                  ***
15050 REM **************************************************
15100 FOR I=1 TO N : X(I)=X9(I) : NEXT I
15120 GOSUB 12000 : REM FUNCTIONS calling
15160 FOR I=1 TO N : F9(I)=F(I) : NEXT I
15200 FOR I3=1 TO N : DI=ABS(X(I3)/10000!)+1E-08
15210   X(I3)=X(I3)+DI : GOSUB 12000
15240   FOR J3=1 TO N : A(J3,I3)=F(J3)
15260   NEXT J3 : X(I3)=X9(I3) : NEXT I3
15300 FOR I3=1 TO N : DI=ABS(X(I3)/10000!)+1E-08
15310   X(I3)=X(I3)-DI : GOSUB 12000
15340   FOR J3=1 TO N : A(J3,I3)=(A(J3,I3)-F(J3))/2/DI
15360   NEXT J3 : X(I3)=X9(I3) : NEXT I3
15999 RETURN
19000 REM **************************************************
19010 REM *** Subroutine: OUTPUT                       ***
19020 REM **************************************************
19100 PRINT
19120 FOR I=1 TO N
19140   PRINT "K("; I; ") =";X9(I); "+/-";
19150   PRINT SQR(ABS(W(I,I)*SS/(NP-N)))
19180 NEXT I
19185 PRINT "Sum of squared errors = "; SS
19190 RETURN
20000 REM **************************************************
20010 REM *** MAIN program                             ***
20020 REM **************************************************
20100 N=2 : REM number of parameters
20130 FF=1 : SM=1E+30
20150 GOSUB 25000
20200 PRINT "Input of the estimated parameters"
20220 PRINT
20300 FOR I=1 TO N : PRINT "K("; I; ")=";
20320   INPUT X(I) : X9(I)=X(I) : NEXT I
20400 GOSUB 15000: REM Partial derivatives
20500   GOSUB 300: REM matrix inversion
20600   FOR I=1 TO N : H(I)=0
```

```
20700       FOR J=1 TO N : H(I)=H(I)+W(I,J)*F9(J)
20720    NEXT J : NEXT I
20750    GOSUB 19000 : REM Output
20800    GOSUB 35000 : REM Optimization factor
21000    FOR I=1 TO N : X9(I)=X9(I)-FF*H(I) : NEXT I
21100 GOTO 20400
21500 REM ###############################################
21510 REM ### MAIN program ends here.            ###
21520 REM ###############################################
25000 REM ********************************************
25010 REM *** Subroutine: READ_DATA                 ***
25080 REM ********************************************
25100 READ NP: REM number of points
25200 FOR I=1 TO NP : READ XX(I), YY(I) : NEXT I
25400 RETURN
30000 REM ********************************************
30010 REM *** Subroutine: SQUARED_SUM               ***
30020 REM *** The sum of the squared deviations     ***
30030 REM *** is evaluated in this section.         ***
30100 REM ********************************************
30200 SS=0
30300 FOR I=1 TO NP
30350    X=XX(I) : GOSUB 50000 : Y=Y-YY(I)
30400    SS=SS+Y*Y : NEXT I
30500 RETURN
35000 REM ********************************************
35001 REM *** Subroutine: OPTIMUM                   ***
35002 REM *** The optimization factor FF is deter-  ***
35003 REM *** mined here.                           ***
35005 REM ********************************************
35200 FF=.6 : FM=0 : DF =.5
35310 GOSUB 35600
35320 IF SS<SM THEN SM=SS : FM=FF : FF=FF+DF : GOTO 35310
35330 FF=FM-DF
35335 GOSUB 35600
35340 IF SS<SM THEN SM=SS : FM=FF : FF=FF-DF : GOTO 35335
35360 FOR J=1 TO 7
35380    DF=DF/2
35390    FF=FM+DF : GOSUB 35600
35400    IF SS<SM THEN SM=SS : FM=FF : GOTO 35430
35410    FF=FM-DF : GOSUB 35600
35420    IF SS<SM THEN SM=SS : FM=FF
35430 NEXT J
35450 FF=FM
35500 RETURN
35600 FOR I=1 TO N : K(I)=X9(I)-FF*H(I) : NEXT I
35620 GOSUB 30000
35650 RETURN
50000 REM ********************************************
50010 REM *** Subroutine: FUNCTION_OF_REGRESSION    ***
50100 REM ********************************************
50200 Y = (1/k(1)/k(2))*LOG(250/x)-(x-250)/k(2)
50300 REM t = (1/k(1)/k(2))*Ln(Co/C)-(C-Co)/k(2)
50999 RETURN
```

```
60000 REM  ############################################
60010 REM  ### Data section:                      ###
60020 REM  ### The first value is the number of   ###
60030 REM  ### data points, followed by the data  ###
60040 REM  ### points as pairs (X,Y).             ###
60050 REM  ############################################
61000 DATA  11      : REM number of data points
62010 DATA  250,0
62020 DATA  233.01,2
62030 DATA  218.44,4
62040 DATA  206.31,6
62050 DATA  196.60,8
62060 DATA  179.61,10
62070 DATA  167.47,12
62080 DATA  157.76,14
62090 DATA  143.20,16
62100 DATA  123.78,20
62200 DATA  101.94,25
63999 END
```

The program of prediction of the theoretical values according to L-H kinetics

with obtained k_1 and k_2 coefficients

```
REM
REM Constants
10  CLS
     INPUT "K1="; K1
     INPUT "K2="; K2
     INPUT "C0="; C0
     INPUT "DATA SET (N)="; N
REM Arrays
     REDIM T(N)
     REDIM C(N)
     REDIM TIME(N)
     C(0)=1
     FOR I=1 TO N
     PRINT "TIME("; I; ")=",
     INPUT TIME(I)  : NEXT I
PRINT TAB(10); "Time(min)"; TAB(30); "Concentration(µM)"
PRINT TAB(10); "---------"; TAB(30); "------------------"
     FOR I=1 TO N
     T(I)=TIME(I)
     IF T(I)=0 THEN END
     C(I)=C(I-1)
     S=0
20 REM Iteration starts here
     S=S+1
     CC=EXP(LOG(C0)-(K1*K2*T(I))-(K1*(C(I)-C0)))
     IF ABS(CC-C(I))<=.0001 THEN 30
     C(I)=CC
```

VI

.

```
      GOTO 20
30 PRINT TAB(13); T(I); USING "$$$.$$$$"; TAB(35); C(I)
   NEXT I
      INPUT " READY FOR NEW DATA SET (Y/N)"; A$
      IF A$="y" THEN 10
      PRINT : PRINT : PRINT : PRINT
      PRINT "               <BYE THEN>"
END
```

.

.

APPENDIX B

Experimental and Computational Data

Data for the annular reactor

B1. Absorbance of thin films of Degussa P-25 and Tioxide PC1 catalyst (data for Figure 8.2).

	Surface loading (mg/cm²)		Wavelength (nm)		
			254	365	440
P-25	0.16	Abs.>	0.786	0.438	0.227
	0.40		1.852	1.168	0.627
	0.63		3.459	2.930	1.834
PC1	0.23	Abs.>	1.622	1.654	1.589
	0.46		1.872	1.889	1.812
	0.80		2.782	2.846	2.486

B2. Effect of catalytic slurry concentration upon the first order rate constant (data for Table 8.1) in annular reactor.

			Slurry conc.(g/lt)			
	Time (min)	0.5	1	2	3
P-25	0	(µM)> 100	100	100	100
	2	77.96	72.47	54.27	50.5
	4	66.66	55.5	48.24	42.57
	6	54.8	48.16	40.7	40.09
	8	45.19	38.53	35.17	29.7
	10	36.72	31.19	29.14	28.21
	12	29.94	27.06	23.61	23.26
	14	27.11	22.01	18.59	20.79
	16	23.16	17.43	16.08	16.33
	20	16.94	11.26	9.54	8.91
	25	11.21	6.74	6.03	5.99
PC1	0	(µM)> 100	100	100	100
	2	55.33	42.08	36.31	45.94
	4	44	32.67	29.47	37.38

6	40	23.26	17.89	31.98
8	34.66	17.32	13.68	27.47
10	26.66	11.88	9.73	23.87
12	21.33	7.92	6.84	21.62
14	16.66	5.44	4.73	20.72
16	12.66	3.21	3.15	19.81
20	8.66	1.485	1.31	18.91
25	4.66	0.742	0.5	17.5

B3. Effect of physical adsorption of organic molecules on two different catalysts surfaces under no light (data for Figure 8.3) in annular reactor.

	Catalyst type			
Time (min)	P-25 (4-CP)	PC1 (4-CP)	P-25 (SA)	PC1(SA)
0	(μM)> 100	100	100	100
2	95	97.56	85.53	60.15
4	94.16	99.18	86.79	60.15
6	95	98.37	87.05	60.15
8	94.16	98.37	87.05	60.9
10	94.16	97.56	86.79	60.15
12	92.66	95.93	86.86	61.65
14	92.83	95.93	86.86	60.9
16	91.66	94.3	85.9	59.4
20	92.83	94.93	86.67	59.64
25	92.5	94.49	86.51	60.2

B4. Effect of liquid flow rate upon the first order rate constant (data for Table 8.2 and Figure 8.4) in annular reactor.

	Flow rate (lt/min)			
Time (min)	0.5	0.75	1	1.25
0	(μM)> 100	100	100	100
2	85.28	79.71	74.09	71.28

4	72.58	67.11	61.65	58.92
6	64.97	60.20	55.44	51.04
8	59.39	51.97	44.55	40.84
10	52.79	45.04	37.3	33.43
12	46.7	38.11	29.53	26.24
14	41.11	33.50	25.9	23.10
16	36.04	29.15	22.27	19.83
20	29.94	24.03	18.13	15.18
25	23.85	18.40	12.95	10.22

B5. Effect of different light sources over two different organics (data for Table 8.3 and Figure 8.5) in annular reactor.

	Lamp type			
Time (min)	LP (4-CP)	LP(SA)	MP(4-CP)	MP(SA)
0	(µM)> 100	100	100	100
2	91.89	78.76	60	74.09
4			53.68	61.65
6			46.31	55.44
8	77.47	67.8	40	44.55
10				37.3
12			30.52	29.53
14				25.9
15	66.66	57.53		
16			25.26	22.27
20	60.36	51.37	21.05	18.13
25	54.95	46.57	16.84	12.95
30	49.54	41.78		
35	45.94			
40		34.93		
42	41.44			
45		32.19		
50	36.93	28.76		
60	32.43	21.91		

B6. Effect of initial concentration upon the degradation of salicylic acid (data for Table 8.4 and Figure 8.6) in annular reactor.

Initial conc.(500µM)

Time (min)	Exper.Points	Lang-Hins	1st order
0	(µM)> 500	500	500
2	456.9	485.36	478.14
4	451.1	471.16	460.76
6	439.6	457.37	445.61
8	433.9	443.99	435.70
10	425.3	431.0	425.99
12	419.5	418.40	416.51
14	402.3	406.16	407.24
16	393.7	394.28	398.17
20	379.3	371.56	380.64
25	367.8	345.0	359.81

Initial conc.(250µM)

Time (min)	Exper.Points	Lang-Hins	1st order
0	(µM)> 250	250	250
2	208.3	226.97	218.81
4	183.7	206.07	193.79
6	168.5	187.10	173.89
8	155.3	169.88	161.01
10	140.1	154.25	149.09
12	130.7	140.06	138.05
14	123.1	127.18	127.83
16	115.5	115.48	118.36
20	102.2	95.22	101.49
25	92.81	74.82	83.73

Initial conc.(100µM)

Time (min)	Exper.Points	1st order
0	(µM)> 100	100
2	74.09	77.09
4	61.65	63.01

6	55.44	53.59
8	44.55	45.57
10	37.3	38.76
12	29.53	32.96
14	25.9	28.03
16	22.27	23.84
20	18.13	17.24
25	12.95	11.50

.

Data for the falling film reactor

B7. Effect of catalyst type on the degradation of salicylic acid in falling film reactor (data for Figure 9.1).

	Catalyst type	
Time (min)	Tioxide	P-25
0	(μM)> 100	100
2	66.97	67.85
4	56.42	51.02
6	50	36.73
8	40.36	26.53
10	34.4	17.85
12	29.81	11.73
14	23.85	7.14
16	19.26	4.08
20	11.46	1.02
25	6.88	0.51

.

B8. Effect of catalyst loading in falling film reactor (data for Figure 9.2 and 9.3).

Catalyst type	Tioxide		P-25	
Time (min)	0.5g/lt	1g/lt	0.5g/lt	1g/lt
0	(µM)> 100	100	100	100
2	66.97	47.42	67.85	61.62
4	56.42	38.14	51.02	41.86
6	50	31.95	36.73	27.9
8	40.36	29.38	26.53	18.6
10	34.4	24.74	17.85	11.04
12	29.81	20.1	11.73	7.56
14	23.85	13.91	7.14	3.49
16	19.26	9.27	4.08	1.74
20	11.46	5.41	1.02	0.87
25	6.88	3.6	0.51	

B9. Destruction of reactants with 100µM initial concentration in falling film reactor (data for Table 9.1 and Figure 9.4).

Time (min)	Exper.Points	Salicylic acid Lang-Hins	1st order
0	(µM)> 100	100	100
2	67.85	74.53	74.51
4	51.02	53.74	50.60
6	36.73	37.52	34.37
8	26.53	25.44	23.34
10	17.85	16.83	15.85
12	11.73	10.92	10.76
14	7.14	6.99	7.31
16	4.08	4.43	4.96
20	1.02	1.75	2.29
25	0.51	0.54	0.87

Time (min)	Exper.Points	4-Chlorophenol Lang-Hins	1st order
0	(μM)> 100	100	100
2	58.06	60.09	58.97
4	33.33	34.87	33.40
6	18.27	19.74	18.92
8	11.29	11.01	10.72
10	6.989	6.08	6.073
12	3.764	3.34	3.44
14	1.613	1.83	1.95
16	1.1	1.0	1.104
20		0.29	0.354
25	·	0.06	0.085

B10. Destruction of reactants with 250μM initial concentration in falling film reactor (data for Table 9.2 and Figure 9.5-9.6).

Time (min)	Exper.Points	Catechol (CA) Lang-Hins	1st order
0	(μM)> 250	250	250
2	233.01	234.94	236.89
4	218.44	220.41	220.55
6	206.31	206.43	205.34
8	196.6	193	191.18
10	179.61	180.14	177.99
12	167.47	167.83	165.72
14	157.76	156.09	154.29
16	143.2	144.91	143.65
20	123.78	124.25	124.52
25	101.94	101.52	104.15

Time (min)	Exper.Points	Hydroquinone (HQ) Lang-Hins	1st order
0	(μM)> 250	250	250
2	225.44	227.59	226.96
4	205.35	207.05	206.2

6	185.26	188.26	187.34
8	169.64	171.08	170.21
10	158.48	155.39	154.64
12	142.85	141.07	140.49
14	125	128.01	127.64
16	116.07	116.12	115.97
20	98.21	95.44	95.72
25	73.66	74.52	75.31

Salicylic acid (SA)

Time (min)	Exper.Points	Lang-Hins	1st order
0	(µM)> 250	250	250
2	220.58	227.42	*227.1*
4	199.57	206.1	203.59
6	182.77	186.04	182.52
8	165.96	167.28	163.62
10	153.36	149.81	146.69
12	136.55	133.63	131.51
14	121.84	118.73	117.89
16	105.04	105.09	105.69
20	79.83	81.42	84.94
25	63.03	58.06	64.64

4-Chlorophenol (4-CP)

Time (min)	Exper.Points	Lang-Hins	1st order
0	(µM)> 250	250	250
2	164.44	163.67	164.16
4	102.94	106.23	105.46
6	67.4	68.55	67.75
8	46.56	44.06	43.52
10	28.18	28.24	27.96
12	18.38	18.07	17.96
14	11.03	11.55	11.54
16	7.35	7.38	7.41
20	3.06	3	3.06
25		0.98	

B11. Light intensity distribution of medium-pressure lamp used in FFR (data for Figure 9.8)

Distance from centre (cm)	a = 1cm b = 15cm	a = 6cm b = 10cm	a = 11cm b = 5cm
	Intensity (quanta/s.cm^2)*10^{17}		
23	0.953	1.072	0.873
21	0.974	1.124	0.919
19	0.995	1.200	1.082
17	1.021	1.301	1.261
15	1.097	1.378	1.419
13	1.225	1.480	1.542
11	1.276	1.582	1.608
9	1.327	1.633	1.71
7	1.352	1.659	1.746
5	1.378	1.684	1.766
3	1.378	1.684	1.786
1	1.403	1.710	1.807

B12. Salicylic acid and 4-Chlorophenol removal with intermediates in falling film reactor (data for Figure 9.9).

Time (min)	SA	4-CP	Catechol	Hydroquinone
0	(μM)> 250	250	0	0
2	220.58	165.44	23.66	26.78
4	199.57	102.94	37.18	56.91
6	182.77	67.4	54.08	72.54
8	165.96	46.56	67.6	80.91
10	153.36	28.18	81.13	78.12
12	136.55	18.38	91.27	75.33
14	121.84	11.03	98.03	65.61
16	105.04	7.35	101.41	58.68
20	79.83	3.06	104.79	46.87
25	63.03		98.03	29.57

X

B13. Effect of oxygen transfer in falling film reactor (data for Figure 9.10).

Time (min)	4-CP (air)	4-CP (N_2)	HQ (air)	HQ (N_2)
0	(μM)> 250	250	0	0
2	165.44	167.3	26.78	29.68
4	102.94	107.69	56.91	52.08
6	67.4	67.3	72.54	65.62
8	46.56	44.23	80.91	72.91
10	28.18	28.84	78.12	78.12
12	18.38	17.3	75.33	80.2
14	11.33	13.46	65.61	81.77
16	7.35	7.69	58.68	79.16
20	3.06	2.88	46.87	77.08
25			29.57	70

B14. pH variation for four organics in slurry system in falling film reactor (data for Figure 9.11).

Time (min)	SA	4-CP	Catechol	Hydroquinone
0	(μM)> 3.64	5.10	5.02	5.32
2	3.66	4.12	4.86	4.90
4	3.68	3.86	4.67	4.70
6	3.68	3.68	4.61	4.59
8	3.68	3.61	4.44	4.50
10	3.69	3.57	4.42	4.44
12	3.72	3.56	4.41	4.41
14	3.73	3.55	4.39	4.39
16	3.75	3.55	4.32	4.35
20	3.80	3.55	4.30	4.34
25	3.84	3.55	4.27	4.33

B15. Salicylic acid and 4-Chlorophenol removal with intermediates using Nutech catalyst coated fibre glass gauze in falling film reactor (data for Figure 9.12).

Time (min)	(µM)→ SA	4-CP	Catechol	Hydroquinone
0	250	250	0	0
2	231.81	121.21	12.05	44.77
4	212.12	53.03	28.71	67.91
6	192.42	24.62	42.37	64.92
8	178.78	9.46	58	62.68
10	165.15	5.68	73.08	55.97
12	148.48	2	84.52	48.50
14	137.87		92.74	
16	128.78		100.79	
20	106.06		112.84	
25	83.33		118.89	35.07

B16. Data obtained from the Langmuir-Hinshelwood and 1st order kinetic models using experimental data for immobilised system (data B14) in falling film reactor (data for Table 9.7).

Time (min)	1st order (µM)→ SA	4-CP	Lang-Hins SA	4-CP
0	250	250	250	250
2	231.40	115.74	230.38	116.74
4	212.10	53	212.06	53.54
6	194.41	24.26	194.98	24.35
8	178.19	11.11	179.10	11.02
10	163.33	5.087	164.34	4.98
12	149.71	2.33	150.66	2.25
14	137.22	1.06	138.0	1.01
16	125.78		126.28	0.46
20	105.67		105.51	
25	85		83.96	

B17. 2nd run to check catalyst stability of Nutech catalyst coated fibre glass gauze (data for Figure 9.13).

Time (min)	1st Run 4-CP	Hydroquinone	2nd Run 4-CP	Hydroquinone
0	(µM)> 250	0	250	0
2	121.21	44.77	145.83	34.77
4	53.03	67.91	62.5	63.79
6	24.62	64.92	29.76	75.86
8	9.46	62.68	13.39	69.82
10	5.68	55.97	5.95	61.02
12	2	48.50	3.5	55.17
14				51.72
25		35.07		36

Data for the spinning disc reactor

B18. Effect of UV lamp type and intensity upon the degradation of 4-chlorophenol in spinning disc reactor (data for Figure 10.1).

Time (min)	Low pressure (W/m^2) 5.52	2.76
0	(µM)> 91	91
30	73.81	75.48
60	57.4	61.83
90	43.72	47.5
120	29.81	33.92
150	17.85	22.52
180	10.06	13.05
210	4.88	7.6
240	2.28	3.75

Time (min)	Medium pressure (W/m²)			
	240	98.2	49	27.9
0	(µM)> 91	91	91	91
30	78.9	80.15	82.12	83.76
60	68.1	70.04	74	76.42
90	57.2	61.12	66.21	68.9
120	45.9	52	58.1	61.2
150	34.88	41.89	49.2	52.65
180	26.85	33	41.55	45.72
210	· 18	24.8	33	38.1
240	10.71	18.1	24.9	30

B19. Photochemical decomposition of 4-Chlorophenol in spinning disc reactor (data for Figure 10.2).

Time (min)	Low press. lamps	Medium press. lamp
0	(µM)> 91	91
30	90.78	91
60	90.59	91
90	90.28	91
120	90.1	91
150	89.92	91
180	89.7	91
210	89.51	91
240	89.28	91

B20. Effect of catalyst type upon the performance of the DSR with 4-Chlorophenol (data for Figure 10.3).

Time (min)	Degussa P-25		Tioxide PC1	
	Low press.	Med. press.	Low press.	Med. press.
0	(µM)> 91	91	91	91
30	73.81	78.9	79.11	81.63
60	57.4	68.1	69.6	72.5

90	43.72	57.2	58.75	63.1
120	29.81	45.9	48.18	53.6
150	17.85	34.88	38.56	43.6
180	10.06	26.85	29	34.9
210	4.88	18	19.98	25.02
240	2.28	10.71	13.5	16.8

B21. Effect of lamp type upon the degradation of salicylic acid with Degussa P-25 (data for Figure 10.4).

Time (min)	Low press.	Med. press.
0	(μM)> 89	89
30	74.8	78.72
60	60.02	68.2
90	46	58.5
120	34.2	49.05
150	23.9	39.88
180	16	31.4
210	9	23.66
240	5.5	16.05

APPENDIX C

Miscellaneous Calculations

C1. Calculation of quantum yield value

Quantum yield calculations are mainly based on the equation below (Eq.5.11 section 5.3) (Calvert and Pitts 1966, Braun et al. 1991):

$$\Phi = \frac{n_t}{I_a t_{1/2}}$$

n_t = the number of moles of reactant consumed

I_a = the number of moles of photons absorbed (*quanta s^{-1}*)

$t_{1/2}$ = the time for half of the degradation of initial reactant concentration(*s*)

$$n_t = C_{1/2} \times V \times N_A$$

$C_{1/2}$ = Half of the concentration degraded (*mol lt^{-1}*)

V = Volume of liquid used in the reactor (*lt*)

N_A = Avogadro constant (*6.02*10^{23} mol^{-1}*)

Sample calculation:

$$\Phi = \frac{50 \mu M \times 10^{-6}\, \dfrac{mol/lt}{\mu M} \times 2lt \times 6.02 \times 10^{23}}{3 \times 10^{18}\, quanta/s \times 12\,\text{min} \times 60\, \dfrac{s}{\text{min}}}$$

C

C2.   Defining of the light output in energy unit (watts)

Quanta is the other name of light particles i.e. photons. Each photon has its own energy at every different wavelength and this energy is defined as:

$$E = h.v.$$

To define light output in watts, 254nm for low pressure and 365nm for medium pressure was chosen because the low pressure lamps emit over 90% of its radiation at 254nm and medium pressure lamp emits predominantly at 365-366nm (section 7.1).

$$E = h.v = h \times \frac{c}{\lambda}$$

h = Planck constant ($6.62*10^{-34}$ J s)

v = Frequency (s^{-1})

c = Speed of light ($2.99*10^{10}$ cm s^{-1})

λ = Wavelength (nm)

$$E = 6.62 \times 10^{-34} \times \frac{2.99 \times 10^{10}}{254 \times 10^{-7}} = 7.82 \times 10^{-19} J(watt.s)$$

Each quanta has 7.82×10^{-19} *watt.s* energy at 254nm

Each quanta has 5.44×10^{-19} *watt.s* energy at 365nm

For the low pressure lamp with 3.10^{18} *quanta.s^{-1}* output :

3.10^{18} *quanta.s^{-1}* = 2.35 *watt*

For the medium pressure lamp with 5.10^{19} *quanta.s^{-1}* output :

5.10^{19} *quanta.s^{-1}* = 27.21 *watt*

For instance in the spinning disc reactor with 38cm diameter disc, power per square area:

for medium pressure lamp with 27.21 *watt*

$27.21/(\pi \times 0.19^2) = 240$ *watt.m^{-2}*

The total power output of medium pressure lamp used in the FFR can be calculated considering the FFR geometry using the value of $I_i = 1.8 \times 10^{17}$ quanta / s cm^2 (section 9.2.2.1).

The surface area of photons absorbed in the FFR is:

$$A = L.W = L\pi D = 80cm.\pi.10cm = 2512.8cm^2$$

and the intensity:

$$I = 1.8 \times 10^{17} \text{quanta / s cm}^2 \times 2512.8cm^2 = 4.5 \times 10^{20} \text{ quanta / s}$$

and the power output in watts using the value of 5.44×10^{-19} *watt.s/quanta* at 365nm is 245 *watt*.

C3. Sample calculation for film thickness and Re number in the falling film reactor

.

In Chapter 9, film thickness and Re number are defined as following (Equation 9.6 and 9.7):

$$\delta = \left(\frac{3\mu Q}{\rho g \pi D}\right)^{1/3} \quad \text{and} \quad Re = \frac{4\rho Q}{\pi D \mu}$$

where ρ is density of the liquid, g is gravity, δ is the average film thickness and μ is viscosity.

$\rho_{25} = 0.997$ g/cm^3 $\quad \mu_{25} = 0.00893$ $g/cm.s$ $\quad g = 980.6$ cm/s^2

$Q = 5$ $lt/min = 83.33$ cm^3/s

$$\delta = \left|\frac{3\mu Q}{\rho g \pi D}\right|^{1/3} = \left|\frac{3 \times 0.00893 \times 83.33}{0.997 \times 980.6 \times 3.14 \times 10}\right|^{1/3} = 0.0417 cm = 0.417 mm$$

$$Re = \frac{4Q\rho}{\pi D \mu} = \frac{4 \times 83.33 \times 0.997}{3.14 \times 10 \times 0.00893} = 1185.2$$

APPENDIX D

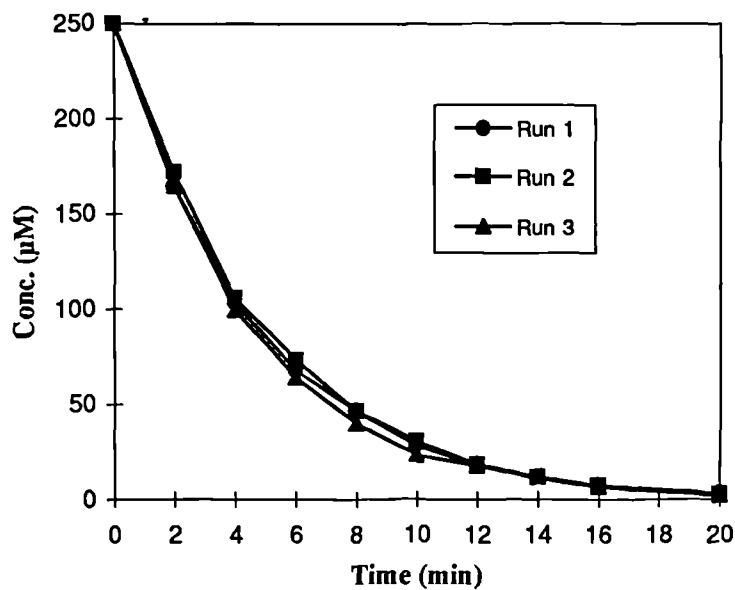Quantifying Errors in Experimental Measurements

D1. Sample -1   Based on the results of the falling film reactor

Catalyst concentration and type = 0.5g/lt P-25   Liquid flow rate = 5lt/min
10lt 100μM Salicylic acid solution

Concentration (μM)

Time	Run 1	Run 2	Run 3	Standard deviation for every collection time
0	100	100	100	0
2	67.85	67.67	66.82	± 0.550
4	51.02	48.87	50.46	± 1.115
6	36.73	36.09	38.31	± 1.142
8	26.53	26.31	27.57	± 0.673
10	17.85	16.91	18.22	± 0.675
12	11.73	10.52	11.68	± 0.684
14	7.14	6.76	6.31	± 0.415
16	4.08	3.57	4.04	± 0.283
20	1.02	1.31	1.21	± 0.147
25	0.51	0.56	0.47	± 0.045
1st order rates (min^{-1})	k 0.19343	k 0.20059	k 0.18719	k 0.1937 ± 0.0067

D2.   Sample -2   Based on the results of the falling film reactor

Catalyst concentration and type = 0.5g/lt P-25   Liquid flow rate = 5lt/min
10lt   250µM 4-Chlorophenol solution

Concentration (µM)

Time	Run 1	Run 2	Run 3	Standard deviation for every collection time
0	250	250	250	0
2	164.44	171.95	164.20	± 4.406
4	102.94	105.82	99.11	± 3.366
6	67.40	72.75	63.60	± 4.596
8	46.56	46.29	39.94	± 3.746
10	28.18	30.42	23.66	± 3.443
12	18.38	18.51	17.75	± 0.406
14	11.03	11.90	11.83	± 0.483
16	7.35	7.28	6.65	± 0.385
20	3.06	2.65	2.21	± 0.425
1st order rates (min^{-1})	k 0.22124	k 0.22099	k 0.22356	k 0.2219 ± 0.0014

APPENDIX E

Engineering Design of the Spinning Disc Reactor (SDR)

Figure E.1 Design of the SDR

Alphabetical key for Figure E.1

A.   UV Lamp
B.   Borosilicate glass disc
C.   Central shaft
D.   Surrounding shaft
E.   Liquid distributor head
F.   V-belt transmission

APPENDIX F

Photocatalysis of Organic Effluents in a Falling Film Reactor

H. C. Yatmaz, C. R. Howarth and C. Wallis

Chemical & Process Engineering Department, University of Newcastle-upon-Tyne
Newcastle-upon-Tyne, NE1 7RU, UK

o

Abstract

The characteristics of a falling film reactor have been investigated using different type of TiO_2 catalysts and salicylic acid, 4-chlorophenol, catechol, hydroquinone. This type of reactor is capable of accommodating a large 2.5kW UV lamp and as a consequence high destruction rates are achieved. Because of the characteristics of the falling liquid film, low catalyst loadings are required and efficient oxygen transfer is achieved within the reactor.

1. INTRODUCTION

Ollis, Pelizzetti and Serpone (1) (2) have emphasised the need for new reactor designs to increase the effective photon utilisation for large scale use. In particular they highlighted problems of the trade-off between increased catalyst surface and decreased photon distribution when increasing photocatalyst particle concentrations in slurry reactors, such as tubular flow or stirred semi-batch types. Another important design aspect is to provide high mass transfer in order to promote:

     a- Improved reactant/catalyst interaction or absorption.

     b- Improved oxygen take up at the gas/liquid interface.

Ollis and Turchi (3) modelled some simple reactors and concluded that falling film or slit flows could have superior performance. Their study (3) was based on slurries, but the advantage of thin liquid film reactors using immobilised catalyst surfaces in terms of elimination of downstream particle separation stages should not be overlooked (2). Two types of reactors which produce thin liquid films have been considered, namely spinning disc and falling film reactors. The former allows a high liquid throughput and spinning disc ozonolysis reactors which produce extremely thin liquid films (4) have demonstrated good mass transfer performance. The thin film characteristics of these suggest that they will be suitable for use with immobilised films and work is ongoing to deposit active TiO_2 films (5). Although falling film reactors produce thicker films they are simpler to design, thus can be used with high intensity lamps and can combine good UV utilisation with mass transfer improvements. The characteristics of this type of reactor has been studied and the work reported here is concerned with the kinetic characteristics using slurries, but this type of reactor is also eminently suitable for use with highly reactive immobilised film surfaces and a logical extension will be to operate with these catalysts (5).
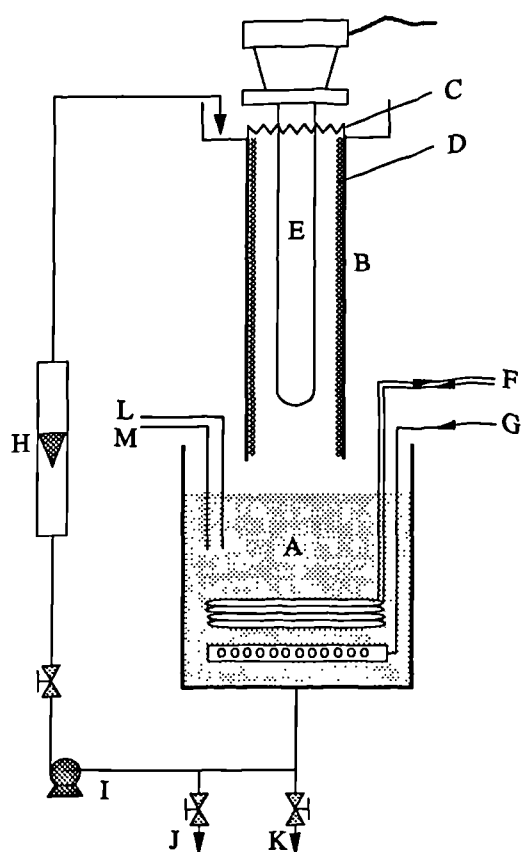
Figure 1. FALLING FILM REACTOR

A- Holding tank
B- Borosilicate glass tube
    coated by reflective aluminium
    Total length = 80 cm , I.D.=10 cm
C- Weir
D- Falling liquid film
E- Medium pressure lamp
    length = 70 cm, O.D.= 4.8 cm
    Power consumption = 2.5 kW
F- Cooling water coil
G- Air or nitrogen to sparger
H- Rotameter to 7.5 lt/min
I- 60 W pump
J- To drain
K- Sampling point
L- Temperature measurement
M-pH measurement

2. EXPERIMENTAL

Figure 1. shows the falling film reactor. Preliminary observations showed that care was needed to produce uniform falling film and it was necessary to adopt a V-profiled weir to provide good film flow. Two type of catalysts, Degussa P-25 and Tioxide were used in concentrations of 0.5 to 1 g/lt. The lamp was a 2.5kW medium pressure Hanovia-UVV. 10 lt of four standard reagents were used salicylic acid, 4-chlorophenol, catechol and hydroquinone at initial concentrations of 100 to 250μM and flowrates in the range 5 to 7.5 lt/min.

3. RESULTS AND DISCUSSION

Choice of catalyst: Average film thicknesses, calculated using the falling film model (6) for flowrates 5 and 7.5lt/min, ranged from only 0.425mm to 0.487mm, UV absorption should not be a limiting factor. Experimental results were obtained using 100μM salicylic acid solutions to compare the efficiency of catalyst types and concentrations. Figure 2. shows Degussa P-25 to more active than Tioxide, but there is an initial rapid fall in the concentration with the Tioxide catalyst which suggests that this type has a stronger physical adsorption. Other workers (1,2) in tubular or batch slurry reactors suggest that a catalyst loading of 1g/lt is the optimum. Work was carried out at this concentration and at a lower figure of 0.5g/lt. From Figure 3. and 4., it is clear that with this type of reactor less catalyst is needed for efficient operation. The reasons

for this are not clear but as in the light of these results all further experiments were carried out using P-25 type catalyst of 0.5g/lt concentrations.

Modelling: In common with other workers (1,2,3), all the data has been analysed using the Langmuir-Hinshelwood equations for the rate r:

$$r = \frac{(k_1 k_2 C)}{(1 + k_1 C)} \qquad \text{where C = reactant concentration,}$$

giving k_1 (binding constant) and k_2 (rate constant).

Kinetics: Using $100\mu M$ initial concentrations Figure 5. shows a rapid rate of destruction for salicylic acid and 4-CP and the rates obtained are shown in Table 1. for both reactants.

Table 1. Kinetic rates for $100\mu M$ initial concentration (0.5g/lt, P-25)

	k_1 (μM^{-1})	k_2 ($\mu M\,min^{-1}$)
Salicylic acid	$8.79*10^{-6}$	30287.04
4-Chlorophenol	$1.23*10^{-4}$	3106.02

Further results were obtained at higher concentrations and other reactants were used namely catechol and hydroquinone. The results are shown in Figure 6. and the kinetic rates are shown in Table 2.

Table 2. Kinetic rates for $250\mu M$ initial concentration (0.5g/lt, P-25)

	k_1 (μM^{-1})	k_2 ($\mu M\,min^{-1}$)
Catechol	$3.13*10^{-3}$	17.47
Hydroquinone	$3.43*10^{-4}$	148.29
Salicylic acid	$7.63*10^{-4}$	78.48
4-Chlorophenol	$8.74*10^{-4}$	323.10

It is not possible to compare the rate constants in Tables 1. and 2. with those obtained by other workers, because different reactors and light intensities are used, however when compared with Table 1. for salicylic acid and 4-CP, these results in Table 2. show higher rate constants (k_2) for lower initial concentrations and higher binding constants (k_1) for higher initial concentrations.

The models produced by Ollis and Turchi (3) suggested that falling film reactors could have superior performance, but for the reasons outlined above it is not possible to produce a direct comparison with tubular/stirred reactors. The removal rates in Table 1. are indeed high but if the falling film reactor is to be fully understood, it is necessary to consider whether to total mineralisation occurs. Figure 7. shows that intermediates are formed with salicylic acid and 4-CP. Other workers using tubular or stirred reactors also found similar intermediates but many workers did not report intermediates primarily because they did not analyse for them.

Oxygen mass transfer: Efficient oxygen transfer is important in reactor design and with a high intensity lamp it was necessary to determine whether the reaction was oxygen limited in the falling film reactor. 4-CP and its intermediate hydroquinone was used for this investigation. In order to establish that the falling film reactor could provide good oxygen transfer at the film/air interface, the holding tank and the bottom of the reactor were sparged and blanketed with nitrogen. Using 4-CP, Figure 8. clearly shows that sufficient oxygen is supplied within the reactor to carry out the primary destruction stage, but the intermediate removal appears to be oxygen deficient.

4. CONCLUSION

The falling film reactor is a simple design which allows efficient light utilisation to be combined with good mass transfer characteristics. The destruction rates of typical reactants appear to be higher than in conventional tubular or stirred slurry reactors and lower catalyst loadings can be used.

It is not necessary to provide external oxygen sparging, because the mass transfer characteristics of a falling film reactor allow sufficient oxygen to be transferred within the reactor to promote the reaction even with a high radiation flux of 1.1 kW/m^2.

5. REFERENCES

1. Ollis, D.F.; Pelizzetti, E.; Serpone, N. in Photocatalysis -Fundamentals and Applications; N.Serpone, E.Pelizzetti, Ed., John Wiley & Sons, USA, 1989, pp. 603-637
2. Ollis, D.F.; Pelizzetti, E.; Serpone, N. *Environ. Sci. Technol.*, 1991, Vol.25, No.9, 1522-1529
3. Ollis, D.F.; Turchi, C., *Environmental Progress*, 1990, Vol.9, No.4, 229-234
4. Barberis, K.; Howarth, C.R., *Ozone Science & Eng.*, 1991, Vol.13, No.5, 501-519
5. Christensen, P.A.; Hamnett, A.; He, R.; Howarth, C.R.; Shaw, K. "Fundamental photocatalytic studies on immobilised films of TiO_2" submitted to *TiO_2 Photocatalytic Purification and Treatment of Water and Air*, Ontario, Nov. 1992
6. Bird, R.B.; Stewart, W.E.; Lightfoot, E.N., Transport Phenomena, John Wiley & Sons, USA, 1960, pp.37
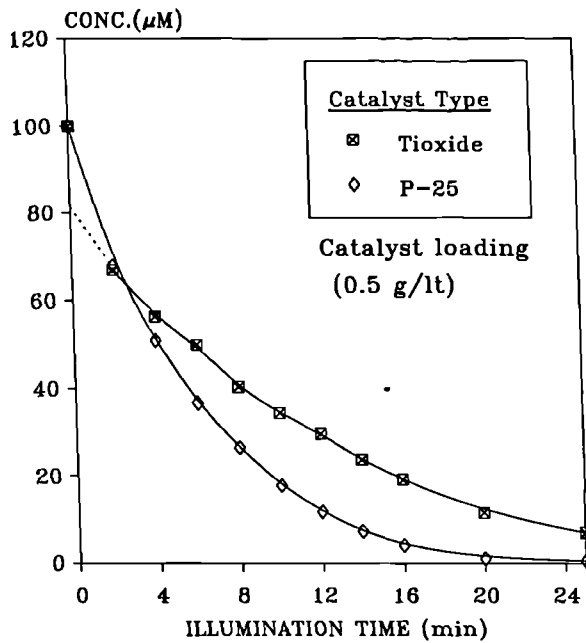
Figure 2. Effect of Catalyst Type
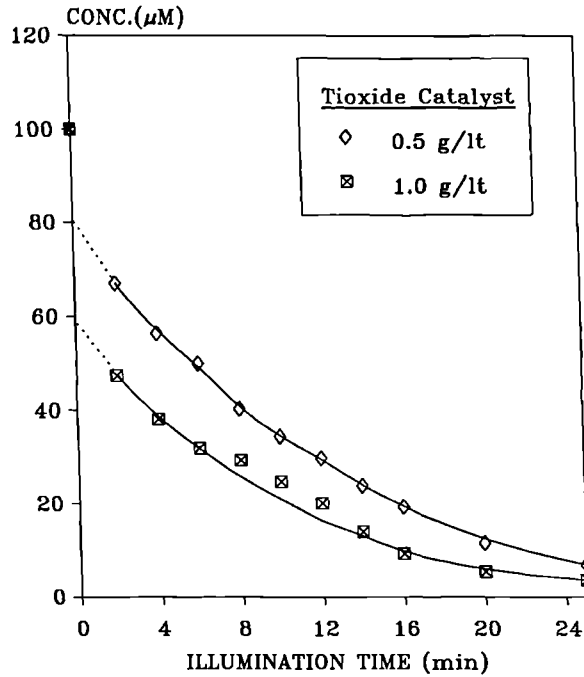on the Degradation of Salicylic Acid
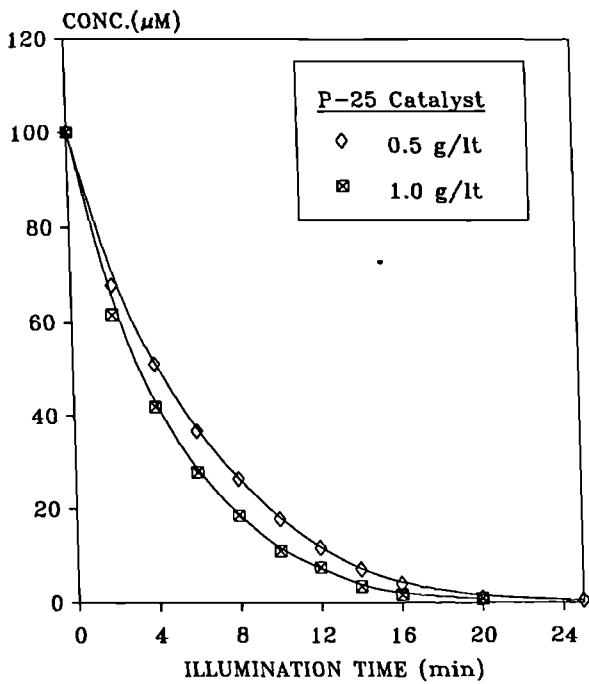

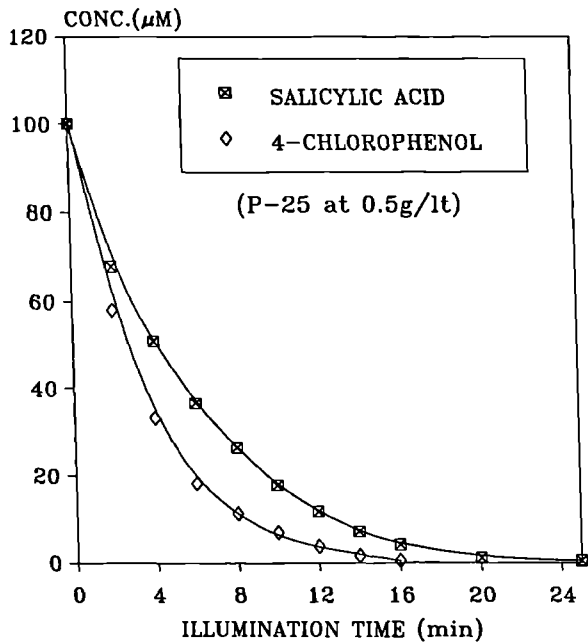Figure 3. Effect of Catalyst Loading

Figure 4. Effect of Catalyst Loading

Figure 5. Destruction of Reactants
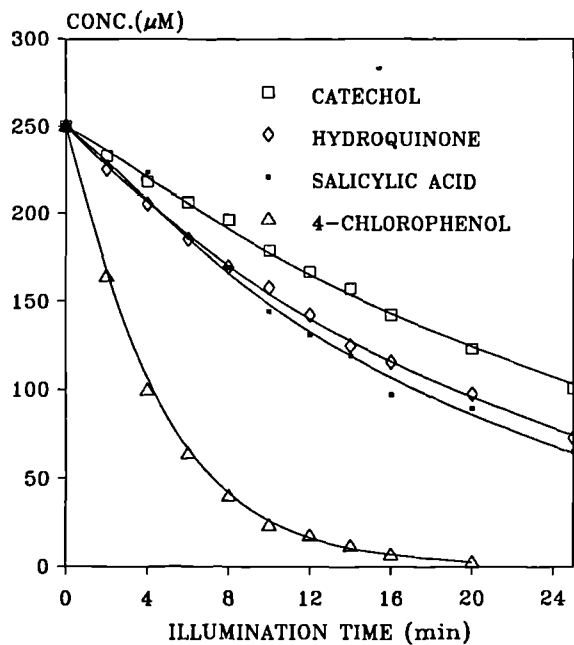with 100μM Initial Concentration

Figure 6. Destruction of Reactants
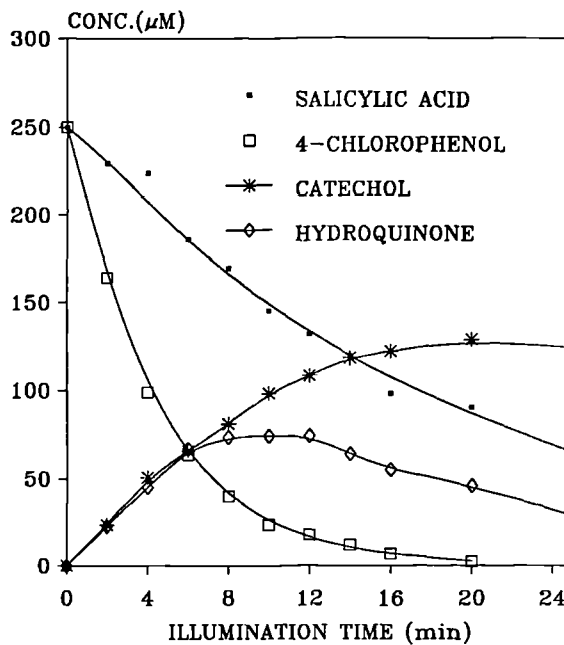with 250μM Initial Concentration
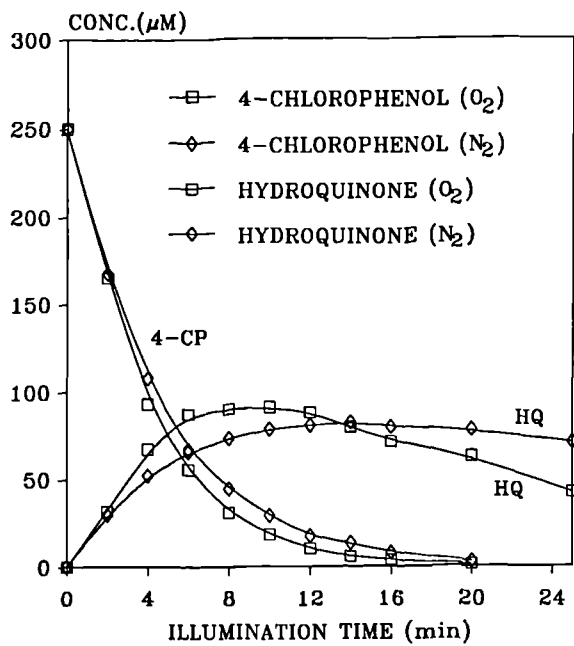

Figure 7. Salicylic Acid, 4-CP
Removal with Intermediates

Figure 8. Effect of Oxygen
Transfer within Reactor